LAND USE IMPACTS ON THE GEOCHEMISTRY AND MICROBIOLOGY OF CAVE STREAMS WITHIN THE KNOXVILLE METROPOLITAN AREA

A Thesis Presented for the
Master of Science
Degree
The University of Tennessee, Knoxville

Maya J. Robles
December 2025

ACKNOWLEDGEMENTS

The accomplishments made during the completion of my degree would not have been possible without support from friends, family, and the Engel lab group. I would especially like to thank Annette Engel for her intellectual inspiration and academic mentorship, and Audrey Paterson for her dedication to the lab and technical assistance. Thank you also goes to my committee, Ania Szynkiewicz and Jill Mikucki, for their advice and expertise.

My research expenses and conference travel were funded by the Donald H. and Florence Jones Endowment for Aqueous Geochemistry, the Department of Earth, Environmental and Planetary Sciences Student Success Fund, and a grant from the Office of Research Innovation & Economic Development that supported NextGen sequencing by the Genomics Core Laboratory at the University of Tennessee.

I appreciate those who assisted me in the field or lab, including Kayla Summerlot, Gabrielle Boggs, Maya Wilson, Oliver Dattilo, Derek Detweiler, and Sara Shields. I'm also grateful for the friendships made during my time in Knoxville because they offered a trusting and reliable support system: Brittan and August Wogsland, Kayla Summerlot, Kaitlyn Gauvey, Everett Williams, and Thomas Frueh. I appreciate my outdoorsy companions who kept in touch and took me on adventures when I could, especially from the caving community. Thanks to all who believed in me despite the challenges I faced.

Finally, thank you to my family for encouraging my curiosity from early on and the pursuit of knowledge.

ABSTRACT

Karst groundwater systems are ubiquitous, reliable aquifers that have higher risks of contamination compared to other aquifer systems due to their connectivity to the surface, such as from sinking streams and sinkholes. Changes to land use / land cover (LULC) above karst systems can impact and alter environmental conditions in the subsurface and affect groundwater biota. Previous studies have focused on understanding how LULC changes affect the geochemistry and microbial communities in surface aquatic systems, but few studies have investigated the impacts of LULC change on water quality and microbiology of cave and karst areas. This study focused on cave systems in the Knoxville Metropolitan Statistical Area, where changes in LULC over a 5-year period (2019–2024), near to and within cave system watersheds, were calculated. Cave stream and sediment geochemistry and microbiology were evaluated and compared to LULC changes. This study also assessed impacts to the caves from a flooding event caused by Hurricane Helene. Overall, watershed boundaries did not predict water quality conditions for the caves, but local LULC around cave entrances, within a 1-km radius buffer, corresponded to the degree of impact, with the highest nutrient measurements coming from cave streams near high intensity development and with higher human populations. Caves with inflowing streams were more affected by LULC changes compared to caves with outflowing streams that were more representative of groundwater conditions and buffered from LULC impacts. Stream water and sediment geochemistry generally suggested stream impairment based on elevated concentrations of chloride, nitrate, and trace metals that were indicative of anthropogenic activities. Some trace metals were only measured from cave sediments, and concentrations were higher from streams experiencing the most LULC change over time. Moreover, the microbial loads of coliforms and *E. coli* were higher than recommended by federal agencies, and the presence of other putative pathogens suggested chronic contamination of the cave streams. Dominant bacterial phyla from cave streams and sediments included Pseudomonadota, Acidobacteria, Bacteridota, Planctomycetota, Verrucomicrobiota, and Chloroflexota. Because there have been limited studies connecting LULC drivers to karst microbial community compositional changes through time, this study provides key information for future research.

TABLE OF CONTENTS

CHAPTER ONE: INTRODUCTION 1
1.1 Problem Statement 1
1.2 Research Objectives and Hypotheses 3
CHAPTER TWO: LITERATURE REVIEW 5
2.1 Karst Aquifers and Contamination Risks 5
2.2 East Tennessee Karst 7
2.3 Groundwater Microbial Ecology 8
CHAPTER THREE: MATERIALS AND METHODS 11
3.1 Study Area and Design 11
3.1.1 Original Site Selection Criteria 11
3.1.2 Site Descriptions 15
3.2 Field Methods 18
3.3 Land Use / Land Cover Analysis 20
3.4 Geochemical Analyses of Water and Sediments 22
3.5 Culture-Based Microbial Colony Counts 23
3.6 DNA Extractions from Water and Sediment 27
3.7 16S rRNA Gene Sequencing and Analysis 28
3.8 Statistical Analysis 28
CHAPTER FOUR: RESULTS AND DISCUSSION 29
4.1 Land Use / Land Change at the Local and Watershed Scales 29
4.2 Environmental Conditions and Geochemistry 37
4.2.1 Physicochemical Measurements 37
4.2.2 Major Ion Chemistry 37
4.2.3 Trace Metal Chemistry 47
4.3 Culture-based Analysis of Aerobic Microbes, Coliforms, and *E. coli* 50
4.4 Sequence Analysis of Microbial Communities 54
4.4.1 Taxonomic Overview of Microbial Communities 54
4.4.2 Putative Pathogens 61
4.5 Correlations Between Taxonomic Groups, LULC, and Environmental Variables 61
CHAPTER FIVE: CONCLUSIONS 67

REFERENCES 69
APPENDICES 83
  Appendix A 83
VITA 91

LIST OF TABLES

Table 3.1. Cave information, including the names, geology, watershed, county, passage length, stream type, and a short summary of the surrounding land use. TCS ID numbers are from the Tennessee Cave Survey database, with letters noting the county. 12

Table 3.2. Selection of study caves in 2019 was done by evaluating aggregated land use / land cover (LULC) categories from the NLCD around each cave and the population within a 5-km radius from the cave using the 2015 NASA SEDAC database. See text for details. NM = not measured. 13

Table 3.3. Parameters used for ICP-OES analysis of water samples. Analytes, selected wavelengths, R^2 values from the calculated calibration curves, the Qtegra Limit of Detection (LOD), and the Method Detection Limit (MDL), following the U.S. EPA method 6010D unless otherwise stated. The metals Al, Cd, Cu, Fe, Mo, Ni, and Zn were below detection in all water samples analyzed. Units for wavelengths are nm, and LOD and MDL values are reported in mg/L. 24

Table 3.4. Parameters used for ICP-OES analysis of sediment extractions. Analytes, selected wavelengths, R^2 values from the calculated calibration curves, the Qtegra software Limit of Detection (LOD), and the Method Detection Limit (MDL), following the U.S. EPA method 6010D, unless otherwise stated. Analytes As, Mo, Ni, and Pb were below detection in all sediment extraction samples analyzed. Units for wavelengths are nm, and LODs and MDLs are mg/L. 25

Table 4.1. Percentage of LULC categories in the NLCD for each 1-km cave buffer zone in 2019. Categories not included in the table had <0.1% coverage (e.g., woody wetlands, emergent herbaceous wetlands, cultivated crops, shrub/scrub). 30

Table 4.2. Percentage of LULC changes from 2014 to 2019 at the 1-km buffer scale for each cave. Categories not included in the table had <0.1% coverage (e.g., woody wetlands, emergent herbaceous wetlands, cultivated crops, and shrub/scrub). Pink-shaded cells note higher percentages from 2014 to 2019; blue-shaded cells note lower percentages from 2014 to 2019. 31

Table 4.3. Percentage of LULC categories from the NLCD for each 1-km cave buffer zone in 2024. Categories not included in the table had <0.1% coverage (e.g., woody wetlands, emergent herbaceous wetlands, cultivated crops, and shrub/scrub). 32

Table 4.4. Percentage of LULC changes from 2019 to 2024 at the 1-km buffer scale for each cave. Categories not included in the table had <0.1% coverage (e.g., woody wetlands, emergent herbaceous wetlands, cultivated crops, shrub/scrub, and barren land). Pink-shaded cells note higher percentages from 2019 to 2024; blue-shaded cells note lower percentages from 2019 to 2024. 33

Table 4.5. Percentage of LULC changes from 2019 to 2024 at the HUC 12 sub-watershed scale. Categories not included in the table had <0.1% coverage (e.g., woody wetlands, emergent herbaceous wetlands, cultivated crops, shrub/scrub, and barren land). Pink-shaded cells note higher percentages from 2019 to 2024; blue-shaded cells note lower percentages from 2019 to 2024. 34

Table 4.6. Field-collected physiochemical data, including pH, temperature in °C, dissolved oxygen (DO) in mg/L, and specific conductance (Cond) in μS/cm. The full sample ID represents the location (East Tennessee, ETN), date (year, month, day), and TCS ID. 38

Table 4.7. Geochemical summary for alkalinity reported as mmol, and total inorganic carbon (TIC), non-purgeable organic carbon (NPOC), total nitrogen (TN), and nitrate reported in mg/L from both the ion chromatography (IC) measurements and CHEMetrics methods. NM = not measured. BDL = below detection limit. Detection limits for nitrate measured by IC were 1.0 mg/L. 39

Table 4.8. Major ion concentrations measured from cave stream water. Concentrations are in mg/L. NM = not measured. 40

Table 4.9. Analysis of variance (ANOVA) results for physicochemical, geochemical, and CFUs tested against LULC, watershed (Clinch, Holston, Watts Bar), and sampling period (2019, 2024, 2024 post-Helene), with statistically significant values (p-value <0.05) highlighted in pink. ND = no data due to too few data points. 44

Table 4.10. Spearman's rank correlation analyses for LULC, physicochemical, and culture-based microbiological characteristics for the cave stream samples. Only significant (p-value <0.05) and moderately strong relationships (ρ >0.5) are shown. Trace metals from water are noted by "(w)" and trace metals from sediments are noted "(s)." 45

Table 4.11. Analysis of variance (ANOVA) results tested for trace metal concentrations from cave streams against LULC, watershed (Clinch, Holston, Watts Bar), and sampling period (2019, 2024, 2024 post-Helene), with statistically significant values (p-value <0.05) highlighted in pink. 48

Table 4.12. Analysis of variance (ANOVA) results tested for weak-acid soluble metal concentrations from cave sediments against LULC, watershed (Clinch, Holston, Watts Bar), and sampling period (2019, 2024, 2024 post-Helene), with statistically significant values (p-value <0.05) highlighted in pink. ND = no data due to too few data points. 48

Table 4.13. Spearman's rank correlation for the top 1% of class-level microbial relative abundances from the cave stream samples. The upper right triangle has p-values, highlighted in pink if significant (p-value >0.05), and the lower left triangle has Spearman's rank (ρ), with moderately to strongly correlated relationships bolded. 59

Table 4.14. Spearman's rank correlation for the top 1% class-level microbial relative abundances from the cave sediment samples. The upper right triangle has p-values, highlighted in pink if significant (p>0.05), and the lower left triangle has Spearman's rank (ρ), with moderately to strongly correlated relationships bolded. 60

Table 4.14. Pearson's significance (r) tests for class-level taxa from the cave streams against LULC for major categories (1-km buffer) and population density within a 5-km radius around the caves. Statistically significant values (p-value <0.05) are highlighted in green, and moderately strong correlations are highlighted in yellow. 63

Table 4.15. Pearson's significance (r) tests for class-level taxa from the cave sediments against LULC for major categories (1-km buffer) and population density within a 5-km radius around the caves. Statistically significant values (p<0.05) highlighted in pink, and moderately strong correlations highlighted in yellow 64

Table A.1. Trace elements concentrations for the cave streams. Concentrations are in ppm (mg/L). BDL = below detection limit, based on the reporting limit for each element. 84

Table A.2. Extracted trace element concentrations and standard deviations measured from the cave sediments, reported duplicates. Concentrations are in ppm. BDL = below detection limit, based on the reporting limit for each element 85

Table A.3. Extracted concentrations of Ca, Mg, Na, P, Si and standard deviations measured from the cave sediments, reported duplicates. Concentrations are in ppm. BDL = below detection limit, based on the reporting limit for each element. 88

Table A.4. Average colony forming units (CFU) and standard deviations per mL for aerobic bacteria, total coliforms, and *E. coli* measured from raw cave stream water. NM= not measured. 90

LIST OF FIGURES

Figure 3.1. Map of the watersheds in the study area in Knox and Roane counties, Tennessee. Cave locations are shown as colored dots. Identification numbers are from the Tennessee Cave Survey (TCS) database, with letters denoting the county. Watershed data are from the U.S. Geological Survey National Watershed Boundaries Dataset (https://www.usgs.gov/national-hydrography/watershed-boundary-dataset). 14

Figure 3.2. (A) Sampling dissolved nitrate inside one of the study caves by using a CHEMetrics field spectrophotometer and colorimetric kit, and (B) filtering water through a Sterivex filter to obtain an eDNA sample (right). 219

Figure 3.3. Map of the land use / land cover (LULC) in the study area. Cave locations are shown as yellow dots. LULC data are from the USGS National Landcover Database (NLCD) 2019 (https://www.usgs.gov/centers/eros/science/national-land-cover-database). The solid black lines separate the three sub-basin watersheds (HUC 8). 21

Figure 3.4. (A) A gridded aerobic Petrifilm sheet with CFUs per 1 cm^2. (B) Coliform/*E. coli* Petrifilm sheet, with the circles indicating coliform bacteria and blue arrow indicating *E. coli*. (C) Close-up of a coliform & *E. coli* Petrifilm sheet, with arrows indicating *E. coli* (in blue) and circles surrounding coliform bacteria (with bubbles). All of the rest of the colonies on the sheet were interpreted as non-coliform cells. 26

Figure 4.1. Cave 1-km buffer zones for 2019 (A) and 2024 (B), classified according to the NLCD. Cave entrances are shown as black triangles. 35

Figure 4.2. Map of the LULC of eight HUC 12 sub-watersheds, classified according to the NLCD. HUC 12 boundaries are outlined and HUC 8 watersheds are circled in black. Cave locations are shown as yellow dots, and there is one per sub-watershed. LULC data are from the USGS National Landcover Database (NLCD) 2019 (https://www.usgs.gov/centers/eros/science/national-land-cover-database). 36

Figure 4.3. pH measured from the cave streams. Caves are listed by their TCS IDs, with shapes (circle, triangle, square) corresponding to the sampling period (2019, 2024, 2024 post-Helene, respectively) and color coded according to watershed (greens for Watts Bar of the Tennessee River, oranges for Holston River, and purples for Lower Clinch River). Caves are also grouped by the dominant LULC classification. 41

Figure 4.4. Nitrate measured from the cave streams. Caves are listed by their TCS IDs, with shapes (circle, triangle, square) corresponding to the sampling period (2019, 2024, 2024 post-Helene, respectively) and color coded according to watershed (greens for Watts Bar of the Tennessee River, oranges for Holston River, and purples for Lower Clinch River). Caves are also grouped by the dominant LULC classification. 45

Figure 4.5. Nitrate, sulfate, and potassium compared to chloride concentrtions in mmol/L. Caves are listed by their TCS IDs, with shapes (circle, triangle, square) corresponding to the sampling period (2019, 2024, 2024 post-Helene, respectively) and color coded according to watershed (greens for Watts Bar of the Tennessee River, oranges for Holston River, and purples for Lower Clinch River). 46

Figure 4.6. Strontium and barium concentrations from the cave streams. Caves are listed by their TCS IDs, with shape (circle, triangle, square) corresponding to the sampling period (2019, 2024, 2024 post-Helene, respectively) and color coded according to watershed (greens for Watts Bar of the Tennessee River, oranges for Holston River, and purples for Lower Clinch River). Caves are also grouped by the dominant LULC classification. Units are in mmol.. 49

Figure 4.7. Counts for colony-forming units (CFUs) for aerobic microbes from the cave streams. Caves are listed by their TCS IDs, with shape (triangle, square) corresponding to the sampling period (2024 and 2024 post-Helene, respectively) and color coded according to watershed (greens for Watts Bar of the Tennessee River, oranges for Holston River, and purples for Lower Clinch River). Caves are also grouped by the dominant LULC classification. 51

Figure 4.8. Total coliform and *E. coli* counts of colony-forming units (CFUs) from the cave streams. Coliform counts are represented by solid shapes and *E. coli* counts are represented by open shapes. Caves are listed by their TCS IDs, with shape (circle, triangle, square) corresponding to the sampling period (2019, 2024, 2024 post-Helene, respectively) and color coded according to watershed (greens for Watts Bar of the Tennessee River, oranges for Holston River, and purples for Lower Clinch River). Caves are also grouped by the dominant LULC classification. 52

Figure 4.9. Relative abundances of 16S rRNA gene sequences from cave streams at the phylum level for Archaea (Thermoprotea) and Bacteria. Only sequences with > 1% abundance are shown. 55

Figure 4.10. Relative abundances of 16S rRNA gene sequences from cave sediments at the phylum level for Archaea (Thermoprotea) and Bacteria. Only sequences with > 1% abundance are shown. 56
Figure 4.11. Relative abundances of bacterial 16S rRNA gene sequences from cave streams at the class level. Sequences with > 1% relative abundance are shown. 57
Figure 4.12. Relative abundances of bacterial 16S rRNA gene sequences from cave sediments at the class level. Sequences with > 1% relative abundance are shown. 58
Figure 4.12. Relative abundances of 16S rRNA gene sequences from cave streams at the order level. Putative pathogens are highlighted while all other orders are grayed out. 62
Figure 4.13. Cannonical correspondence analysis of selected class-level taxa which were statistically significant among different LULC caves. Colored shapes indicate caves. The first axis explains 68.1% of the variance and second axis explains 22.0% of the variance.. 66

CHAPTER ONE: INTRODUCTION

1.1 Problem Statement

Groundwater reservoirs contain about 95% of the available freshwater on Earth and are the primary drinking water source globally (Griebler and Avramov, 2015). Karst aquifers, formed by the chemical dissolution of soluble carbonate rock, serve about a quarter of human populations (Goldscheider et al., 2020). Unfortunately, the quality of groundwater resources worldwide is decreasing due to anthropogenic activities, such as urbanization, industrial activity, and agriculture. Urbanization is defined as a shift from natural, wild landscapes to urban landscapes with impervious land cover that can increase the detrimental impacts of flooding.

Karst landscapes rapidly respond to flood events, notably by increasing conduit flow velocities, raising aquifer water levels and spring discharge rates, and shifting water quality (Ford and Williams, 2007). Flood events also elevate microbial loads and introduce opportunistic pathogens (Mapili et al., 2022), as well as mobilize sediments and solutes (Bahar and Yamamuro, 2008) and organic compounds, such as manure and pesticides (Allison and Martiny, 2008). In urbanized areas, stream solute concentrations, bacterial loads, and conductivity values increase (Clinton and Vose, 2005), and karst stream water quality and cave microbial ecology distinctly change (Zhao et al., 2010; Liu et al., 2014). However, although karst ecosystems have been investigated from a hydrogeological and hydrogeochemical perspective (Gibert et al., 1994; Drew and Hötzl, 1999; Ford and Williams, 2007), knowledge about biogeochemical and microbial processes is limited for most karst systems. Caves offer an accessible window to the subsurface and studying cave streams provides access to groundwater in karst regions.

Studies in southern Appalachian watersheds demonstrate that the percent of land use / land cover (LULC) is one of the most influential factors on baseline water quality (Bolstad and Swank, 1997), and similar studies demonstrate this trend in other states (Hunsaker and Levine, 1995). Appalachia has some of the richest water resources in the United States, but coverage of water treatment systems is below the national average, as private unregulated groundwater wells or springs are the primary drinking water sources for three quarters of households in rural areas (Hughes et al., 2005). Wastewater systems are also highly varied throughout the region. Many households rely on septic tanks that can clog or leak into the soil or surface water, especially in drain fields of urban systems (Clinton and Vose, 2005; Hughes et al., 2005).

In the Appalachian Valley and Ridge (AVR) of East Tennessee, the Knoxville Metropolitan Statistical Area (KMSA) currently encompasses nine counties and has just under one million residents (United States Census Bureau, 2023), which makes it the third largest city in Tennessee. Since Knoxville's establishment in 1792, the city expanded from a small urban center into surrounding karst-rich areas (Jiang and O'Neill, 2017). Karst springs with high discharge, formed along fault zones, fractures, or solutional openings in the carbonate rocks of the Chickamauga, Knox, and Conasauga groups (Fashina et al., 2022), had been used for freshwater (Hughes et al., 2005). Over time, demand surpassed supply (Jiang and O'Neill, 2017), and Knoxville switched to a municipal water source of treated river water (e.g., reservoirs on dammed rivers). Karst springs still serve about 10% of households in Tennessee, with public utilities serving about 520,000 people in Knox County (Tennessee Department of Health, 2003; Centers for Disease Control and Prevention, 2021; Fashina et al., 2022).

In urban watersheds, fecal indicator bacteria (i.e., coliforms, including *E. coli*) strongly correlate with population density (Frenzel and Couvillion, 2002). Contaminants like fecal material can be transported through watersheds from runoff, whereby the rate of transport is dependent on the type of land use. Urban streams in Knoxville surpass the State of Tennessee bacteriological standards (Hampson et al., 2000), predominately because Knoxville uses sewer overflow systems. Sewage overflow events have led to *E. coli* levels that are two orders of magnitude higher than background levels in karst springs in Gallusquelle, Germany (Heinz et al., 2008), for example. Moreover, *E. coli* and total coliform bacteria were found in 63% of the KMSA surface streams assessed, which also surpassed State standards (Bickford et al., 1996; Hampson et al., 2000; Johnson et al., 2011). Where there is agriculture over karst in the region, mismanagement of animal waste has resulted in fecal coliform bacteria levels greater than 400 colony forming units (CFU)/mL in cave streams draining dairy operations, whereas pasture operations have less than 1 CFU/mL (Boyer and Pasquarell, 1999).

Unique species with low trait variability and specific adaptations to the subsurface are found in caves and karst aquifers. These species are often endemic to a specific region and are vulnerable to disturbances in their habitat. The rare and endemic Berry Cave Salamander (*Gyrinophilus gulolineatus)* is found in only a few caves within the KMSA and within the Knoxville city limits. This salamander is especially sensitive to declining water quality due to microbial contaminants. Its population has significantly declined since the 2000s (Neimiller et al., 2021). The microbial diversity of cave streams throughout the range of *G. gulolineatus*, or elsewhere in Tennessee, has not yet been investigated.

1.2 Research Objectives and Hypotheses

The overarching goal of the thesis was to assess water quality and microbiology of cave streams in the KMSA over the 5-year period.

The following questions were asked as part of the research:

1) What is the microbial community composition from cave streams in the KMSA?
2) Are there significant relationships between LULC and cave stream geochemical properties, and between LULC and cave stream microbial communities?
3) Were there changes in cave stream and cave sediment microbial communities following local LULC changes around the caves or after Hurricane Helene?

The following objectives were met:

1) Assess the geochemistry and microbiology of cave stream water and sediment from 2019 and 2024, and before and after Hurricane Helene, to determine what, if any, changes occurred in the systems over that time period and due to flood disturbance.
2) Calculate the microbial loads for cave streams from 2019 and 2024, as well as after Hurricane Helene, by using culture-based methods for total aerobic microbes, coliforms, and *E. coli* to evaluate whether these groups of microbes are entering and living within the cave streams, which could be an indication of chronic sources for these microbes within a cave's local watershed.
3) Determine the LULC changes around the caves and within their watersheds from 2014 to 2019 and from 2019 to 2024 that could be tied to changes in cave stream geochemistry and microbiology.
4) Evaluate environmental, land use, and geochemical drivers that could explain differences in microbial community compositions and potential disturbance responses, such as caused by Hurricane Helene flooding.

The following hypotheses guided the research:

1) Because urban land use affects major ion chemistry, cave streams from systems surrounded by high intensity development (HID) will have higher concentrations of nitrate and chloride, as well as dissolved organic carbon.

2) Cave sediment from systems surrounded by HID will have higher trace metal concentrations, such as zinc and lead.
3) Cave streams surrounded by similar LULC classification types will have similar microbial community compositions.
4) Caves with inflowing versus outflowing streams will have different microbial communities that do not correlate to LULC classifications because the communities in the outflowing streams are sourced from groundwater where impacts from LULC could be buffered, compared to inflowing streams that are impacted by surface runoff and other LULC effects.

CHAPTER TWO: LITERATURE REVIEW

2.1 Karst Aquifers and Contamination Risks

Karst landscapes contain surface and subsurface water systems, sinkholes, and caves that form from the chemical dissolution of soluble carbonate rocks (e.g., limestone, gypsum, marble). Carbonate rocks are estimated to cover about 12% of the earth's dry, ice-free land (Ford and Williams, 2007). An estimated 9% of the total world population relies on karst aquifers for drinking water (Stevanović, 2019). Many cities, such as San Antonio (USA), Rome (Italy), Damascus (Syria), Taiyuan (China), and Vienna (Austria), are predominantly or completely dependent on karst groundwater (Krescic and Stevanovic, 2010; Chen et al., 2017). Karst springs can provide water to people due to their high yields but often receive little to no treatment prior to use compared to surface water resources (Hughes et al., 2005). An estimated 10.2 million people in the United States are dependent on untreated, noncommunity groundwater resources (U.S. Environmental Protection Agency, 2006), which is unregulated and often receives no treatment before consumption. This is problematic because karst groundwater is highly susceptible to contamination because contaminants can rapidly migrate into the subsurface through fractures, conduits, or sinkholes (Vesper, 2001; White, 2002; Bakalowicz, 2005; Ford and Williams, 2007; Fernández-Ortega et al., 2024).

The consequence of the world's rapidly growing populations and human-driven land use / land cover (LULC) changes have resulted in environmental problems that can impact water resources and negatively impact karst, including deforestation (Drew and Hötzl, 1999; Trajano, 2000), urbanization (Schirmer et al., 2013; Liu et al., 2014; He et al., 2021), unsustainable resource extraction from mining and industry (Reboleira et al., 2011; Magesh et al., 2017), tourism (Jurado et al., 2010; Chiarini et al., 2022), non-native species introduction (Howarth, 1983; Howarth et al., 2007), persistence of antibiotic resistance among microbes (Kaiser et al., 2022), and heavy metal use and intensive agrochemical practices (Reboleira et al., 2013; Zhang et al., 2014). In rural areas, water contamination can include fertilizers, animal waste, elevated nutrient and heavy metal levels, and fecal coliform bacteria (Huebsch et al., 2013; Fernández-Ortega et al., 2024). Comparatively, in urban areas, contamination risks depend on the levels of industrialization, land management practices, and disposal practices for industrial, commercial, and residential waste containing heavy metals (Pérez-Castresana et al., 2019; Justus et al., 2020; Choudhury et al., 2024; Motta et al., 2025). In particular, landscape changes that increase impervious cover also increase runoff and decrease the ability of solutes and particulates to trickle into the subsurface (Schirmer et al., 2013). Urbanization is associated with increased solute concentrations, bacterial loads, and conductivity values in surface streams (Clinton and Vose, 2005). Urban karst groundwater can have elevated levels of antibiotic-resistant microbes (Kaiser et al., 2022). Additionally, the combination of anthropogenic activities with climate change can also impact karst (Medina et al., 2023), specifically causing more frequent and intense storm events that force contaminants into the subsurface. Other disturbances caused by climate change can include higher exposure of systems to elevated CO_2 concentrations and changes in water and air temperatures (Viles, 2003; He et al., 2021).

Heavy metal contamination is closely associated with anthropogenic activities that can compromise aquatic ecosystem health and lead to poor water quality and negative human health consequences. Contaminants are present and persist in the environment above normal background concentrations but are not necessarily directly tied to environmental or human health conditions, such as neurological, respiratory, or kidney diseases, and cancer. Heavy metals like Cd, Pb, Cu, Ni, Cr, Zn, As, Fe, Mn, Hg can result from industrial metalworking (Pérez-Castresana et al., 2019; Al-Asadi et al., 2020; Fadlillah et al., 2023; Choudhury et al., 2024). Sphalerite and pyrite, as well as other sulfide mineral mine tailings, can cause increased concentrations of Cd, Pb, As, Ni, Zn in water (Pérez-Castresana et al., 2019; Luo et al., 2020; Choudhury et al., 2024). Coal combustion and petrochemical industry and manufacturing can release Cd, Pb, Ni, Cr, and Hg (Pérez-Castresana et al., 2019; Justus et al., 2020; Fadlillah et al., 2023; Choudhury et al., 2024). The mechanical industry and improper disposal practices for battery or fuel contribute to Cd, Pb, Cu, and Cr (Pérez-Castresana et al., 2019; Fadlillah et al., 2023; Choudhury et al., 2024). Phosphate fertilizers and pesticides result in Cd, Pb, Cu, As, and Mn in runoff from agricultural areas or residences (Pérez-Castresana et al., 2019; Al-Asadi et al., 2020; Fadlillah et al., 2023; Choudhury et al., 2024). Untreated domestic (including household chemicals and detergents) and industrial wastewater can generate elevated concentrations of Cd, Pb, Fe, Mn, and Hg (Al-Asadi et al., 2020; Justus et al., 2020; Fadlillah et al., 2023), and Ni and Mn can result from excess cooling water discharged into streams from power plants (Biedunkova and Kuznietsov, 2024).

The southwest region of China has extensive karst that has been studied recently because rapid urbanization and industrialization are causing heavy metal contamination and impacting groundwater dynamics. Most studies center on the Guizhou Province and its highly populated capital, Guiyang. Natural groundwater evolution is controlled by cation exchange and the dissolution/precipitation of carbonates, gypsum, and halite minerals (Yuan et al., 2017), but municipal and industrial wastewater disposal and excessive pesticide/fertilizer use are changing groundwater compositions regionally (Zhang and Yuan, 2004). Around mining districts, heavy-metal contamination is also impacting rivers (Liao et al., 2023), and cave streams have heavy metal concentrations above background levels, including for Zn, Ni, Cr, Cu, As, and Hg, with Cr and As accounting for the most concerning health risks and need for management (Xu et al., 2020). Aquatic biota also appear impacted, with cave fish containing excessive concentrations of (listed from most to least) Zn, Cu, Cr, Ni, Cd, As, Pb, Hg (Xu et al., 2021). Collectively, the results from these investigations in Guizhou Province can inspire similar studies in the United States.

2.2 East Tennessee Karst

Major cities in the Appalachian Valley and Ridge (AVR) include Knoxville and Chattanooga in eastern Tennessee, and the Tri Cities of northeastern Tennessee and eastern Virginia. The AVR physiographic providence is characterized by erosion-resistant siliciclastic rocks holding up ridges and carbonate rocks in the valleys. The repeated geologic units within the sub-parallel ridges and valleys were created by thrust faulting. The AVR is one of the largest karst regions of the United States and stretches for about 1200 km from northern Alabama to Pennsylvania.

In general, the AVR has some of the richest water resources in the United States due to extensive karst aquifer systems, but use of water treatment systems is below the national average in the region (Hughes et al., 2005). Many people, predominately in suburban and urban areas, get their drinking water from community or city systems, which treat the water before delivery. However, wells are the primary drinking water source for three-quarters of households in rural areas (Hughes et al., 2005), and many people provide for themselves with wells that are unmonitored and unregulated by the State, and lack filtration or disinfectant use. Wastewater treatment systems are also highly variable throughout the region. Many households rely on septic tanks or cesspools, which may develop problems, such as clogs or septic leakage into the soil, especially in drain fields of urban systems (Clinton and Vose, 2005; Hughes et al., 2005). Widespread septic tank use in the region has the potential to contaminate groundwater and surface water. However, there have been relatively few studies of the microbiology of cave streams in the AVR and KMSA specifically (Boyer and Pasquarell, 1999).

2.3 Groundwater Microbial Ecology

In the 1970s, microbial diversity and activity was understood to be limited to the shallow rhizosphere (Alexander, 1971). Even after decades of research, a modern understanding of microbial diversity and distribution patterns is still lacking for deeper subsurface environments, such as groundwater (Griebler et al., 2022) and caves and karst (Lee et al., 2012; Addesso et al., 2021; Zhu et al., 2021; Prescott et al., 2022). Early studies of shallow and deep groundwater microbiology uncovered isolates from culture-based methods that were closely related to surface heterotrophs, including from phyla like Pseudomonadota (formerly Proteobacteria), Bacteroidota (formerly Bacteroidetes), Actinomycetota (formerly Actinobacteria), and Bacillota (formerly Firmicutes) (Hirsch and Rades-Rohkol, 1983; Stim, 1995). Microbiota from groundwater were also found attached to sediment particles, rock surfaces, and detritus as biofilm-forming communities that were optimized to living on surfaces rather than as plankton (Bouwer and McCarty, 1984).

Following the advent and improvement of gene sequencing technologies, novel lineages have been recovered extensively from groundwater (Probst et al., 2018), and microbial communities have distinct metabolisms (Pedersen et al., 1996; Farnleitner et al., 2005). Some communities are supported by chemolithoautotrophs that use inorganic electron donors, though research and understanding of this group from groundwater lags behind that of heterotrophic microbes. Much of the modern focus on groundwater microbiology aims to understand the role of microbes as drivers of biogeochemical processes, and of the resilience of aquifers against anthropogenic impact, such as from contamination (Griebler and Lueders, 2009; Kaiser et al., 2022; Guan et al., 2023) or LULC changes (He et al., 2021; Guan et al., 2023). For instance, some microbial groups identified from groundwater can biodegrade anthropogenic contaminants, such as fertilizers, pesticides, and herbicides. Similarly, several modern hydrochemical studies lean into the subject of anthropogenic chemical impacts on microbial communities (Panno et al., 2001; Wang and Zhang, 2019; Wang et al., 2020; Yang et al., 2020a), but fewer studies have connected anthropogenic hydrochemical and LULC drivers to groundwater microbial community compositional changes.

Caves offer direct access to groundwater in karst landscapes without the need for drilling. Microbial community dynamics in karst systems may reflect differences in microbial transport and exchange in karstic flow paths that include cells introduced from surface runoff into karst conduits or sinkholes, or from seepage from the overlying soil-vegetation groundcover, or flushed from the epikarst or from flowing phreatic water (Farnleitner et al., 2005). Therefore, karst habitats that are hydrologically connected to the surface can contain a continuum of microbial communities sourced from the surface to the subsurface (Freckman et al., 1997) and with transition zones that represent ecotones (e.g., soil, epikarst, open-channel underground streams, groundwater) (Gibert et al., 1990; Griebler and Lueders, 2009). Although the microbiology of pristine, uncontaminated karst aquifers is not well described (Griebler and Lueders, 2009), many studies have centered around novel systems, such as lava tubes or caves with hydrogen sulfide springs (Cunningham et al., 1995; Engel et al., 2004; Hathaway et al., 2012; Brad et al., 2021), or tourist caves (Jurado et al., 2010; Bontemps et al., 2022; Piano et al., 2023). Other cave and karst studies have identified previously unknown or unculturable microbial taxa (Engel et al., 2003; Barton et al., 2004; Farnleitner et al., 2005). Characterizing the microbiology of cave streams may inform about possible disturbance responses caused by LULC changes within a watershed and may provide information about public health risks caused by opportunistic pathogens (Mapili et al., 2022).

Controls on microbial diversity in karst groundwater are generally tied to environmental conditions. In general, most karst ecosystems are oligotrophic or nutrient-poor because they are limited by the nature and type of allochthonous organic matter input (Culver, 1985; Ghiorse and Wilson, 1988; Madsen and Ghiorse, 1993) and redox conditions (Frindte et al., 2016). Particulate and dissolved organic carbon (DOC) are the primary resources available to karst groundwater ecosystems, although knowledge about DOC is limited for many systems, especially in how these resources change over time (Hofmann and Griebler, 2018). Lastly, despite having low oxygen concentrations and lack of sunlight for photosynthesis, the mixing of organic matter with different electron acceptors can also impact microbial abundance and community composition (Baker et al., 2000; Fillinger et al., 2019; Karwautz et al., 2022). For example, from a study on alpine, dolomitic and limestone karst springs (Farnleitner et al., 2005), microbial community diversity varied year-round, except that the community was consistently dominated by

Nitrospirota (formerly Nitrospirae) and Bacillota, which suggested stability in the environmental conditions and resource needs of these taxa over time compared to other groups that changed.

CHAPTER THREE: MATERIALS AND METHODS

3.1 Study Area and Design

Tennessee is one of the most cave-rich states in the United States. According to the Tennessee Cave Survey (TCS), the KMSA has approximately 400 known caves, and a cave density of about 0.5 to 1.5 caves per kilometer. Caves selected for this study inside the KMSA were located within a 50-km radius of each other.

Cave selection and sampling was initially done in 2019 by a graduate student in Dr. Engel's group (Victoria Frazier). See additional details in Section 3.1.1, below. In 2024, some of the caves were revisited after using the Tennessee Property Viewer to gather cave landowner information and consultation with members of the TCS. Some caves were no longer accessible due to landownership changes, a blocked cave entrance, or because there was no longer a flowing cave stream. Ultimately, eight caves with cave streams were selected for further study, each formed in similarly aged stratigraphic units of the upper Cambrian to Middle Ordovician that had similar limestone, and some marble characteristics **(Figure 3.1, Table 3.1**).

Caves were visited in August and September 2024 and then re-visited in late September and early October after Hurricane Helene made landfall along the Gulf coast on September 26, 2024, as a category 4 hurricane. Prior to landfall, a multi-day rainfall event drenched some counties in east Tennessee, and then the region experienced more rainfall from Tropical Storm Helene. Most of the heavily flooded and affected counties were north and east of the KMSA, but Knoxville recorded about 127 mm of rainfall from the pre- and post-landfall events (Kiehl, 2024). Re-sampling the caves after Hurricane Helene provided an opportunity to examine how the cave systems responded to a flood event, although not all of the caves were equally impacted by flooding due to their hydrology and watershed properties.

3.1.1 Original Site Selection Criteria

The caves were originally selected in 2019 after determining the intensity of urbanization and population density in a 5-km radius around each cave and within each cave's watershed (**Table 3.2**). Population density was based on the NASA Socioeconomic Data and Applications Center (SEDAC) Population Estimator (https://www.earthdata.nasa.gov/centers/sedac-daac). Urban LULC was defined according to the abundance of impermeable surfaces (e.g., roads, parking lots, and buildings) using the National Land Cover Database (NLCD) 2016 classification system and Geographical Information Systems (GIS) incorporated into the computer program

Table 3.1. Cave information, including the names, geology, watershed, county, passage length, stream type, and a short summary of the surrounding land use. TCS ID numbers are from the Tennessee Cave Survey database, with letters noting the county.

TCS ID	Cave name	Rock unit	Watershed	County	Cave Length	Stream Type	General Land use
KN14	Carter	Kingsport Dolomite	Holston	Knox	275 m	Outflow	Public park
KN24	Cruze	Holston Limestone	Watts Bar	Knox	300 m	Inflow	Residential, forestry
KN62	Kirkpatrick	Maryville Limestone	Lower Clinch	Knox	90 m	Inflow	Roadway, residential
KN82	Thumping	Holston Limestone	Holston	Knox	850 m	Inflow	Agriculture, residential
KN103	Pedigo	Maynardville Limestone	Lower Clinch	Knox	93 m	Outflow	Residential, forestry
KN145	Lost Puddle	Maynardville Limestone	Lower Clinch	Knox	156 m	Outflow	Residential, forestry
RN5	Cave Creek	Mascot Dolomite	Watts Bar	Roane	310 m	Outflow	Residential, forestry
RN6	Eblen	Maynardville Limestone	Lower Clinch	Roane	1020 m	Outflow	Agriculture, forestry

Table 3.2. Selection of study caves in 2019 was done by evaluating aggregated land use / land cover (LULC) categories from the NLCD around each cave and the population within a 5-km radius from the cave using the 2015 NASA SEDAC database. See text for details. NM = not measured.

TCS ID	% Development	% Agriculture	% Forest	Population
KN14	21.97	37.86	38.81	7,599
KN24	59.02	6.47	27.55	42,856
KN62	13.56	24.33	62.07	5,750
KN82	46.58	17.52	34.30	NM
KN103	18.51	21.11	59.34	19,635
KN145	17.95	18.03	54.29	24,017
RN5	11.77	29.76	51.66	3,000
RN6	18.49	20.40	55.98	2,933

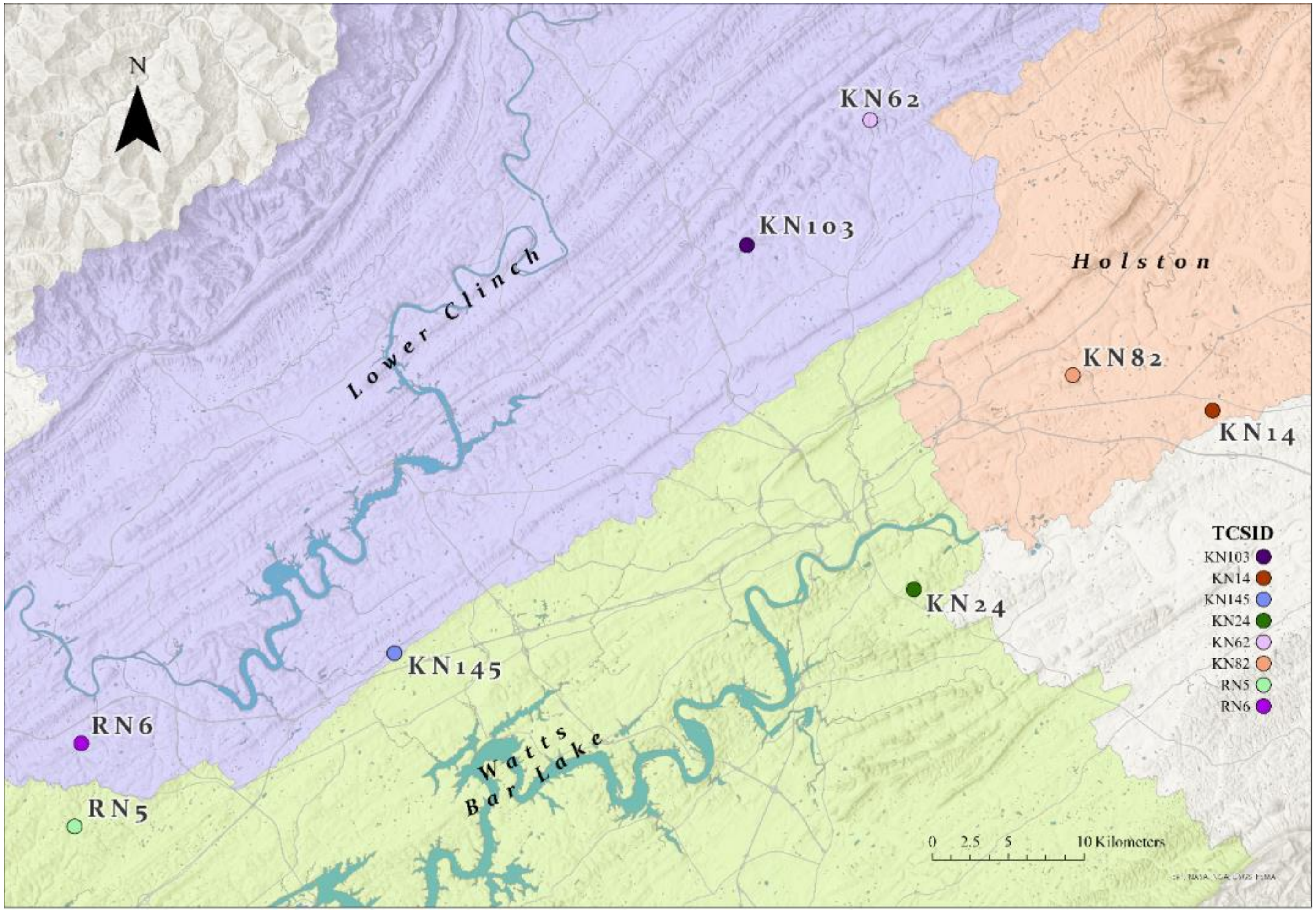

Figure 3.1. Map of the watersheds in the study area in Knox and Roane counties, Tennessee. Cave locations are shown as colored dots. Identification numbers are from the Tennessee Cave Survey (TCS) database, with letters denoting the county. Watershed data are from the U.S. Geological Survey National Watershed Boundaries Dataset (https://www.usgs.gov/national-hydrography/watershed-boundary-dataset).

ArcMap (Esri). Each cave location (as XY coordinates) was uploaded into ArcPro as a .csv file and plotted on a base map layer available in ArcPro Living Atlas.

The NLCD assigns values to pixels at a resolution of 24 m^2/pixel. Major LULC categories included: open water, developed areas, agricultural areas (e.g., pasture or cultivated crops), and vegetated areas (e.g., deciduous forest, mixed forest, etc.). Developed land was divided into open space, barren land, low intensity, medium intensity, and high intensity development. Developed open space (DOS) can be vegetated and has less than 20% impervious cover (e.g., parks and residential areas). Low intensity development (LID) was mostly comprised of single-unit family homes, as a combination of vegetated areas and constructed materials with between 20 and 49% impervious cover. Medium intensity development (MID) was defined by 50-79% impervious cover and developed residential areas. High intensity development (HID) areas had 80-100% impervious cover and included commercial or industrial areas and apartment complexes. For the overall study, caves were then selected that either had primarily agricultural LULC, primarily forested LULC, or primarily a mix of development LULC (**Table 3.2**).

3.1.2 Site Descriptions

The eight study caves sampled in 2024 were in Knox and Roane counties (**Table 3.1**). Caves are identified by a TCS ID code that corresponds to county (i.e., KN or RN) and number. More information about the TCS can be found on the website: https://tennesseecavesurvey.org/dashboard.html. Although not all of the caves in the study have been mapped by TCS members, each of the caves has a narrative description that includes geological, hydrological, and other cave details. The narratives were adapted and amended for brief descriptions of each cave.

<u>KN14</u>: Carter Cave is a well-known cave located in a small, forested valley in a public park in East Knoxville. KN14 formed within the Kingsport Dolomite of the lower Ordovician Knox Group. The cave entrance is small (1.5 meters by 1 meter), as is the rest of the passage. The cave passages follow strike and dip of 30 degrees (Moneymaker, 1929). The cave spring is located left of the main entrance after following a tight crawl into a small room. Water from the cave spring emerges outside the cave entrance and forms a stream that flows along the park trail. Outside the park, residential properties lie within 250 meters of the cave entrance. Over the years, local visitors regularly accessed the cave, and passages are well-traveled and generally littered with glass and aluminum bottles. Initially, there were no obvious debris or floodline on the passage walls to indicate recent flooding events. Following Hurricane Helene, a tree trunk

fell and blocked the main entrance with boulders and rubble, so the cave stream could not be reached for post-Helene sampling.

KN24: Cruze Cave is within Knoxville city limits and closest to downtown, being in the South Knoxville Urban Wilderness, a neighborhood encased by green space and trails, and primarily low to medium intensity development. KN24 formed in the Holston Limestone of the Middle Ordovician Chickamauga Group. The passage follows the steep local dip of the rock. The cave entrance is situated between two private residences and a Knoxville Utility Board (KUB) property, and dozens more residences occur within half a kilometer of the entrance. A stream flows into the entrance and proceeds underground for about 300 meters until it ends in a sump. During intense rainfall events, the stream washes debris, such as clothing and shoes, bottles, and even lawn chairs, into the cave. Debris lines are up to 4 meters in height in some areas of the cave. Biofilms cover the walls of the cave passages, suggesting high nutrient loads from the cave stream. Several spring salamanders were observed during sampling. This cave has the first Tennessee cave snail record (Keenan et al., 2017), which was formerly described in 2021 as *Fontigens orolibas*, the Blue Ridge Springsnail (Gladstone et al., 2021).

KN62: Kirkpatrick Cave is in north Knoxville and located off a steep road embankment of Highway 33. KN62 formed in the Maryville Limestone of the Conasauga Group from the Middle Cambrian. A few houses surround the cave entrance property, but development in the area is minimal except for the large highway. A stream flows in a small sinkhole and into the cave entrance, then flows for about 30 meters in the cave before reaching several pools and eventually over flowstone before the stream sumps. During precipitation events, water quickly fills the entrance of the cave, funneling in from the sinkhole. Surface debris covered the walls of the cave and was about 3 meters high in some places, and the floor of the cave was covered with gravel from nearby road construction. Piles of animal scat, some at late stages of decomposition, were also present along the cave floor and on ledges. For the first sampling time in 2024, water levels were too low to sample flowing water. Following Hurricane Helene, the volume of water flowing through the cave was much higher, and flowing water was sampled in the flowstone passage area. No scat piles were observed along the stream passage during the second visit.

KN82: Thumping Cave is located on a farm in east Knoxville, just south of the Holston River. KN82 formed within the Middle Ordovician, Holston Limestone of the Chickamauga Group. A stream flows through a cow pasture and into the cave entrance. Cows were found sheltering inside the entrance during sampling, and fungi were found on cave floors and on woody debris inside the cave. KN82 is the largest cave of this study and has a stream passage that opens up from the entrance room into a large hall with a lake. The main passage is muddy and contains several pools, many of which had crawfish and salamanders. Older TCS narratives describe a warning associated with the lake, “Warning: Lake should not be traversed until checking with the East Knoxville Water Treatment Plant northeast of the entrance on the Holston River. Thousands of gallons of surplus water are frequently emptied into a sinkhole beside the plant. This water quickly finds its way into the cave causing the lake to back up and siphon completely across the passage (TCS, 1971).” Surplus water no longer empties into the sinkhole (personal communication with landowner), but the lake still floods when the Holston River levels are high. Following Hurricane Helene, water levels were still high during sampling and the lake sumped before the rest of the cave could be explored. Small fish were present in the cave, as were cow bones and vertebrae, after Helene.

KN103: Pedigo Cave is located in a hilly, forested north Knoxville neighborhood, with houses located along winding roads. KN82 formed in the Maynardville Limestone of the Conasauga Group from the Middle Cambrian. The cave entrance is near its spring resurgence, where the cave water is used for gardening and drinking water (personal communication with landowner). The cave entrance is small, 2 meters wide and less than a meter high, and the passage is barely tall enough to stand. Sculpin fish were seen in the upper stream passage. Pedigo Cave also has a population of snails morphologically similar but genetically distinct from a recently described cave-adapted snail, *Antrorbis tennesseensis*, the Tennessee Cavesnail (Gladstone et al., 2019).

KN145: Lost Puddle Cave is located below a ridge downslope of several densely packed residential properties in west Knoxville. The cave formed in Maynardville Limestone. Southwest of the entrance, a stream flows out of the cave from a narrow tube and feeds the creek running along the ridge. There is a brief crawl before reaching a perched ledge overlooking a 3-meter deep “puddle” that is 9-meter wide and continues for 30 meters into the cave. The cave contains Berry Cave salamanders (*Gyrinophilus palleucus gulineatus*), which are only known from a handful of east Tennessee caves (Neimiller et al., 2021). Additionally, this cave contains long-tailed salamanders (*Eurycea longicauda*) and cave salamanders (*Eurycea lucifuga*).

RN5: Cave Creek Cave is in Roane County, west of Knoxville. The outflowing stream, Cave Creek, flows into Watts Bar Lake on the Tennessee River. RN5 formed in the Mascot Dolomite of the uppermost Ordovician Knox Group. The cave stream follows the passage for about 134 meters. A layer of silt resides on the sediment on the bottom of the stream, which is easily disturbed, and a dark layer of clay distinct from the carbonate rock indicates the stream floods up to half a meter in height. Spring and cave salamanders, and sculpin fish, inhabit the stream. RN5 is the type locality for *A. tennesseensis* (Gladstone et al., 2019).

RN6: Eblen Cave is a large, locally well-known cave explored by recreational cavers. RN6 formed in Copper Ridger Dolomite and Maynardville Limestone. It is near RN5, but its cave stream flows into Mill Creek on the surface, which is a tributary of Caney Creek that joins the Clinch River. Beyond the impressive 5-meter-tall entrance of the cave at the top of a large 200-meter hill, the stream is at the lowest level of the cave and emerges below the entrance. The stream passage is small, about 1 to 2 meters high, and the stream bed consists of rocks and pebbles without overlying clay or silt, while the stream banks have accumulated deposits of clay. No noticeable debris was in the cave stream, and clay layers indicated that flooding levels did not surpass a half a meter height. Personal communication with the landowner suggested that the stream passage does not often flood due to its elevation. Sculpin and *E. lucifuga* reside in the stream passage, and paratypes of *A. tennesseensis* were also from RN6 (Gladstone et al., 2019).

3.2 Field Methods

Caves sampled in both 2019 (early June through early August) and 2024 before Hurricane Helene (early August through September) were done at base-flow stream conditions, following days of no rainfall. Sampling after Hurricane Helene was done after at least two days of no rainfall, but water levels had not reached base-flow in all of the caves sampled. Geochemical and microbiological sampling methods for 2019 and 2024 were the same. Stream temperature and pH were measured by using an Accumet AP110 meter with a double-junction electrode. Dissolved oxygen (DO) and specific conductance were measured with a YSI 2030 multiprobe. Nitrate was measured from the cave water directly by using a CHEMetrics (AquaPhoenix Scientific) cadmium reduction method test kit and field spectrophotometer (**Figure 3.2A**).

To obtain environmental DNA (eDNA) from the cave streams and sediments, duplicate Sterivex filters were collected at each cave during each visit. Up to 2 L of cave stream water

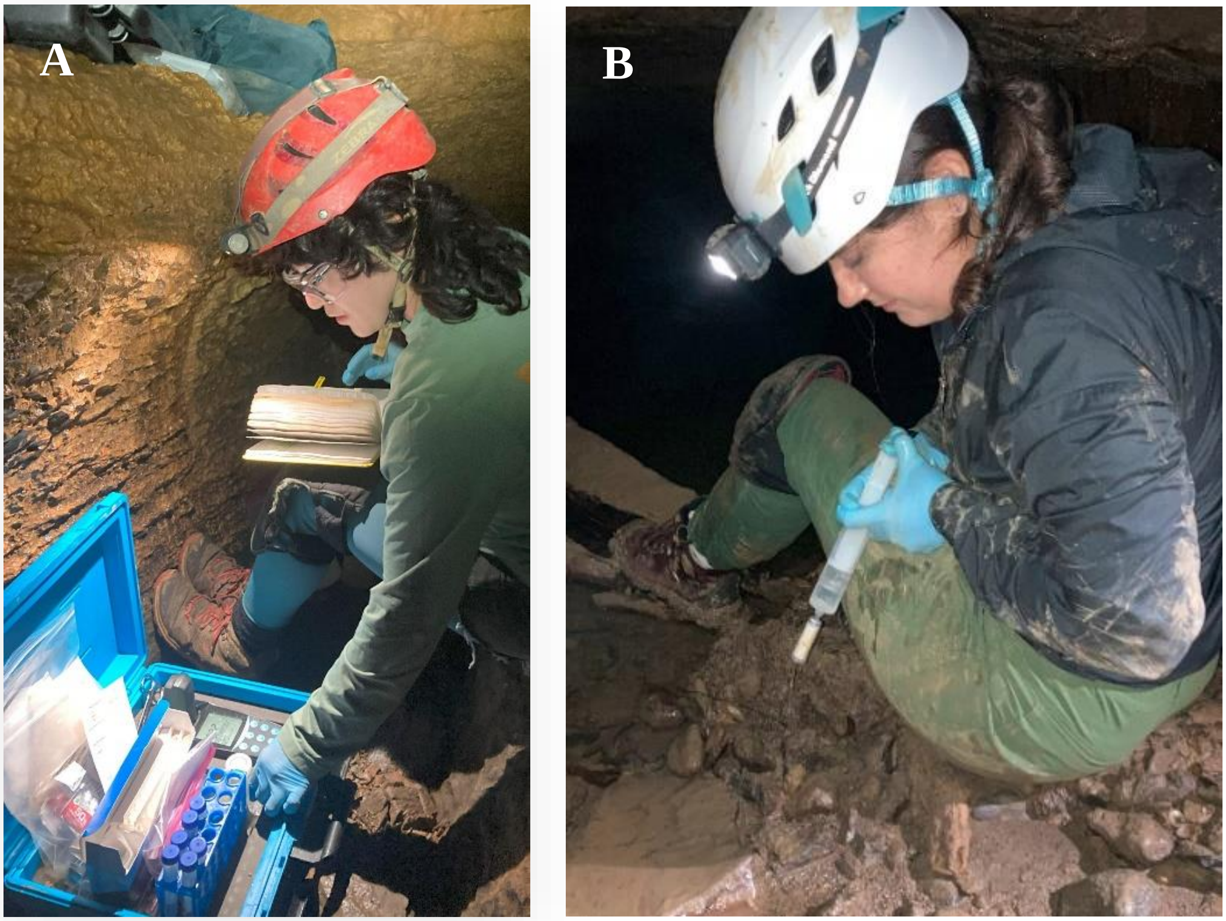

Figure 3.2. (A) Sampling dissolved nitrate inside one of the study caves by using a CHEMetrics field spectrophotometer and colorimetric kit, and (B) filtering water through a Sterivex filter to obtain an eDNA sample (right).

were filtered through 0.22 µm Sterivex (Millipore Sigma) PES filters (**Figure 3.2B**) into clean and prepared HDPE bottles for anions or ashed borosilicate glass containers for dissolved carbon analyses. HDPE bottles for cations were acid-washed in trace-metal grade nitric acid and then water was acidified with nitric acid after filtering into the bottle. Raw water was also collected in a sterile 50-mL Falcon tube. Filtered and raw water samples were transported on ice to the laboratory and stored at 4 ^{o}C until analysis. Filters were preserved with 1 mL 2% CTAB in the field, capped, and sealed, then placed in individual Whirl-Pak bags for transport on ice to the laboratory and storage at -20 ^{o}C until analysis.

At least 100 g of sediment was collected from cave streams where water samples were collected and placed into sterile Whirl-Pak bags. Sediment was transported on ice to the laboratory, then stored at -20 ^{o}C until analysis.

3.3 Land Use / Land Cover Analysis

ArcGIS Pro (Esri) was used to evaluate LULC and watershed characteristics for the caves in Knox and Roane counties for the five years prior to each sampling period. XY coordinates of the caves from the TCS database were uploaded as a .csv file using *Add XY Coordinates* onto a base map with the NLCD time series layer ranging from 2001–2024. LULC classification was based on the Anderson Land Cover classification system (Anderson et al., 1976) and included vegetation type, agricultural use, and a range of development intensity levels. NLCD imagery from 2014, 2019, and 2024 was trimmed into polygons for watershed boundaries and buffer areas around the caves. Watershed polygons were created using the *Extract by Mask* tool using the NLCD raster and Tennessee State data for U.S. Geological Survey Hydrologic Unit Code (HUC) 8 (i.e., subbasin) boundaries, which included the Watts Bar Lake, Holston River, and Clinch River watersheds (**Figure 3.3**). However, hydrologic connection from the caves and the surface may not follow these boundaries, while immediate land use could offer a more detailed view of relationships between LULC and water quality (Zampella et al., 2007). Each cave buffer was created with the *Extract by Mask* tool for the NLCD raster to be a 1-km radius from each cave entrance generated by the *Buffer* tool. The buffer represented a region where LULC or other surface processes may influence the cave environment. Processing was confined to one area at a time to retrieve individual buffers.

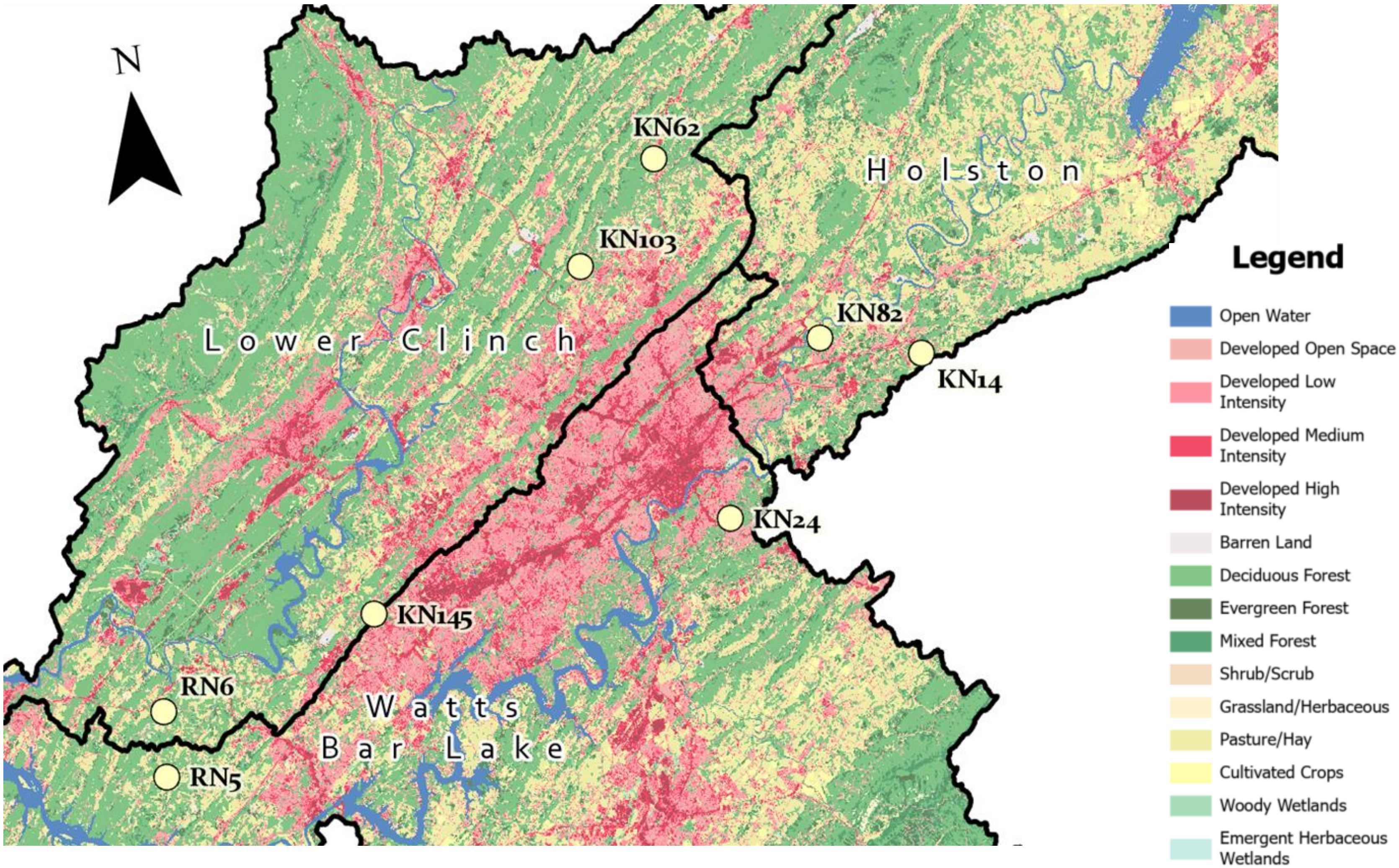

Figure 3.3. Map of the land use / land cover (LULC) in the study area. Cave locations are shown as yellow dots. LULC data are from the USGS National Landcover Database (NLCD) 2019 (https://www.usgs.gov/centers/eros/science/national-land-cover-database). The solid black lines separate the three sub-basin watersheds (HUC 8).

To calculate percentages of the LULC classification type of the polygons (i.e., for a watershed or cave buffer), the *Calculate Field* tool was used with pixel data in the attribute table with the following parameters,

$$LULC\ type\ (\%) = \frac{C_n}{C_{total}} \times 100$$

where C_n represents the pixel count of each LULC type in the polygon and C_{total} is the total number of pixel counts within the polygon. These data were exported to excel with the *Table to Excel* conversion tool.

The different NLCD categories were aggregated to reflect four major categories for further statistical analysis–water, forested, developed, agriculture. The water category was formed by aggregating cover amounts for open water, woody wetlands, and emergent herbaceous wetlands. The forested category was formed by aggregating deciduous forest, evergreen forest, mixed forest, and shrub/scrub cover. Developed was formed by aggregating barren land, developed open space, developed medium intensity, developed low intensity, and developed high intensity. Lastly, the agriculture category was formed by aggregating the cover amounts for grassland, pasture, and cultivated crops.

3.4 Geochemical Analyses of Water and Sediments

A suite of geochemical analyses was obtained for each cave water sample after each visit. Alkalinity, as bicarbonate concentration based on the pH of cave water, was determined by end-point titration to pH 4.5 with 0.1 N sulfuric acid on the day of collection. Anion concentrations were measured on a reagent-free system high-pressure Integrion ion chromatograph (IC) (ThermoFisher Scientific, Dionex). Major cations were measured on a Thermo Dionex ICS-2100 using a CS16 column with 26 mM methanesulfonic acid eluent (US EPA Method 9056A). Non-purgeable organic carbon (NPOC), total inorganic carbon (TIC), and total nitrogen (TN) were measured on a Shimadzu TOC-L with a TNML add-on (Shimadzu method No. SCA-130-101). Only two caves from 2019 were analyzed for TOC, NPOC, TIC, and TN (KN145 and KN103), compared to all caves for 2024.

From the cave sediment, exchangeable and weak-acid soluble trace metals were extracted with acetic acid using methods modified from Pueyo et al. (2008) and Rauret et al. (1999). Briefly, sediment samples were dried in an oven until they achieved constant mass, which was generally after about 16 hours. One gram of each sample was weighed in triplicate into separate 15 mL Falcon tubes and mixed with 40 mL of 0.11M acetic acid. The sediment-acetic acid solution was agitated at 30 rpm using a wrist-action shaker at room temperature for 16 hours (Rauret et al., 1999; Pueyo et al., 2008). The acid-extracted supernatant was filtered and diluted to 1:10 with 2% nitric acid. Final concentrations of trace metals from sediments were calculated by multiplying by 40, for the dilution with acetic acid, and by 10, for the dilution with nitric acid.

A suite of elemental concentrations was measured by inductively coupled plasma-optical emission spectroscopy (ICP-OES) from the cave water and extracted sediment samples using an iCAP 7400 (Thermo Scientific) and Qtegra software. Water samples were analyzed using a 2% nitric acid rinse and sediments were analyzed with an acid-matched rinse of 1:10 0.11 M acetic acid and 2% nitric acid. Analytical blanks were the rinse solutions. The OES wavelengths were selected based on EPA method 6010D unless otherwise stated in **Table 3.3** and **Table 3.4** (U.S. Environmental Protection Agency, 2018; Jianfeng and Timothy, 2021). The instrument limit of detection (LOD) was determined by the Qtegra software as,

$$LOD = \frac{3(\sigma_{blanks})}{a_1}$$

The method detection limit (MDL) based on the EPA method 6010D was calculated by using the concentrations from the method blank as,

$$MDL = Method\ blank + t_{(n-1,1-\propto=0.99)} * \sigma_{blanks}$$

where $t_{(n-1,1-\propto=0.99)}$ is the Student's *t*-test value for a single-tailed, 99% *t*-statistic with n-1 degrees of freedom (U.S. Environmental Protection Agency, 2016). The LOD and MDL values were rounded up to the nearest power of ten, and R^2 values for calibration curves, for each metal analyzed are reported on **Table 3.3** and **Table 3.4.**

Data were graphically analyzed for element ratios and against LULC data to compare strength of the relationship (R^2) and assess how variation in solute or trace metal concentrations could be explained by variation of the concentrations of conservation tracers, such as Cl or Ca.

3.5 Culture-Based Microbial Colony Counts

Estimations for culturable aerobic and coliform microbes, including *E. coli*, from the cave streams were determined using 3M Petrifilms (Neogen) (3M, 2017a, 2017b) (**Figure 3.4**). Within approximately 3–6 hours of initial sampling, 1 mL of raw, unfiltered cave water was dispensed onto separate sheets in triplicate per each medium. Following the manufacturer guidelines (Neogen, 2023), aerobic sheets were incubated at 35 °C for 48 hours and coliform

Table 3.3. Parameters used for ICP-OES analysis of water samples. Analytes, selected wavelengths, R^2 values from the calculated calibration curves, the Qtegra Limit of Detection (LOD), and the Method Detection Limit (MDL), following the U.S. EPA method 6010D unless otherwise stated. The metals Al, Cd, Cu, Fe, Mo, Ni, and Zn were below detection in all water samples analyzed. Units for wavelengths are nm, and LOD and MDL values are reported in mg/L.

Analyte	**Wavelength**	**R^2**	**LOD**	**MDL**
Al	394.4	0.9991	0.001	0.1
As	189.04	0.9999	0.001	0.01
Ba	233.52**	0.9997	0.01	0.01
Cd	214.43	0.9998	*	0.001
Cu	324.7	0.9994	0.000001	0.001
Fe	259.94	0.9998	0.001	0.1
Mg	280.27**	0.9991	0.01	0.1
Mn	257.61	0.9990	0.00001	0.001
Mo	203.84	0.9976	0.1	0.1
Ni	341.48	0.9997	0.001	0.01
P	177.49	0.9999	0.01	0.1
Pb	220.35**	0.9995	0.001	0.001
Si	251.61**	0.9998	0.001	0.1
Sr	421.55**	0.9996	0.000001	0.001
Zn	213.86	0.9972	0.001	0.01

*This sample did not produce positive blank values due to spectral interference
**Wavelengths were selected according to Zarcinas (2002) and Yang et al. (2020).

Table 3.4. Parameters used for ICP-OES analysis of sediment extractions. Analytes, selected wavelengths, R^2 values from the calculated calibration curves, the Qtegra software Limit of Detection (LOD), and the Method Detection Limit (MDL), following the U.S. EPA method 6010D, unless otherwise stated. Analytes As, Mo, Ni, and Pb were below detection in all sediment extraction samples analyzed. Units for wavelengths are nm, and LODs and MDLs are mg/L.

Analyte	**Wavelength**	**R^2**	**Instrument LOD**	**MDL**
Al	394.4**	0.9880	0.1	10
As	189.04	0.9987	*	10
Ba	455.4	0.9991	0.001	1
Ca	315.88	0.9989	10	100
Cd	226.5	0.9986	0.1	0.1
Cu	224.7	0.9989	1	1
Fe	259.94	0.9989	1	10
Mg	279.07	0.9947	0.1	10
Mn	259.37**	0.9992	1	1
Mo	202.03	0.9995	*	1
Na	589.59	0.9943	0.001	10
Ni	231.6	0.9988	1	1
P	177.49**	0.9904	10	10
Pb	220.35	0.9988	*	1
Si	251.61	0.9978	1	100
Sr	421.55	0.9993	0.0001	0.1
Zn	213.85	0.9978	1	10

*These samples did not produce positive blank values due to spectral interference
**Wavelengths were selected according to (Cordeiro et al., 2018)

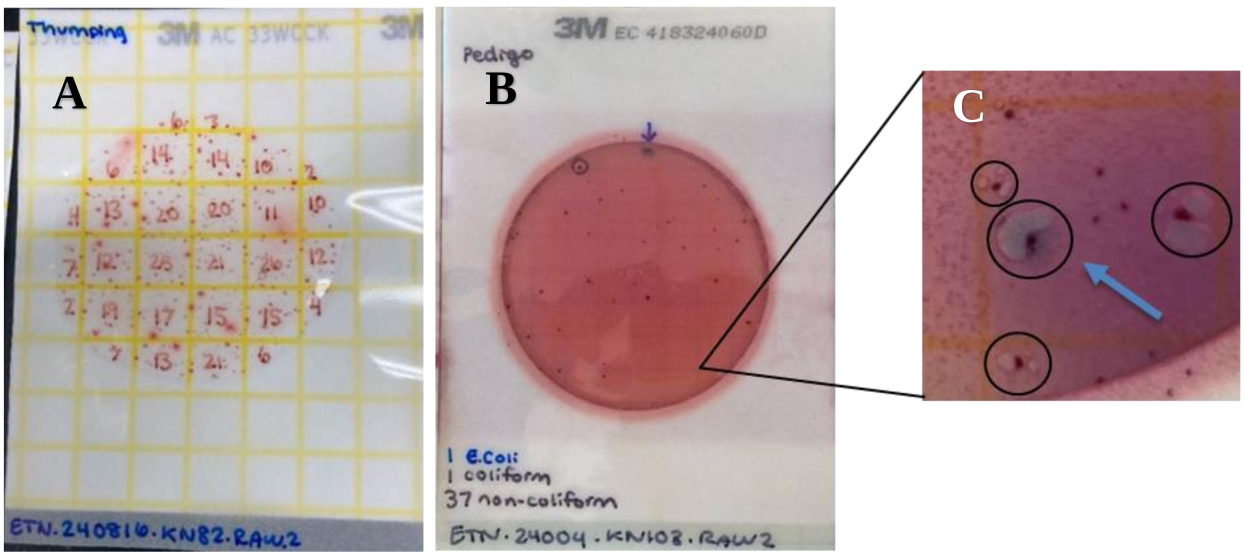

Figure 3.4. (A) A gridded aerobic Petrifilm sheet with CFUs per 1 cm^2. (B) Coliform/*E. coli* Petrifilm sheet, with the circles indicating coliform bacteria and blue arrow indicating *E. coli*. (C) Close-up of a coliform & *E. coli* Petrifilm sheet, with arrows indicating *E. coli* (in blue) and circles surrounding coliform bacteria (with bubbles). All of the rest of the colonies on the sheet were interpreted as non-coliform cells.

sheets were incubated at 30 °C for 24 hours. Enumeration was assisted by a 1 cm x 1 cm grid over the sheet (**Figure 3.4A**). If a sheet had more than 10 colony forming units (CFU)/cm^2, then each square was counted, and the total was noted. For sheets that had too many CFUs to count, two squares within the grid were counted and the average was multiplied by 20 for the entire area of the sheet. For aerobic microbes, all colonies were counted in the same manner, regardless of color or morphological differences. For coliform and *E. coli*, only blue colonies were interpreted as *E. coli* and coliform microbes were counted if there were small air bubbles surrounding a colony (**Figure 3.4B, C**). Non-coliform microbes were identified as colonies without air bubbles. The average CFU values, with standard deviation, were reported.

3.6 DNA Extractions from Water and Sediment

Total eDNA was extracted from Sterivex filters using the Qiagen DNeasy DNA Isolation Kit with manufacturer supplied buffers with modifications from Spens et al. (2016) to optimize for water samples having low biomass. Briefly, proteinase K and the ATL Buffer were added directly to the filter unit, followed by an incubation at 56°C for 24 hours. Recoverable lysate was transferred into a conical tube containing cold molecular grade ethanol and incubated at -20 °C for 4 to 6 hours to promote DNA precipitation. Manufacturer steps were followed to remove cell debris using centrifugation, pellet washing, then pellet air-drying prior to eluting DNA pellets in AE Buffer. Yield was checked on a Nanodrop spectrophotometer. The extracted DNA was stored at -80 °C until use.

Total eDNA was extracted from cave stream sediments using a protocol adapted from Guerry (1973), Somerville et al. (1989), Zhou (1996), and Mitchell and Takacs-Vesbach (2008). Briefly, in duplicate, 2 grams of each sample were mixed with sucrose lysis buffer prepared with lysozyme (1 mg/mL) prior to incubation at 37 °C for an hour. The solution was mixed with a freshly made Proteinase K/CTAB/SDS solution then incubated at 55 °C for 16 hours. Particulate material, cell debris, and humics were removed by centrifugation and the addition of 10 M ammonium acetate for protein precipitation. Nucleic acid precipitation was done in triplicate for each extraction with isopropanol at -20 °C for 24 hours, followed by washing with molecular grade ethanol and drying for 2 hours prior to resuspension in TE buffer. Aliquots of each extraction were cleaned with the Qiagen DNeasy cleaning kit, following manufacturer instructions, then homogenized to generate a single sediment DNA extraction. All extracted DNA was checked for yield on a Nanodrop spectrophotometer, then stored at -80 °C until use.

3.7 16S rRNA Gene Sequencing and Analysis

DNA extractions were sent to the University of Tennessee, Knoxville, CORE Genomics Laboratory for sequencing of the V4–V5 region of the 16S rRNA gene. After PCR amplification using the 515F and 806R primers (Apprill et al., 2015; Parada et al., 2016), extractions were pair-end sequenced using the Illumina NextSeq platform to produce 2x300 base pair reads. The resulting gene sequences were processed using a modified version of the MOTHUR v.1.47.0 pipeline for Illumina MiSeq platform reads (Schloss et al., 2009; Schloss, 2020). Reads were aligned and combined based on a quality score cutoff of 30 with the *make.contigs* command, then screened to exclude sequences with fewer than 288 or greater than 296 base pairs, before alignment to the SILVA 138.2 reference database and making taxonomic assignments (Quast et al., 2012). Sequences with poor alignment were removed and screened for length again. Chimeric sequences were identified and removed using the *vsearch* command. Reads assigned to the taxonomic lineages of Eukarya, mitochondria, chloroplasts, or unidentified sequences were removed. Samples which did not amplify well (noted as "failed" by sequencing lab) were not included in downstream analysis to avoid problems due to variable sequence lengths.

3.8 Statistical Analysis

Environmental, LULC, geochemical, and relative abundances of microbial taxa were analyzed statistically in PAST v. 5.2.1 (Hammer et al., 2001). Data were transformed by adding a constant value of 1, then transforming with a base ten logarithmic transformation, and dividing all data points by the maximum value in the dataset to create a scale of 0 to 1. Strengths and significance of relationships between environmental, LULC, and microbial variables were determined by R^2 values calculated in Excel, and by Spearman's significance (ρ and p-value) or Pearson's correlation (i.e., product-moment correlation) and correlation coefficient (r) and p-value. Alpha was set at 0.05 for all tests. Analysis of variance (ANOVA) was performed using LULC, sampling time (2019, 2024, 2024-post), and watershed (Clinch, Holston, Watts Bar) as independent variables, and culture-based CFUs and environmental and geochemical parameters as dependent variables. Canonical correspondence analysis (CCA) of relative abundances for cave stream taxa, LULC, and selected environmental parameters was done to evaluate variables and potential drivers controlling the presence of major taxa.

CHAPTER FOUR: RESULTS AND DISCUSSION

4.1 Land Use / Land Change at the Local and Watershed Scales

Although the caves in this study were all within the KMSA, the 1-km buffer zone around each cave entrance revealed a range of LULC categories that could influence the cave environment (**Figure 4.1**). Overall, buffer zones around the caves experienced declines in grassland, shrub, and forested cover, and increases in barren land, and mid- and high intensity development (MID, HID) over the decade of analysis. Specifically, five years prior to the first sampling events in 2019, deciduous forests (45.40%) were the dominant vegetation surrounding all of the caves, followed by pastureland (22.13%) and mixed forests (7.88%). All development around the caves comprised an average of 20.36%, with most of the development being DOS (13.51%) or low intensity development (LID) (4.90%). In 2019, KN145 had the greatest HID cover within its buffer zone, with developed open space (DOS) and all other development categories adding up to 34.64% (**Table 4.1**). KN82, RN5, and RN6 had the highest agricultural LULC, comprising an average of 36.62% for the three buffer zones. As such, from 2014 to 2019 (**Table 4.2**), there was an increase by an average of 1.12% in all development categories for all cave buffers zones. Total vegetation and agricultural LULC decreased by an average of 0.55% and 0.52%, respectively, for all buffers. Over the next five years, from 2019 to 2024 (**Table 4.3**), LULC changes were smaller (Table 4.4), but generally showed a loss of forest cover and gain of open land and grassland. By 2024, the LULC classifications with the greatest gains were LID (0.50 %) and HID (0.40 %), and classifications with the greatest losses were grasslands (-0.61 %) and pastures (-0.53 %) (**Table 4.4**).

LULC changes for the caves were also assessed at the sub-basin watershed scale (HUC 12) for Watts Bar of the Tennessee River (drainage area = 2,042 km), the Holston River (drainage area = 6,030 km), and Lower Clinch River (drainage area = 1,015 km) (Tennessee Department of Environmental Conservation, 2007) **(Figure 4.2**). In 2019, the KN14 sub-watershed had the highest amount of pasture (36.57%) and the KN24 watershed had the highest percentage of total developed cover (58.79%). Despite the KN145 buffer zone having the highest development cover in 2019, the dominant cover at the sub-watershed scale was forest. The KN62 sub-watershed also had the most forested cover in 2019 (61.85%). In general, from 2019 to 2024, most sub-watersheds experienced a decline in the amount of shrub and pastureland or agricultural coverage and an increase in barren land, MID, and HID cover (**Table 4.5**).

Table 4.1. Percentage of LULC categories in the NLCD for each 1-km cave buffer zone in 2019. Categories not included in the table had <0.1% coverage (e.g., woody wetlands, emergent herbaceous wetlands, cultivated crops, shrub/scrub).

TCS ID	Open Water	Baren Land	Developed Open Space	Developed Low Intensity	Developed Medium Intensity	Developed High Intensity	Deciduous Forest	Evergreen Forest	Mixed Forest	Grassland	Pasture
KN14	0	0	23.83	4.78	0.79	0.08	44.9	1.82	7.63	0.63	14.43
KN24	0	0	28.7	5.75	2.17	0.16	47.22	0.91	11.35	0.32	3.43
KN62	0.16	0.35	6.81	6.65	3.92	0.79	58.49	1.42	7.72	3.24	8.94
KN82	4.54	0	6.6	3.71	2.13	0.43	34.1	0.99	4.5	1.5	39.71
KN103	0.04	0	18.33	5.37	1.62	0.16	53.08	0.87	7.9	0.43	12.05
KN145	0.2	0.23	13.6	13.88	4.56	2.16	30.15	0.75	6.92	1.89	24.06
RN5	0	0	6.02	2.12	0.39	0.08	41.76	1.61	9.08	0.04	38.46
RN6	0	0	4.73	0.91	0.16	0	52.64	0.28	8.55	0.12	31.68

Table 4.2. Percentage of LULC changes from 2014 to 2019 at the 1-km buffer scale for each cave. Categories not included in the table had <0.1% coverage (e.g., woody wetlands, emergent herbaceous wetlands, cultivated crops, and shrub/scrub). Pink-shaded cells note higher percentages from 2014 to 2019; blue-shaded cells note lower percentages from 2014 to 2019.

TCS ID	Open Water	baren	Developed Open Space	Developed Low Intensity	Developed Medium Intensity	Developed High Intensity	Deciduous Forest	Evergreen Forest	Mixed Forest	Grassland	Pasture
KN14	0.00	0.00	-0.24	0.00	0.24	0.00	0.32	0.00	0.16	-0.24	0.04
KN24	0.00	0.00	0.00	0.20	0.59	0.00	0.43	0.00	0.04	0.00	-0.59
KN62	0.09	0.15	-0.08	0.47	0.67	0.08	0.00	-0.08	-0.24	-0.71	-0.28
KN82	0.00	0.00	-0.24	-0.04	0.20	0.08	-0.51	0.00	0.00	-1.58	0.40
KN103	0.07	0.00	0.87	0.59	0.28	0.00	-0.20	-0.04	0.04	0.43	-1.78
KN145	0.15	0.86	0.04	2.67	0.79	0.86	-1.97	-0.20	0.00	-2.20	-1.02
RN5	0.00	0.00	0.16	0.08	0.16	0.00	0.16	-0.20	0.59	0.00	-0.90
RN6	0.00	0.00	-0.04	0.00	0.04	0.00	0.75	0.00	0.00	-0.63	-0.08

Table 4.3. Percentage of LULC categories from the NLCD for each 1-km cave buffer zone in 2024. Categories not included in the table had <0.1% coverage (e.g., woody wetlands, emergent herbaceous wetlands, cultivated crops, and shrub/scrub).

TCS ID	Open Water	Barren Land	Developed Open Space	Developed Low Intensity	Developed Medium Intensity	Developed High Intensity	Deciduous Forest	Evergreen Forest	Mixed Forest	Grassland	Pasture
KN14	0	0	23.83	4.78	0.79	0.08	44.31	1.58	7.27	1.82	14.43
KN24	0	0	28.66	5.79	2.17	0.16	47.22	0.91	11.35	0.32	3.43
KN62	0.16	0.36	6.81	6.65	3.92	0.79	58.49	1.42	7.72	3.24	8.94
KN82	4.55	0	6.60	3.72	2.13	0.43	34.11	0.99	4.51	1.50	39.60
KN103	0	0	18.33	5.37	1.62	0.16	53.08	0.91	7.90	0.43	12.05
KN145	0.20	0.24	13.52	13.92	4.60	2.16	30.15	0.75	6.92	1.89	24.06
RN5	0	0	6.02	2.12	0.39	0.08	40.23	1.61	9.04	1.61	38.46
RN6	0	0	4.73	0.91	0.16	0.00	52.64	0.28	8.55	0.12	31.68

Table 4.4. Percentage of LULC changes from 2019 to 2024 at the 1-km buffer scale for each cave. Categories not included in the table had <0.1% coverage (e.g., woody wetlands, emergent herbaceous wetlands, cultivated crops, shrub/scrub, and barren land). Pink-shaded cells note higher percentages from 2019 to 2024; blue-shaded cells note lower percentages from 2019 to 2024.

TCS ID	Open Water	Barren Land	Developed Open Space	Developed Low Intensity	Developed Medium Intensity	Developed High Intensity	Deciduous Forest	Evergreen Forest	Mixed Forest	Grassland	Pasture
KN14	0.00	0.00	0.00	0.00	0.00	0.00	-0.59	-0.24	-0.36	1.19	0.00
KN24	0.00	0.00	-0.04	0.00	0.00	0.00	0.00	0.00	0.00	0.00	0.00
KN62	0.00	0.01	-0.03	0.01	-0.02	0.00	-0.23	-0.01	-0.03	-0.01	-0.04
KN82	0.00	0.00	0.00	0.00	0.00	0.00	0.01	0.00	0.00	0.00	-0.10
KN103	0.00	0.00	0.00	0.00	0.00	0.00	0.00	0.04	0.00	0.00	0.00
KN145	0.00	0.01	-0.08	0.01	0.04	0.00	0.00	0.00	0.00	0.00	0.00
RN5	0.00	0.00	0.00	0.00	0.00	0.00	-1.53	0.00	-0.04	1.57	0.00
RN6	0.00	0.00	0.00	0.00	0.00	0.00	0.00	0.00	0.00	0.00	0.00

Table 4.5. Percentage of LULC changes from 2019 to 2024 at the HUC 12 sub-watershed scale. Categories not included in the table had <0.1% coverage (e.g., woody wetlands, emergent herbaceous wetlands, cultivated crops, shrub/scrub, and barren land). Pink-shaded cells note higher percentages from 2019 to 2024; blue-shaded cells note lower percentages from 2019 to 2024.

TCS ID	Open Water	Barren Land	Developed Open Space	Developed Low Intensity	Developed Medium Intensity	Developed High Intensity	Deciduous Forest	Evergreen Forest	Mixed Forest	Grassland	Pasture
KN14	0.00	0.05	-0.01	0.00	0.01	0.00	-0.07	-0.06	-0.01	0.11	-0.04
KN24	-0.01	0.03	-0.09	0.05	0.12	0.02	-0.10	0.01	-0.06	0.07	-0.05
KN62	0.01	0.00	0.00	0.00	0.00	0.00	0.09	-0.05	-0.05	0.22	-0.01
KN82	-0.01	0.08	-0.03	-0.02	0.03	0.09	-0.11	-0.07	-0.02	0.20	-0.14
KN103	-0.01	0.02	0.00	0.01	0.01	0.00	-0.17	0.03	-0.03	-0.05	-0.02
KN145	-0.02	0.06	0.00	0.02	0.05	0.02	-0.40	0.02	-0.06	0.24	-0.09
RN5	-0.02	0.02	0.00	0.00	0.01	0.00	-0.31	0.15	0.02	0.17	-0.03
RN6	-0.02	0.04	0.00	0.00	0.01	0.00	-0.21	-0.03	-0.01	0.32	-0.02

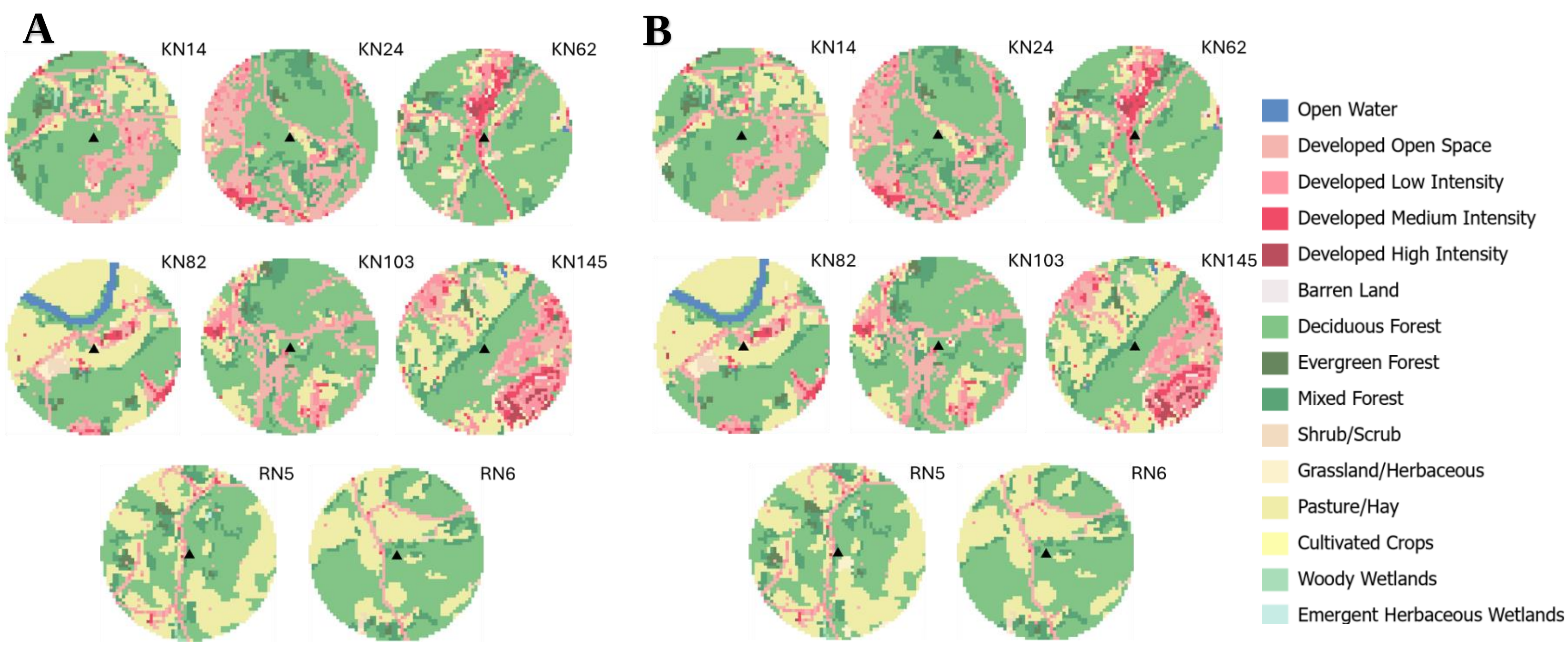

Figure 4.1. Cave 1-km buffer zones for 2019 (A) and 2024 (B), classified according to the NLCD. Cave entrances are shown as black triangles.

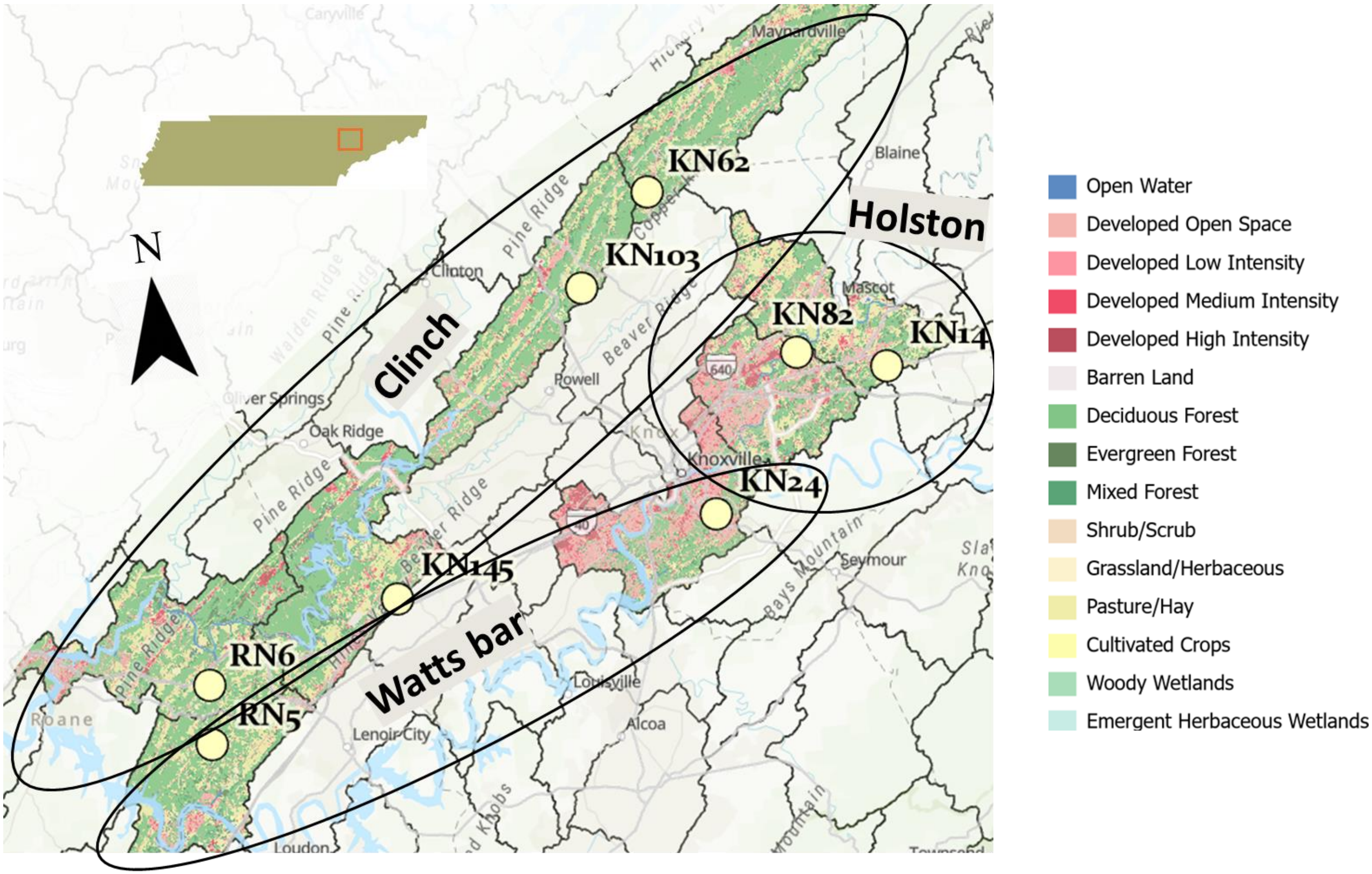

Figure 4.2. Map of the LULC of eight HUC 12 sub-watersheds, classified according to the NLCD. HUC 12 boundaries are outlined and HUC 8 watersheds are circled in black. Cave locations are shown as yellow dots, and there is one per sub-watershed. LULC data are from the USGS National Landcover Database (NLCD) 2019 (https://www.usgs.gov/centers/eros/science/national-land-cover-database).

Moreover, all sub-watersheds except for KN62 also experienced forest losses and gains in grassland or barren land cover, which could signify the next LULC change would be a development category. Development also expanded in the KN24 and KN145 sub-watersheds over the 5-year period.

4.2 Environmental Conditions and Geochemistry

4.2.1 Physicochemical Measurements

All caves were assessed for environmental conditions like temperature, pH, DO concentrations, and specific conductance in the field (**Table 4.6**). Water samples were collected from June through August in 2019 compared to August and September for 2024, and cave water temperatures in 2024 were slightly elevated compared to 2019, except for RN5. Lower water temperatures generally correlated with lower dissolved oxygen concentrations. Cave water pH ranged from 6.61 to 7.58, and pH was generally higher from inflowing cave streams compared to outflowing cave streams (**Table 4.6**). For all caves, pH was lower in 2019 (average = 6.88) compared to 2024 for every cave except KN62 (**Figure 4.3**), which also had the highest specific conductance (452.33 µS/cm) (**Table 4.6**). Similarly, specific conductance was generally higher from inflowing cave streams (average = 333.83 µs/cm, n = 3) compared to outflowing cave streams (average = 259.96 µS/cm, n = 3) but was not significantly different among different cave LULC conditions. Alkalinity was generally higher in 2024 than 2019 (p-value = 0.002), except for KN103 and KN145 (**Tables 4.7**). TN was highest from KN24 post-Helene (**Table 4.7**). The maximum recommended concentration of TN in freshwater should be <0.59 mg/L (Dein et al., 2019), and all caves and sampling periods, besides KN82 post-Helene, surpassed this limit.

4.2.2 Major Ion Chemistry

Major ion chemistry is shown in **Table 4.8**. Dissolved anion concentrations increased following Hurricane Helene, with few exceptions. Chloride concentrations were highest in KN62 in 2019 and 2024, and post-Helene concentrations were double the 2019 levels. Chloride concentrations in KN82 post-Helene were also double 2019 and 2024 sampling events. Sulfate concentrations were highest in KN82 before Helene and decreased post-Helene. Nitrate concentrations (**Table 4.7**) were highest from KN24 compared to the other locations, but most notably in 2019 (**Figure 4.4**). The lowest measured nitrate concentration from KN24 was still higher than all other water samples and surpassed the EPA's maximum contaminant level (MCL) of 10 mg/L in 2019 and 2024 post-Helene (U.S. Environmental Protection Agency, 2024).

Table 4.6. Field-collected physiochemical data, including pH, temperature in °C, dissolved oxygen (DO) in mg/L, and specific conductance (Cond) in µS/cm. The full sample ID represents the location (East Tennessee, ETN), date (year, month, day), and TCS ID.

Sample ID	**Cave name**	**pH**	**Temp**	**DO**	**Cond**
ETN.190711.KN14	Carter	6.73	14.9	8.01	340.5
ETN.240816.KN14	Carter	7.19	14.9	9.02	276.7
ETN.190627.KN24	Cruze	6.79	12.3	5.36	281.8
ETN.230813.KN24	Cruze	7.29	13.6	3.19	273.3
ETN.240930.KN24	Cruze	7.57	14.5	3.41	337.2
ETN.190709.KN62	Kirkpatrick	7.48	13.3	6.39	452.6
ETN.241004.KN62	Kirkpatrick	6.93	14.5	7.86	374.9
ETN.190625.KN82	Thumping	7.50	20.4	8.29	381.2
ETN.240816.KN82	Thumping	7.62	17.0	5.81	346.2
ETN.241005.KN82	Thumping	7.74	22.3	5.38	223.4
ETN.190803.KN103	Pedigo	6.65	14.2	8.41	334.3
ETN.240908.KN103	Pedigo	7.19	14.2	8.14	285.7
ETN.241004.KN103	Pedigo	6.97	14.3	7.80	282.4
ETN.190808.KN145	Lost Puddle	6.61	14.6	5.35	343.6
ETN.240915.KN145	Lost Puddle	6.79	14.7	8.60	141.3
ETN.241002.KN145	Lost Puddle	6.91	14.8	8.13	185.3
ETN.190728.RN5	Cave Creek	6.58	14.5	8.83	249.4
ETN.240911.RN5	Cave Creek	6.87	14.5	8.54	220.0
ETN.241006.RN5	Cave Creek	6.80	14.5	8.43	253.5
ETN.190728.RN6	Eblen	6.68	15.1	8.79	212.4
ETN.240918.RN6	Eblen	7.58	14.9	8.29	276.1
ETN.241006.RN6	Eblen	7.19	15.0	8.48	238.3

Table 4.7. Geochemical summary for alkalinity reported as mmol, and total inorganic carbon (TIC), non-purgeable organic carbon (NPOC), total nitrogen (TN), and nitrate reported in mg/L from both the ion chromatography (IC) measurements and CHEMetrics methods. NM = not measured. BDL = below detection limit. Detection limits for nitrate measured by IC were 1.0 mg/L.

Sample ID	**Alkalinity**	**TIC**	**NPOC**	**TN**	**Nitrate IC**	**Nitrate CHEMetrics**
ETN.190711.KN14	1.05	**68.24	NM	NM	5.6	NM
ETN.240816.KN14	3.62	55.38	0.37	1.55	4.5	0.3
ETN.190627.KN24	0.77	**48.75	NM	NM	21.7	NM
ETN.240813.KN24	4.79	47.05	1.14	2.74	7.5	0.9
ETN.240930.KN24	3.54	47.41	1.61	4.21	11.5	1.0
ETN.190709.KN62	1.35	**64.50	NM	NM	3.7	NM
ETN.241004.KN62	3.61	51.42	29.68	1.64	BDL	0.4
ETN.190625.KN82	1.13	**68.07	NM	NM	1.2	NM
ETN.240816.KN82	3.74	55.02	1.96	3.42	BDL	0.6
ETN.241005.KN82	1.49	**58.46	4.18	0.54	BDL	0.4
ETN.190803.KN103	*4.14	49.53	0.77	1.06	5.6	NM
ETN.240908.KN103	3.94	60.55	1.77	1.32	BDL	0.2
ETN.241004.KN103	4.55	56.58	0.86	1.62	4.6	0.2
ETN.190808.KN145	*4.13	49.62	1.28	0.96	5.0	NM
ETN.240915.KN145	4.54	59.76	0.52	1.22	BDL	0.2
ETN.241002.KN145	3.84	49.72	0.27	1.28	4.2	0.6
ETN.190728.RN5	0.78	**57.73	NM	NM	5.6	NM
ETN.240911.RN5	3.99	53.21	0.27	1.18	3.3	0.2
ETN.241006.RN5	5.32	55.84	0.99	1.34	3.7	0.3
ETN.190728.RN6	0.67	**45.28	NM	NM	3.7	NM
ETN.240918.RN6	3.64	52.50	0.71	0.65	1.7	0.1
ETN.241006.RN6	3.05	**155.34	0.90	0.70	1.8	0.1

*Alkalinity concentrations were calculated from TIC.
**TIC were calculated from alkalinity.

Table 4.8. Major ion concentrations measured from cave stream water. Concentrations are in mg/L. NM = not measured.

Sample ID	Cl^-	SO_4^{2-}	PO_4^{3-}	Na^+	Ca^{2+}	Mg^{2+}	K^+	NH_4^+
ETN.190711.KN14	4.61	2.88	BDL	2.07	50.50	20.90	1.56	0.02
ETN.240816.KN14	3.90	4.90	BDL	2.09	49.90	21.26	1.52	0.01
ETN.190627.KN24	6.74	1.92	0.38	3.68	58.52	4.13	0.39	0.04
ETN.240813.KN24	4.10	8.40	0.33	3.44	73.41	3.83	1.93	0.03
ETN.240930.KN24	4.70	10.80	0.37	3.96	71.00	4.15	2.45	0.03
ETN.190709.KN62	14.18	17.29	BDL	14.02	95.79	8.02	2.35	0.02
ETN.241004.KN62	34.00	10.00	BDL	28.61	103.1	9.32	2.40	0.02
ETN.190625.KN82	4.61	7.68	BDL	4.37	70.94	5.10	1.17	0.07
ETN.240816.KN82	5.10	25.30	BDL	6.40	89.14	4.91	1.82	0.06
ETN.241005.KN82	12.10	16.10	BDL	11.11	30.97	8.34	1.90	0.11
ETN.190803.KN103	3.55	4.80	BDL	2.30	45.69	24.55	1.17	0.03
ETN.240908.KN103	3.30	4.10	BDL	2.12	47.94	26.77	1.31	0.02
ETN.241004.KN103	4.60	4.70	BDL	3.56	52.94	28.64	1.61	0.14
ETN.190808.KN145	3.90	7.68	BDL	2.53	45.69	25.52	1.17	0.04
ETN.240915.KN145	4.40	8.50	BDL	2.65	48.42	26.82	1.26	0.03
ETN.241002.KN145	5.90	7.20	BDL	3.61	48.59	26.87	1.39	0.07
ETN.190728.RN5	2.48	1.92	BDL	1.15	32.87	17.50	1.17	0.07
ETN.240911.RN5	2.00	1.30	BDL	1.09	43.87	23.61	1.03	0.02
ETN.241006.RN5	2.40	1.40	BDL	1.04	42.30	22.69	1.05	0.03
ETN.190728.RN6	2.13	1.92	BDL	0.92	27.66	15.31	0.78	0.23
ETN.240918.RN6	1.90	2.80	BDL	0.93	39.24	22.25	0.91	0.04
ETN.241006.RN6	2.00	2.90	BDL	0.96	38.67	22.01	0.92	0.11

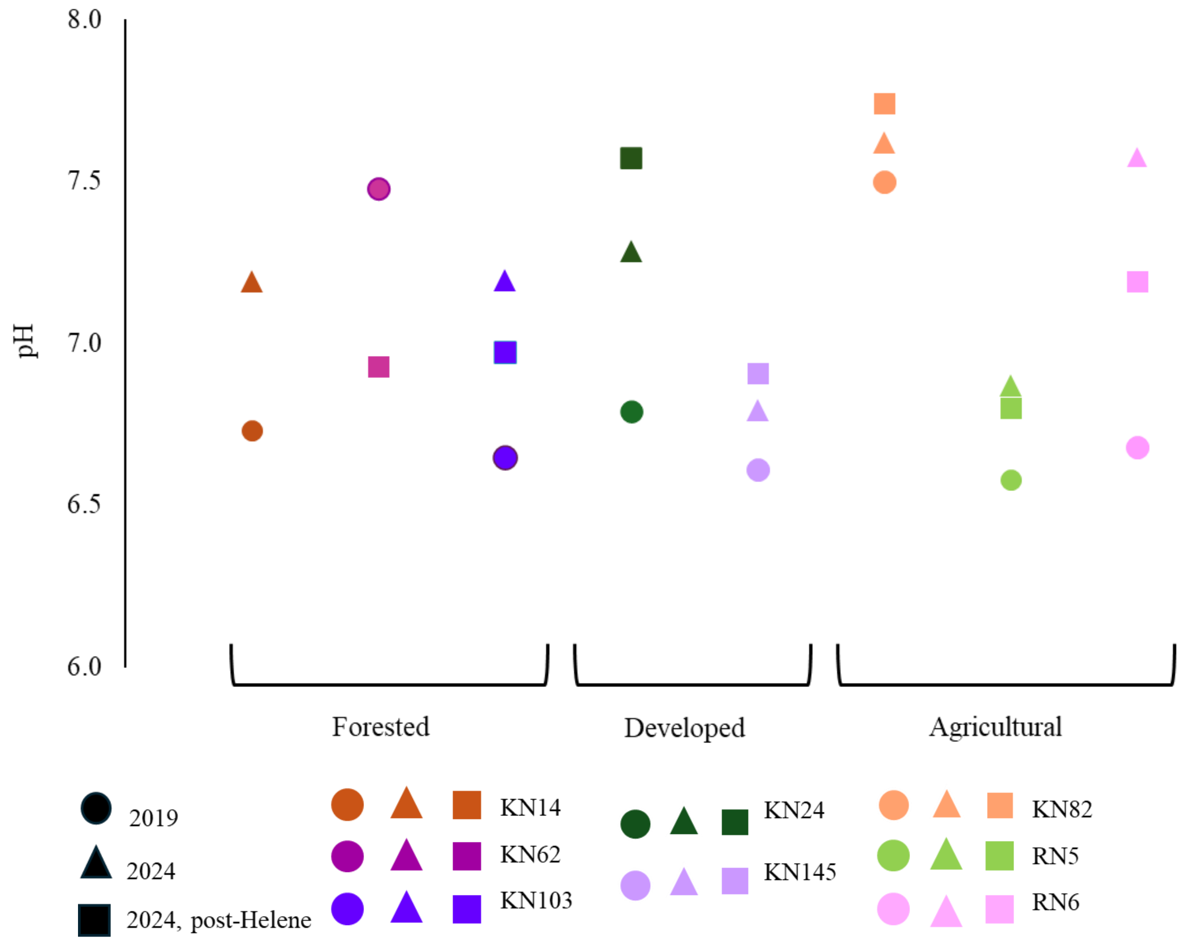

Figure 4.3. pH measured from the cave streams. Caves are listed by their TCS IDs, with shapes (circle, triangle, square) corresponding to the sampling period (2019, 2024, 2024 post-Helene, respectively) and color coded according to watershed (greens for Watts Bar of the Tennessee River, oranges for Holston River, and purples for Lower Clinch River). Caves are also grouped by the dominant LULC classification.

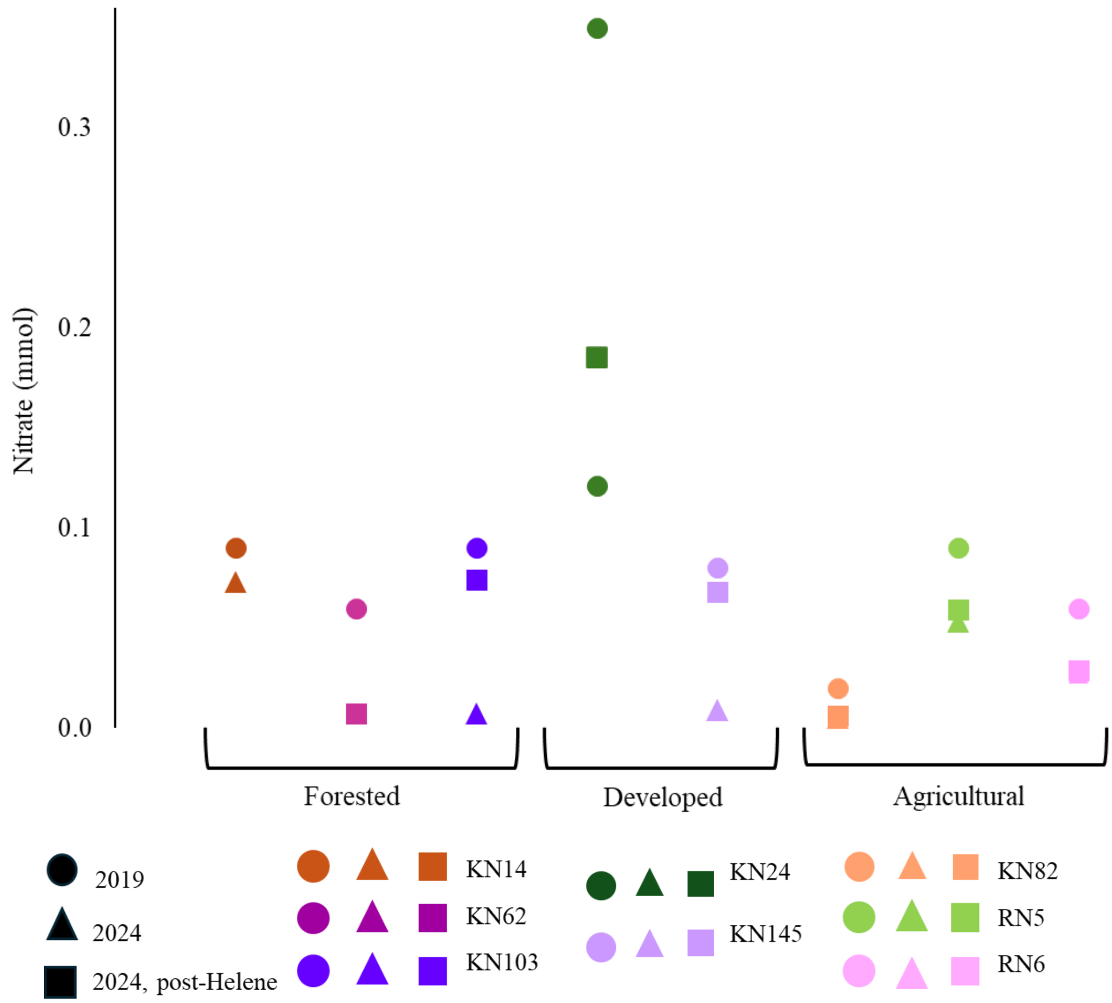

Figure 4.4. Nitrate measured from the cave streams. Caves are listed by their TCS IDs, with shapes (circle, triangle, square) corresponding to the sampling period (2019, 2024, 2024 post-Helene, respectively) and color coded according to watershed (greens for Watts Bar of the Tennessee River, oranges for Holston River, and purples for Lower Clinch River). Caves are also grouped by the dominant LULC classification.

Although KN82 had elevated TN concentrations (**Table 4.7**), the cave did not have elevated nitrate concentrations (**Figure 4.4**) but instead high ammonium concentrations (**Table 4.8**), likely due to decomposing organic matter washed in by the cave stream. Ammonium concentrations mostly decreased from 2019 to 2024, except for RN6, and concentrations increased after Hurricane Helene, most notably in KN103 (**Table 4.8**).

Analysis of variance (ANOVA) showed that there were significant differences in DO, nitrate, and phosphate concentrations among the caves having different LULC coverage classifications (i.e., forested, developed, agriculture) (**Table 4.9**). Spearman's rank correlation analyses also showed there were moderately to strongly significant relationships (i.e., $\rho > 0.5$) among the percentage of agricultural cover and temperature, DO, and nitrate concentrations, and weaker but significant relationships between the percentage of development cover and phosphate concentrations (**Table 4.9**), supporting previous research that suggests LULC influences stream temperature, DO, and nutrient conditions. Moreover, the concentrations of phosphate, chloride, sodium, and other nutrients in the cave streams moderately correlated to the aerobic CFUs, but DO negatively correlated to many of the anion and cation concentrations (**Table 4.10**).

Major cation concentrations did not change appreciably from 2019 and 2024 and from before and after Hurricane Helene, with a few exceptions that could be attributed to hydrology and bedrock (**Table 4.8**). Sodium concentrations from KN62 in 2019 and 2024 were higher than in the other caves, with the next highest concentrations being from KN82 post-Helene. Calcium concentrations were also high from KN62, as well as from KN24 and KN82, which both had inflowing cave streams. Caves formed in the Maynardville Limestone (e.g., KN103, KN145, RN6), which has layers of straticulate dolomite and thick beds of non-cherty dolomite (Milici, 1973), had higher magnesium concentrations, but also caves KN14 and RN5 formed in dolomitic Kingsport Dolomite and Mascot Dolomite had higher magnesium concentrations than caves formed within limestone units (e.g., KN62, KN24, and KN82). Potassium concentrations from KN24 had the greatest increase from 2019 to 2024 post-Helene. In general, KN62 had elevated cation concentrations compared to the other caves, which could be due to its proximity to a major highway.

Comparing chloride, a conservation tracer not altered by biota, to nitrate, sulfate, and potassium concentrations (**Figure 4.5**), indicated a generally positive relationship for all of the caves, except for KN82 where chloride concentration increased but not nitrate concentrations.

Table 4.9. Analysis of variance (ANOVA) results for physicochemical, geochemical, and CFUs tested against LULC, watershed (Clinch, Holston, Watts Bar), and sampling period (2019, 2024, 2024 post-Helene), with statistically significant values (p-value <0.05) highlighted in pink. ND = no data due to too few data points.

Parameter	**LULC**	**Watershed**	**Sampling period**
Temperature	0.052	0.001	0.733
DO	0.022	0.233	0.925
pH	0.610	0.162	0.165
Conductivity	0.092	0.612	0.177
Alkalinity	0.498	0.347	0.002
NPOC	0.327	0.723	0.972
TN	0.098	0.161	0.270
C:N	0.417	0.684	0.186
NO_3	0.049	0.016	0.197
PO_4	0.029	ND	0.993
Aerobic CFUs	0.191	0.592	0.899
Coliform CFUs	0.692	0.223	0.101
E. coli CFUs	0.516	ND	0.414

Table 4.10. Spearman's rank correlation analyses for LULC, physicochemical, and culture-based microbiological characteristics for the cave stream samples. Only significant (p-value <0.05) and moderately strong relationships (ρ >0.5) are shown. Trace metals from water are noted by "(w)" and trace metals from sediments are noted "(s)."

Variable	Variable	Spearman's rank	p-value
% Agriculture	Temperature	0.574	0.005
	DO	0.611	0.003
	NO_3^-	-0.697	0.000
% Forest	Temperature	-0.575	0.005
Population (5-km)	Temperature	-0.544	0.009
	Aerobic microbes	-0.682	0.001
	Mn	-0.894	0.0001
pH	SO_4^{2-}	0.551	0.008
	Sr(w)	0.560	0.007
	Ba(s)	0.521	0.013
	Mn(s)	0.600	0.003
Temp	NO_3^-	-0.514	0.014
	Zn(s)	-0.566	0.006
DO	PO_4^{3-}	-0.567	0.006
	SO_4^{2-}	-0.542	0.009
	Cl^-	-0.612	0.002
	Na^+	-0.660	0.001
	Ca^{2+}	-0.555	0.007
	K^+	-0.523	0.013
	Zn(s)	-0.557	0.007
Alkalinity	NH_4^+	-0.521	0.013
	Ni(s)	-0.564	0.007
Conductivity	Cu(s)	0.501	0.016
	Zn(s)	0.508	0.01
Aerobic CFUs	PO_4^{3-}	0.553	0.011
	Cl^-	0.547	0.013
	Na^+	0.579	0.008
	Ba(w)	-0.531	0.016
	Si(w)	-0.715	0.000
	Sr(w)	0.565	0.009
	Coliform CFUs	0.612	0.019
Coliform CFUs	Cd(s)	0.752	0.0001

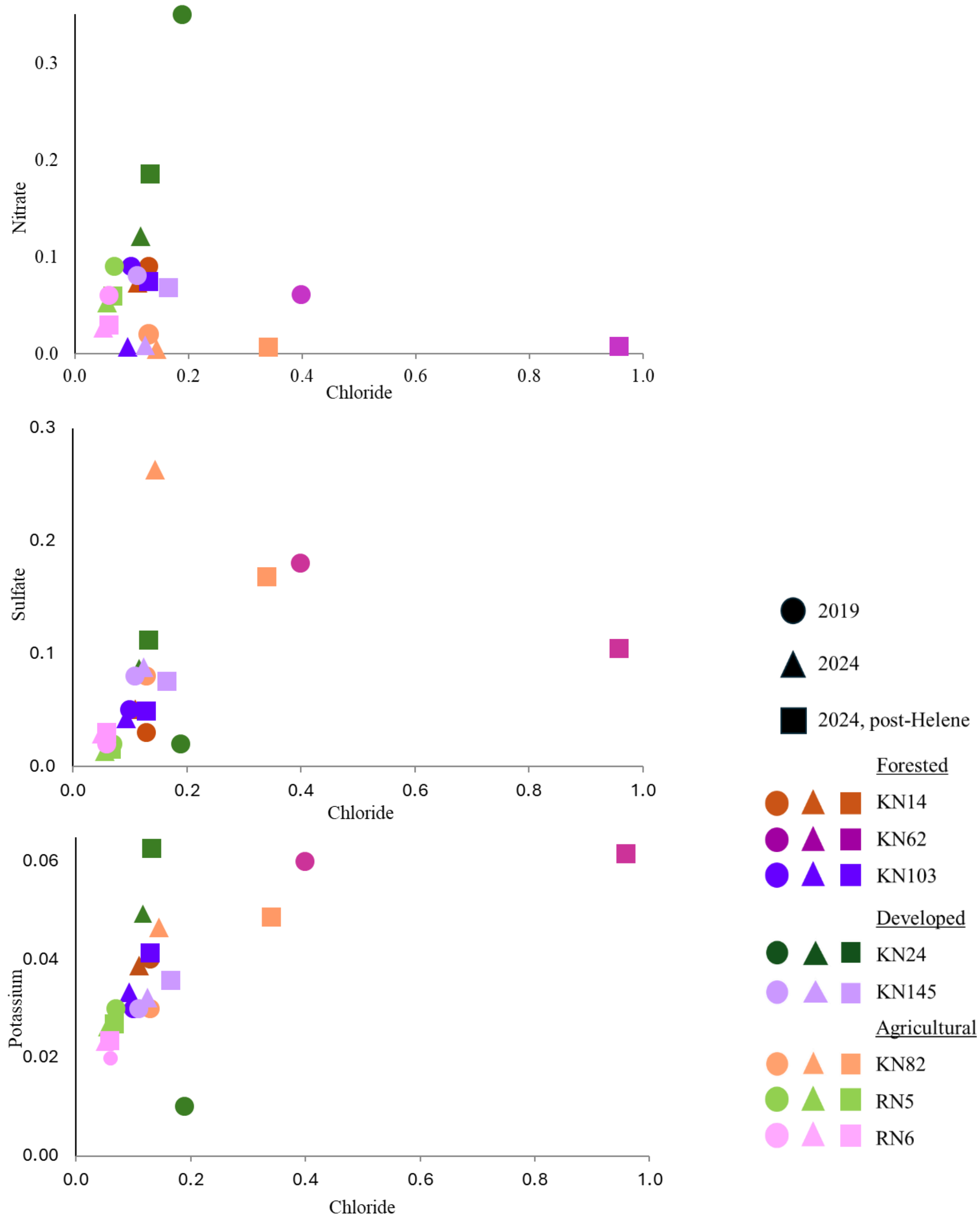

Figure 4.5. Nitrate, sulfate, and potassium compared to chloride concentrtions in mmol/L. Caves are listed by their TCS IDs, with shapes (circle, triangle, square) corresponding to the sampling period (2019, 2024, 2024 post-Helene, respectively) and color coded according to watershed (greens for Watts Bar of the Tennessee River, oranges for Holston River, and purples for Lower Clinch River).

Also, as an example, KN62 had high chloride concentrations, which the literature strongly relates to wastewater inputs in urban watersheds (Overbo et al., 2021), as well as high nitrate concentrations. Concentrations above 3 mg/L could suggest contamination from human or animal wastes and fertilizers, or from septic tank leakage (Power and Schepers, 1989).

4.2.3 Trace Metal Chemistry

Trace metal concentrations were measured from the cave streams (**Table A.1**) and from cave sediments following weak-acid digestions (**Table A.2**). Most of the analyzed trace metal concentrations in the cave streams were below 50 ppb, except for magnesium, silicon, and strontium concentrations were either similar over time or slightly decreased over time, except for KN62, which had higher metal concentrations in 2024 compared to 2019 and RN5 stream water also had a slight increase in trace metal concentrations over time. Barium concentrations were generally highest from the cave streams within the Lower Clinch River watershed (p-value = 0.000002) compared to other watersheds, with KN82 having the highest concentration. According to ANOVA results (**Table 4.11**), barium and strontium concentrations from the cave streams significantly correlated to the watershed (**Figure 4.6**).

Arsenic concentrations in the cave waters did not correlate with calcium concentrations, suggesting arsenic may not be of geologic origin, but may be from an anthropogenic source, such as from atmospheric pollution or fertilizers. KN24 had the highest concentrations of arsenic and lead in the water in 2019 (**Table A.1**). Incidentally, this also coincided with KN24's elevated nitrate that surpassed the EPA's MCL, and the highest phosphate concentrations measured from all samples (i.e., with concentrations above detection limit) (**Table 4.8**).

The weak-acid soluble trace metal concentrations from the cave sediment were generally below 100 ppm, except for several manganese samples and two aluminum samples (**Table A.2)**. Aluminum samples surpassing 100 ppm were in RN6 post-Helene and KN82 post-Helene. High concentrations (>1000 ppm) of manganese were measured from KN24, KN82, KN103, and RN6. In RN6, the highest manganese concentrations were in post-Helene sediment samples, whereas in KN24, KN82, and KN103, the highest concentrations were in 2019 sediment samples. KN24, which has the highest percentage of developed LULC, had the highest manganese concentrations overall. Cadmium was present in all samples above detection, with the highest measurements made in KN82 across sampling periods. Concentrations were also higher in KN24 and KN145

Table 4.11. Analysis of variance (ANOVA) results tested for trace metal concentrations from cave streams against LULC, watershed (Clinch, Holston, Watts Bar), and sampling period (2019, 2024, 2024 post-Helene), with statistically significant values (p-value <0.05) highlighted in pink.

Trace metals	LULC	Watershed	Sampling Period
As	0.638	0.968	0.687
Ba	0.360	2.25E-08	0.766
Sr	0.575	0.021	0.996

Table 4.12. Analysis of variance (ANOVA) results tested for weak-acid soluble metal concentrations from cave sediments against LULC, watershed (Clinch, Holston, Watts Bar), and sampling period (2019, 2024, 2024 post-Helene), with statistically significant values (p-value <0.05) highlighted in pink. ND = no data due to too few data points.

Trace metals	LULC	Watershed	Sampling Period
Al	0.490	0.032	0.837
As	0.484	0.630	0.312
Ba	0.025	0.624	0.751
Cd	0.002	0.007	0.893
Cu	0.002	0.205	0.774
Fe	0.502	0.401	0.312
Mn	0.834	0.758	0.183
Mo	0.286	0.120	0.626
Ni	0.076	0.014	0.109
Pb	0.257	0.544	0.329
Sr	0.073	0.002	0.777
Zn	0.017	0.007	0.967

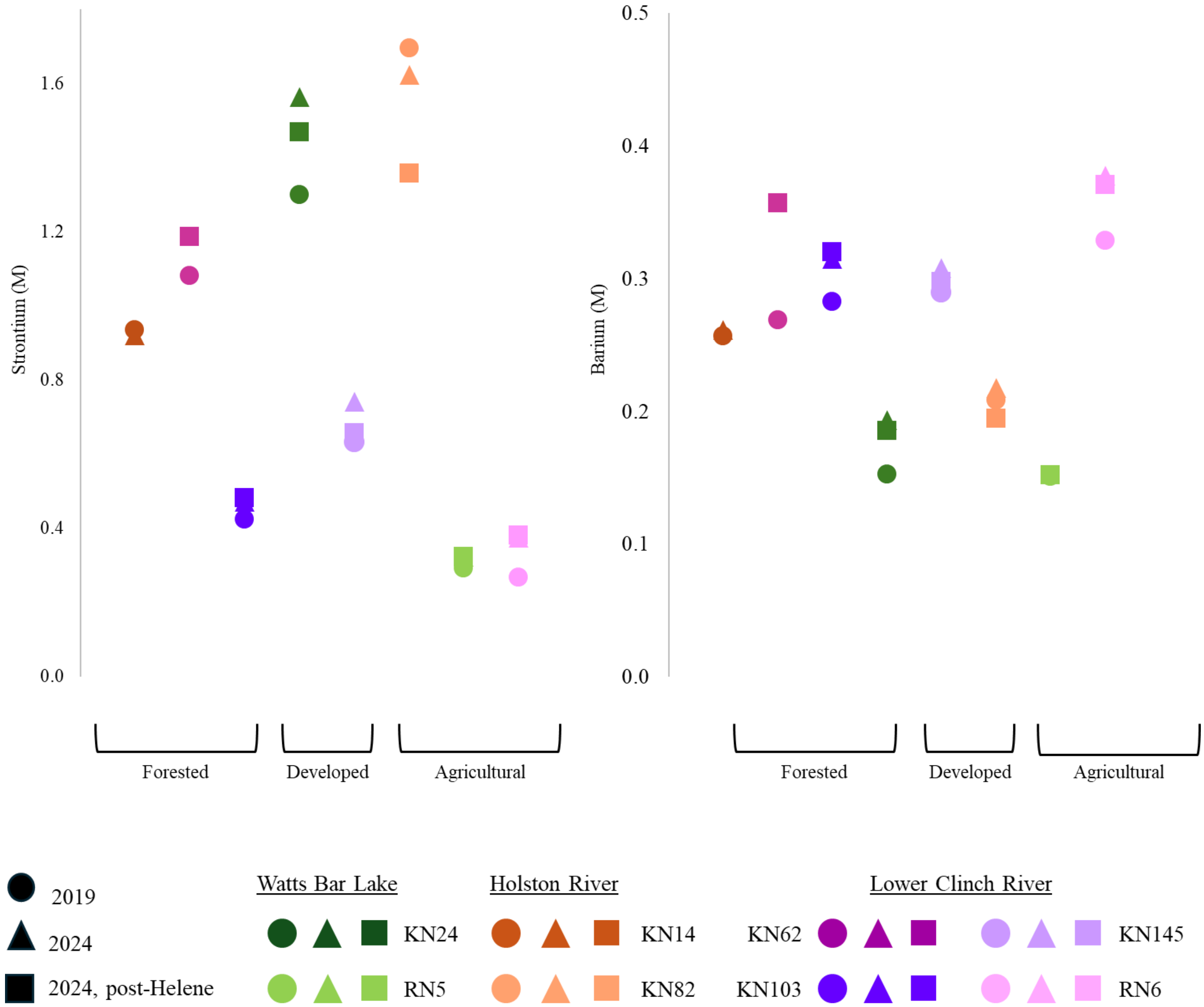

Figure 4.6. Strontium and barium concentrations from the cave streams. Caves are listed by their TCS IDs, with shape (circle, triangle, square) corresponding to the sampling period (2019, 2024, 2024 post-Helene, respectively) and color coded according to watershed (greens for Watts Bar of the Tennessee River, oranges for Holston River, and purples for Lower Clinch River). Caves are also grouped by the dominant LULC classification. Units are in mmol.

compared to others. Barium, cadmium, and copper significantly correlated to LULC type, generally being in higher concentrations in developed or agriculture categorized caves.

Additionally, aluminum, cadmium, nickel, strontium, and zinc sediment concentrations significantly correlated with the sub-basin watersheds (Table 4.12). Phosphate concentrations from sediments were highest from developed and agricultural sites KN145 and RN6 (Table A.3). The presence of metals from both water and sediment suggested variable partitioning and bioavailability, with metal concentrations generally being higher from weakly leached sediment samples than in water.

RN6 also had the highest sediment barium and cadmium concentrations (average = 0.7 ppb) of all the caves, although cadmium values decreased below the reporting limit of 1 ppb. KN62 sediment had slightly higher barium and strontium concentrations over time, but all other metal concentrations decreased. Overall, KN24, KN62, and KN82 also had some of the highest sediment trace metal concentrations, despite being from different watersheds and having dominant agricultural LULC. However, these caves experienced the most gain in development cover at the sub-watershed scale over time. This suggested that the cave sediments could accumulate trace metals from LULC change, and from increasing development in the watershed, which would impact the cave biota through time.

4.3 Culture-based Analysis of Aerobic Microbes, Coliforms, and *E. coli*

Petrifilms for specific types of microbes (i.e., aerobes, coliforms, and *E. coli*) were used to assess microbial loads in the cave streams (**Table A.4**). Notably, other metabolic groups that could not grow on the different media would not be enumerated. Also, the petrifilms used in 2019 did not distinguish between coliforms and *E. coli*, as was done for 2024 sampling events. The EPA Maximum Contaminant Level Goal (MCLG) for total coliforms in drinking water is zero, and a maximum contaminant level (MCL) for total coliforms is 0.05 CFU/mL (U.S. Environmental Protection Agency, 2024). All of the caves during all sampling times surpassed the MCL and, as such, did not meet the MCLG. High occurrences of total coliforms and *E. coli* have been found to co-occur with culturable viruses in other studies (Lindsey et al., 2002; Johnson et al., 2011) and may possibly suggest viral contamination in karst aquifers. Moreover, aerobic CFUs from the cave streams (**Figure 4.7**) did not necessarily correlate to coliform counts (**Figure 4.8**), as KN145 and RN5 had the highest aerobic CFUs, which may be related to having highest amount of urban and agricultural LULC, respectively, but the coliform CFUs from KN24

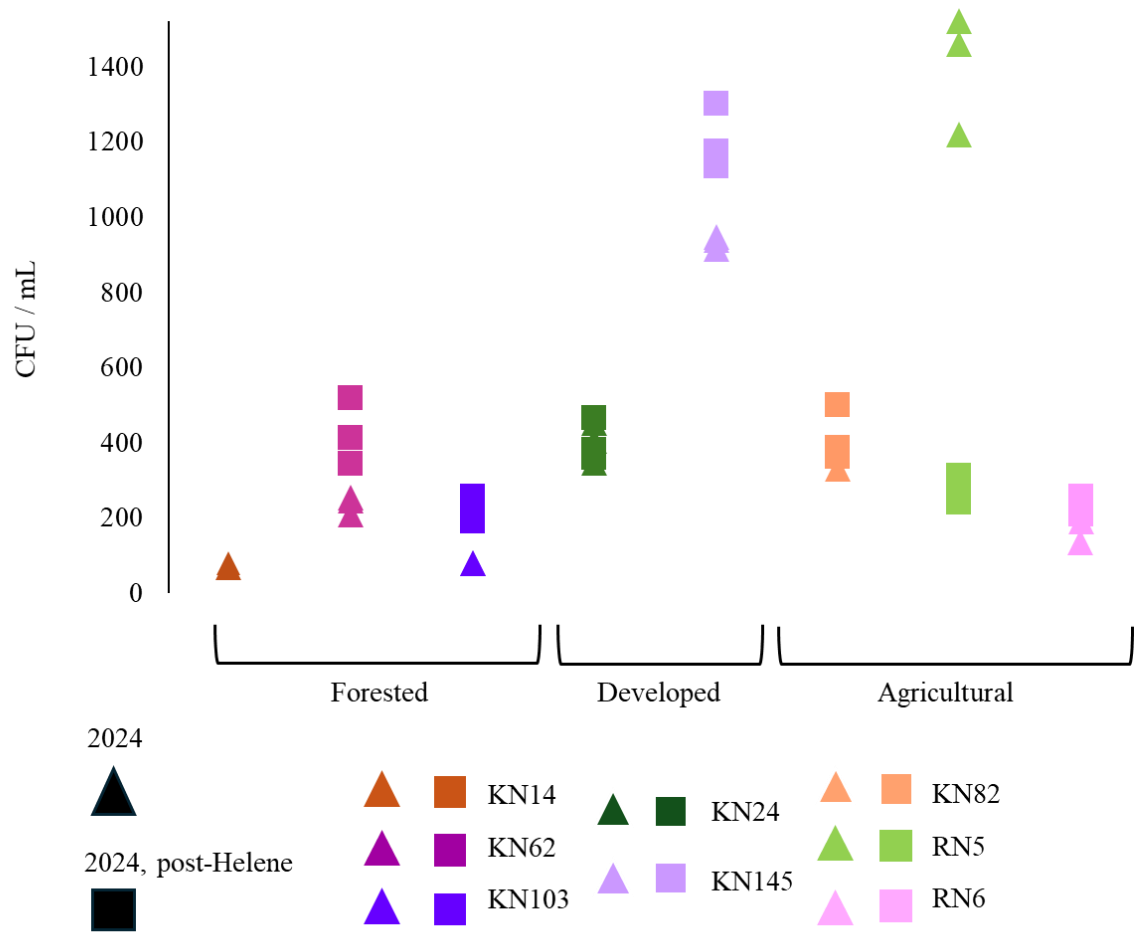

Figure 4.7. Counts for colony-forming units (CFUs) for aerobic microbes from the cave streams. Caves are listed by their TCS IDs, with shape (triangle, square) corresponding to the sampling period (2024 and 2024 post-Helene, respectively) and color coded according to watershed (greens for Watts Bar of the Tennessee River, oranges for Holston River, and purples for Lower Clinch River). Caves are also grouped by the dominant LULC classification.

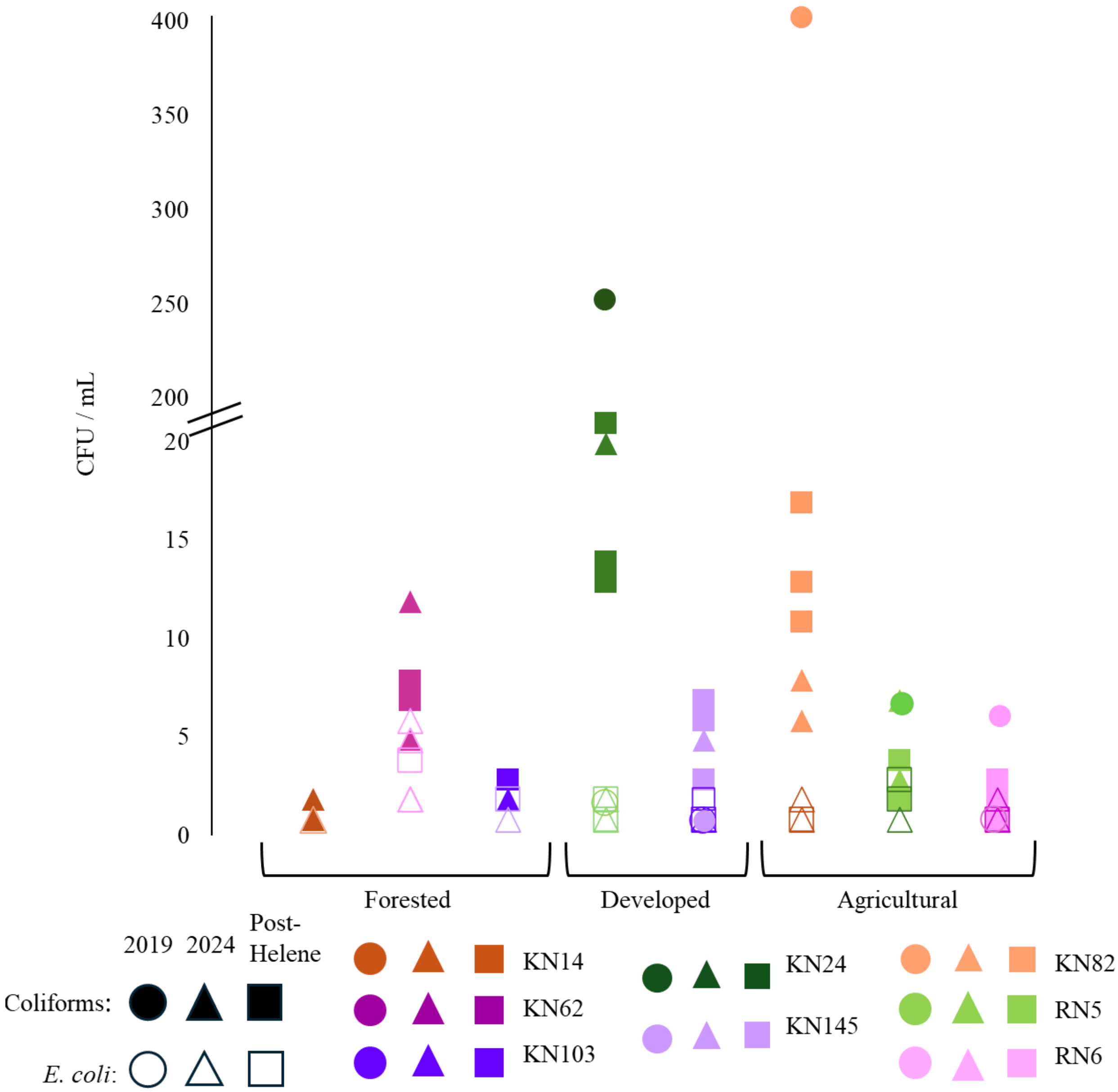

Figure 4.8. Total coliform and *E. coli* counts of colony-forming units (CFUs) from the cave streams. Coliform counts are represented by solid shapes and *E. coli* counts are represented by open shapes. Caves are listed by their TCS IDs, with shape (circle, triangle, square) corresponding to the sampling period (2019, 2024, 2024 post-Helene, respectively) and color coded according to watershed (greens for Watts Bar of the Tennessee River, oranges for Holston River, and purples for Lower Clinch River). Caves are also grouped by the dominant LULC classification.

and KN82 were higher by an order of magnitude, particularly in 2019. Additionally, although the aerobic CFUs from KN82 increased after Hurricane Helene, this cave had the highest coliform CFUs in 2019 and CFUs after Helene were not as high as from the other caves. This cave receives flood water from the nearby Holston River, which could impact which types of microbial groups enter the cave. In general, total coliforms were also elevated from caves with higher nitrate concentrations ($R^2 = 0.71$), except for KN82 that had low nitrate. KN24 had high nitrate concentrations and also among the highest total coliform CFUs. Spearman's rank analyses supported these results by revealing a moderately significant correlation between aerobic CFUs and coliform CFUs, as well as significant correlations among aerobic CFUs and phosphate, chloride, and sodium concentrations (**Table 4.10**). There were no significant relationships between coliform CFUs and environmental variables, besides a very weak and insignificant relationship between coliform CFUs and human population within the buffer zone ($\rho = 0.35$, p-value = 0.1).

Notably, caves having the lowest CFUs for aerobic microbes and coliforms were KN14, KN103, and RN6, which were all outflowing cave streams (**Figure 4.7**). These findings could suggest that the streams have communities more representative of groundwater than caves with inflowing streams sourced from the surface. As such, these cave streams may be less influenced by land use changes on the surface. Using the 16S rRNA gene sequence analyses, it will be possible to determine if the KN14, KN103, and RN6 streams have distinct microbial communities, and fewer putative pathogens, compared to inflowing cave streams.

All cave streams except KN14 also tested positive for *E. coli* in at least one of the replicates and sampling times (**Figure 4.8**). The MCLG for *E. coli* in drinking water is also zero (U.S. Environmental Protection Agency, 2024). According to agency reports and previous studies, *E. coli* counts that surpass an average of 1.26 CFU/mL from recreational streams indicate poor water quality and potential fecal contamination from agriculture runoff or septic leakage (U.S. Environmental Protection Agency, 2012; Dein et al., 2019). The cave water from KN62 in 2024, pre- and post-Helene surpassed 1.26 CFU/mL, which suggested that the water should not be used. However, personal communication with landowners revealed that the cave spring water had previously been considered safe for drinking.

4.4 Sequence Analysis of Microbial Communities

4.4.1 Taxonomic Overview of Microbial Communities

Microbial community composition and diversity were evaluated from the cave streams and cave sediment. A total of 44,320,281 bacterial and archaeal 16S rRNA gene sequences were obtained. Bacteria were assigned to 95% of all reads. There was a high proportion of unclassified bacteria at the phylum level from the cave streams and cave sediments, which could suggest novel taxonomic diversity from these caves. From all of the cave water samples, an average of 38% of all reads were classified to the phylum Pseudomonadota, followed by the phyla Bacteroidota (11%) and Verrucomicrobiota (6%) (**Figure 4.9**). Pseudomonadota was also the most abundant phylum from all of the cave sediments, at 21% of all reads, followed by 15% classified to Acidobacteriota and 7% to Planctomycetota (**Figure 4.10**). The only archaeal phylum having more than 1% relative abundance for all of the sequence reads was Thermoprotea, with relative abundances of 2% and 6% for cave water and sediment, respectively. At the class level for the streams and sediments (**Figure 4.11** and **Figure 4.12**, respectively), Gammaproteobacteria represented 30% of all reads from the water and 16% of all reads from the sediment, followed by Bacteriodia (10%) and Alphaproteobacteria (8%) from the cave water, and Vicinamibacteria (13%) and Alphaproteobacteria (6%) from the cave sediments.

Caves with inflowing streams had a closer tie to what could be considered surface water taxa. For example, after flooding from Hurricane Helene, KN82 experienced an increase in the order Methylococcales, which are heterotrophic microbes that can use organic compounds and that can also oxidize methane. Additionally, the order Pseudomonadales, considered to be comprised of heterotrophs, was abundant from KN62 (which receives road runoff), KN24, and KN145. KN62, and KN24 also had higher relative abundances of these groups, in particular, post-Helene. Taxa associated with oligotrophic systems based on the literature (Yavari-Bafghi et al., 2023), such as Burkholderiales, had higher relative abundances in KN14 and RN6, as well as KN24 and KN82 with inflowing cave streams.

Statistical significance based on Spearman's rank correlation was determined for all major class-level taxa from water (**Table 4.13**) and sediments (**Table 4.14**). For water, a handful of correlations were moderately strong (>0.5), including for the relative abundances between Planctomycetes and Verrucomicrobiia, Vicinamibacteria and Polyangiia, Cyanobacteria and Acidimicrobiia, Omnitrophia and Parcubacteria, and Omitropha and Oligoflexia. Spearman's

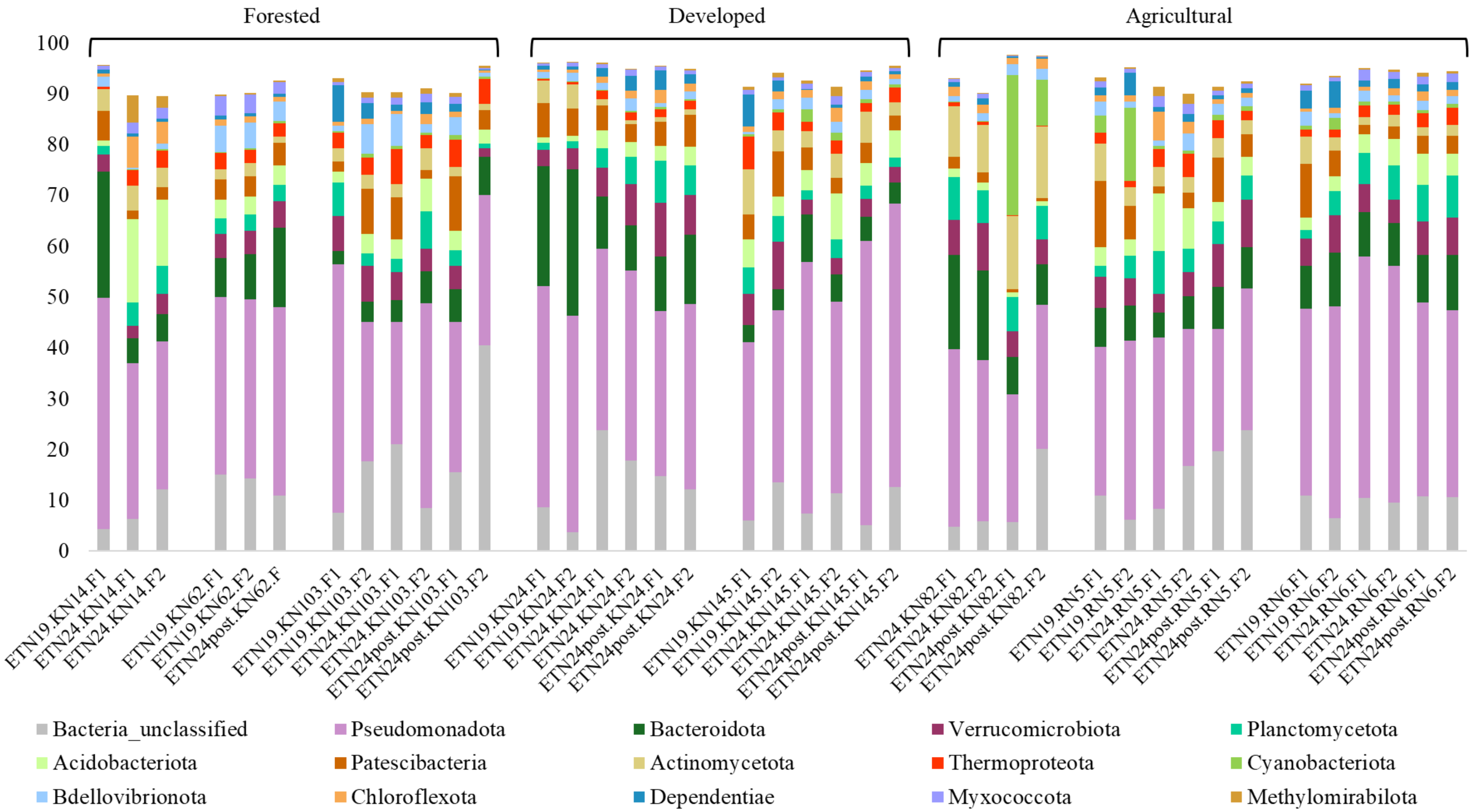

Figure 4.9. Relative abundances of 16S rRNA gene sequences from cave streams at the phylum level for Archaea (Thermoprotea) and Bacteria. Only sequences with > 1% abundance are shown.

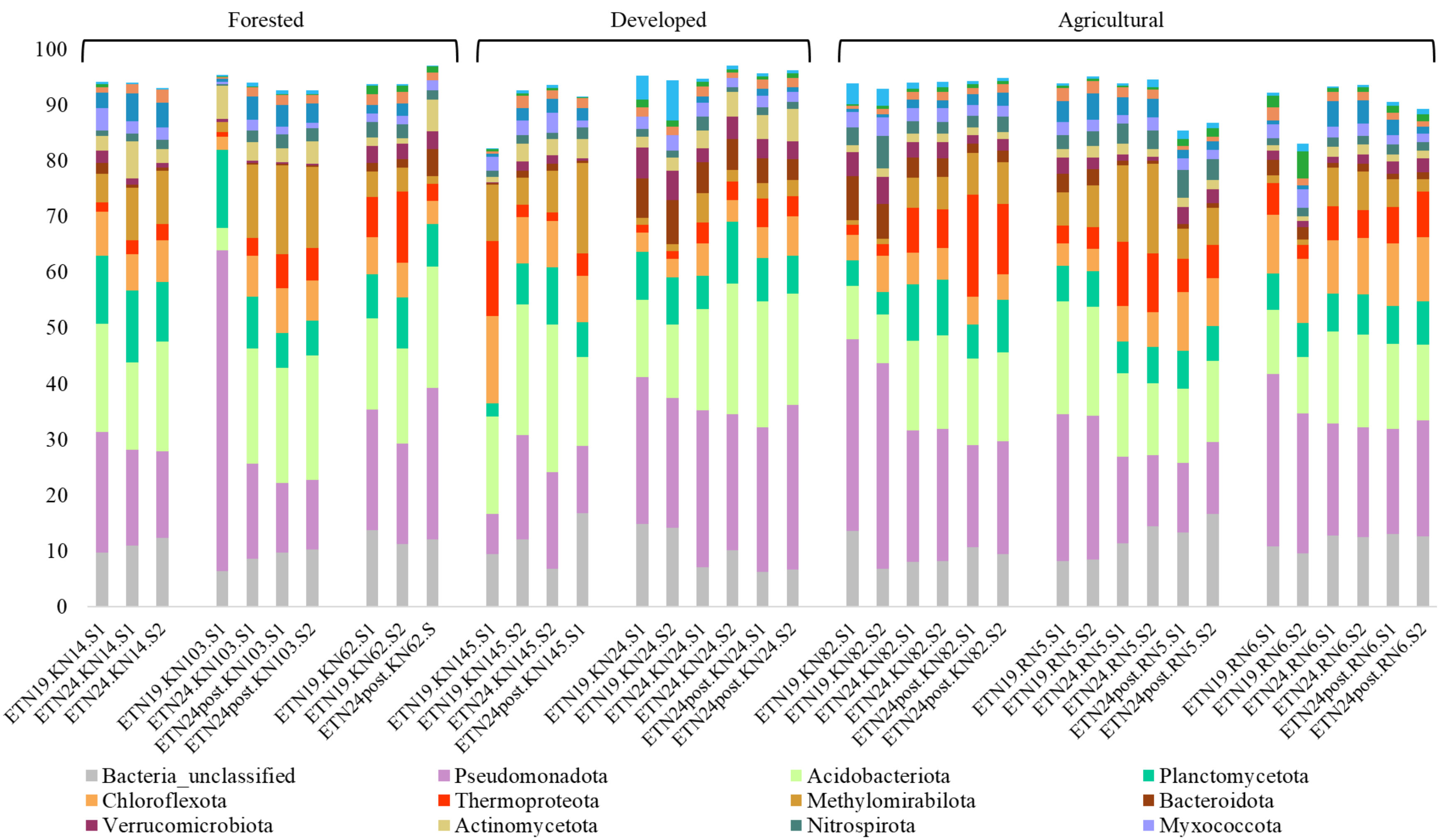

Figure 4.10. Relative abundances of 16S rRNA gene sequences from cave sediments at the phylum level for Archaea (Thermoprotea) and Bacteria. Only sequences with > 1% abundance are shown.

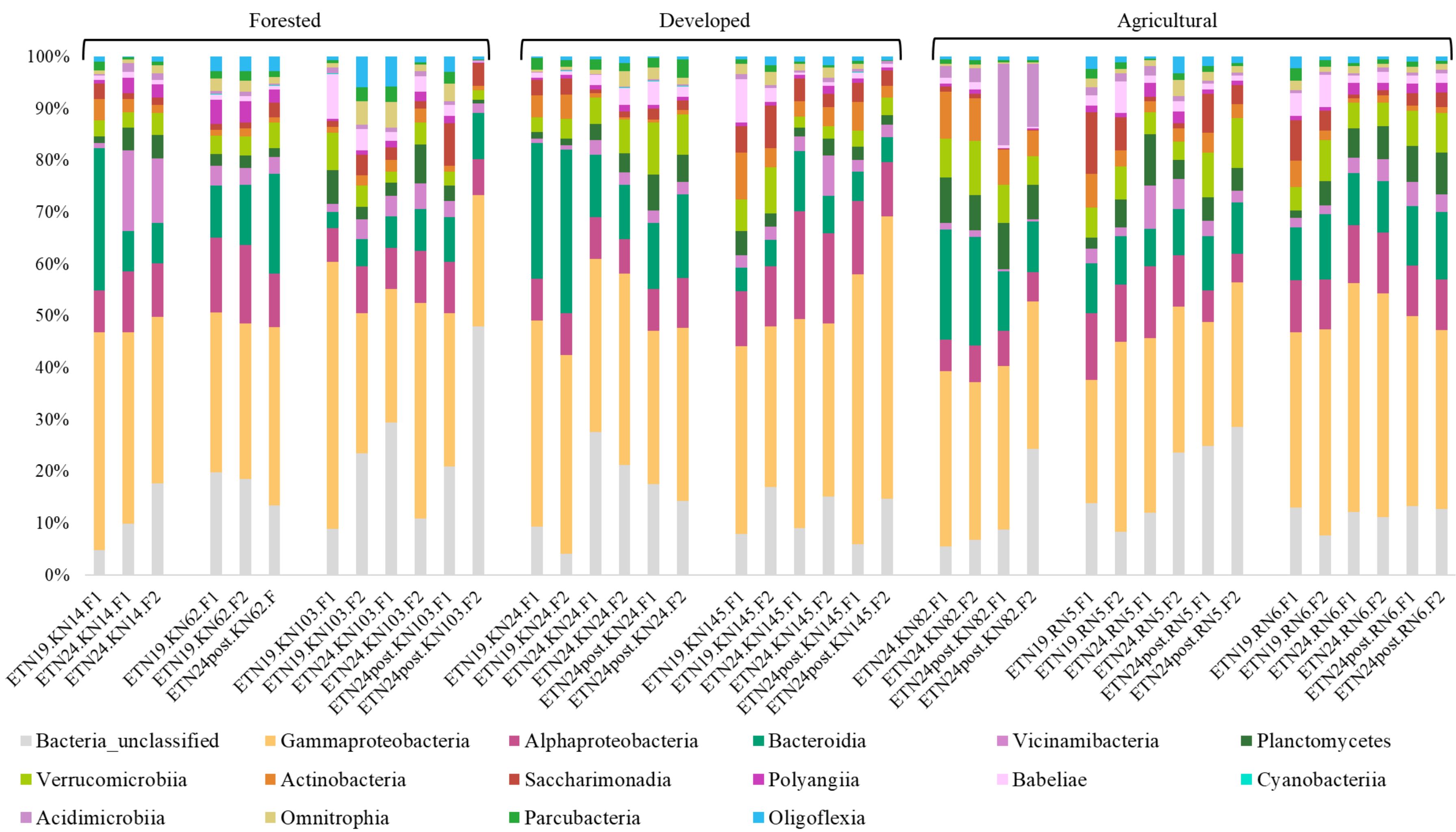

Figure 4.11. Relative abundances of bacterial 16S rRNA gene sequences from cave streams at the class level. Sequences with > 1% relative abundance are shown.

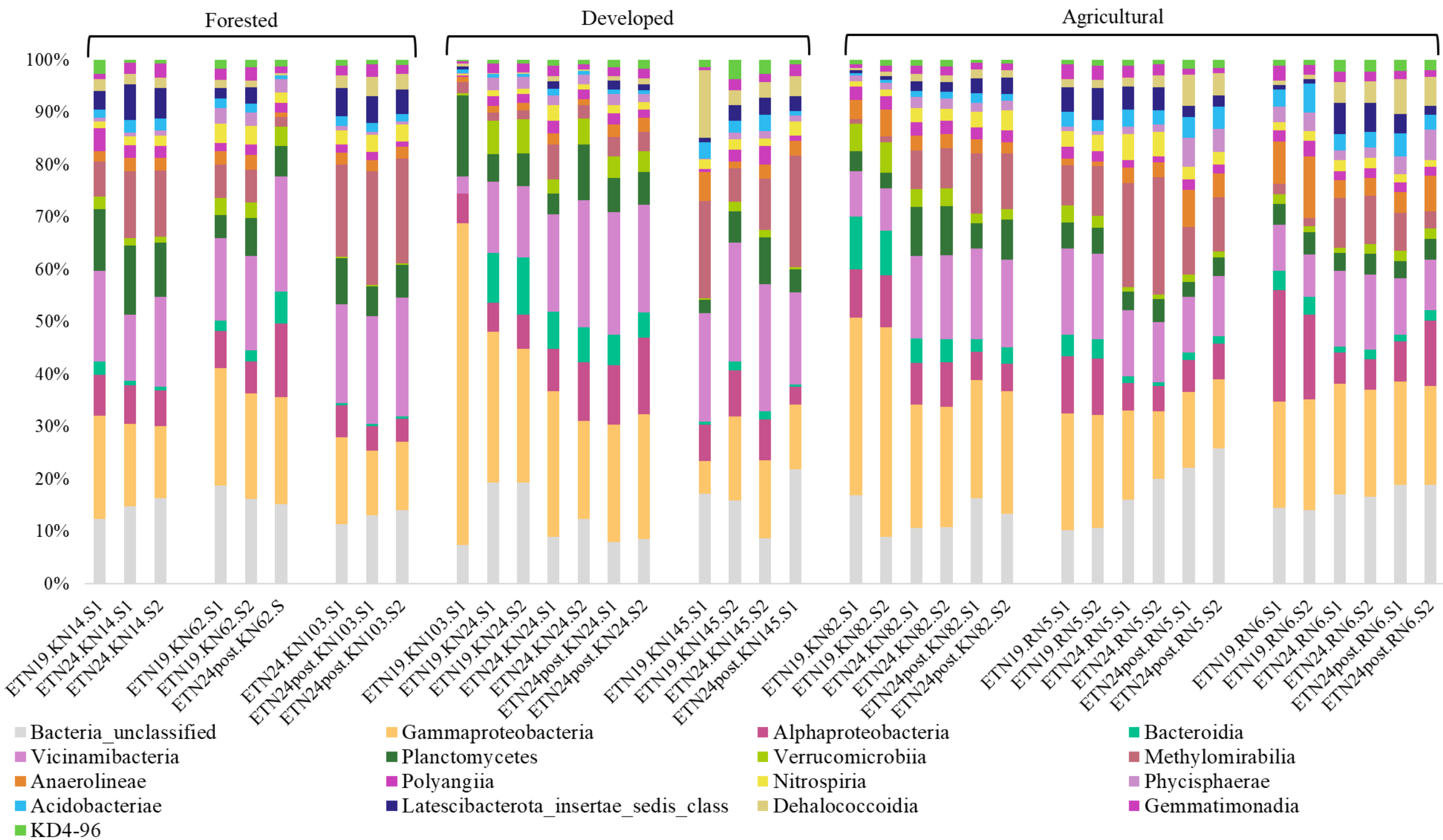

Figure 4.12. Relative abundances of bacterial 16S rRNA gene sequences from cave sediments at the class level. Sequences with > 1% relative abundance are shown.

Table 4.13. Spearman's rank correlation for the top 1% of class-level microbial relative abundances from the cave stream samples. The upper right triangle has p-values, highlighted in pink if significant (p-value >0.05), and the lower left triangle has Spearman's rank (ρ), with moderately to strongly correlated relationships bolded.

p-value / ρ	Gammaproteobacteria	Bacteria_unclassified	Bacteroidia	Alphaproteobacteria	Verrucomicrobiia	Planctomycetes	Saccharimonadia	Actinobacteria	Vicinamibacteria	Cyanobacteriia	Babeliae	Acidimicrobiia	Omnitrophia	Parcubacteria	Oligoflexia	Polyangiia
Gammaproteobacteria		0.002	0.323	0.099	0.854	0.958	0.799	0.852	0.201	0.140	0.253	0.034	0.022	0.360	0.008	0.435
Bacteria_unclassified	-0.481		0.088	0.202	0.574	0.227	0.743	0.001	0.240	0.326	0.424	0.280	0.025	0.465	0.008	0.737
Bacteroidia	0.160	-0.273		0.470	0.231	0.544	0.825	0.332	0.006	0.783	0.063	0.384	0.070	0.036	0.204	0.686
Alphaproteobacteria	0.265	-0.206	-0.118		0.007	0.053	0.148	0.548	0.011	0.068	0.718	0.010	0.237	0.893	0.486	0.003
Verrucomicrobiia	0.030	-0.092	0.194	-0.423		<0.001	0.995	0.640	0.026	0.172	0.004	0.370	0.702	0.434	0.117	0.158
Planctomycetes	0.009	-0.195	-0.099	-0.309	**0.600**		0.001	0.744	0.776	0.070	0.076	0.003	0.396	0.127	0.010	0.814
Saccharimonadia	-0.042	0.054	-0.036	0.233	-0.001	-0.498		0.189	0.542	0.517	0.167	0.006	0.157	0.084	0.076	0.118
Actinobacteria	-0.031	**-0.515**	0.157	-0.098	0.076	-0.053	0.212		0.006	0.128	0.526	0.005	0.090	0.574	0.493	0.008
Vicinamibacteria	-0.207	0.190	-0.426	0.400	-0.351	0.046	-0.099	-0.427		0.002	0.745	0.044	0.025	0.296	0.399	<0.001
Cyanobacteriia	-0.238	-0.159	-0.045	-0.291	0.220	0.290	-0.106	0.245	-0.467		0.931	<0.001	0.022	0.299	0.403	0.031
Babeliae	0.185	-0.130	-0.297	-0.059	0.441	0.284	0.223	-0.103	-0.053	-0.014		0.232	0.020	0.028	0.834	0.576
Acidimicrobiia	-0.336	-0.175	-0.141	-0.404	0.146	0.452	-0.428	0.435	-0.320	**0.740**	-0.193		0.023	0.026	0.331	0.104
Omnitrophia	-0.362	0.354	-0.289	0.191	-0.062	-0.138	0.228	-0.272	0.353	-0.362	0.367	-0.359		0.0002	<0.001	0.010
Parcubacteria	-0.149	0.119	0.333	-0.022	0.127	-0.245	0.276	-0.092	-0.170	-0.168	0.347	-0.351	**0.563**		0.003	0.829
Oligoflexia	-0.414	0.414	-0.205	0.114	-0.251	-0.401	0.284	-0.112	0.137	-0.136	0.034	-0.158	**0.747**	0.453		0.037
Polyangiia	-0.127	0.055	-0.066	0.462	-0.227	0.038	-0.251	-0.416	**0.679**	-0.341	-0.091	-0.261	0.403	0.035	0.331	

Table 4.14. Spearman's rank correlation for the top 1% class-level microbial relative abundances from the cave sediment samples. The upper right triangle has p-values, highlighted in pink if significant (p>0.05), and the lower left triangle has Spearman's rank (ρ), with moderately to strongly correlated relationships bolded.

p-value / ρ	**Gammaproteobacteria**	**Vicinamibacteria**	**Bacteria_unclassified**	**Alphaproteobacteria**	**Methylomirabilia**	**Planctomycetes**	**Bacteroidia**	**Anaerolineae**	**Verrucomicrobiia**	**Nitrospiria**	**Latescibacterota_ insertae_sedis_class**	**Phycisphaerae**	**Dehalococcoidia**	**Polyangiia**	**Acidobacteriae**	**Gemmatimonadia**	**KD4-96**
Gammaproteobacteria		0.023	0.011	0.056	<0.0001	0.050	0.001	0.138	0.0002	0.068	0.045	0.959	<0.0001	0.235	0.002	0.523	0.202
Vicinamibacteria	-0.367		0.448	0.846	0.016	0.232	0.499	0.003	0.515	0.017	0.179	0.374	0.739	0.122	0.247	0.021	0.063
Bacteria_unclassified	-0.410	-0.127		0.013	0.312	0.007	0.203	0.261	0.350	0.224	0.748	0.010	0.085	0.184	0.142	0.847	0.877
Alphaproteobacteria	0.312	-0.033	-0.399		<0.0001	0.812	0.0004	0.286	0.002	0.036	0.016	0.096	0.005	0.009	0.952	0.493	0.341
Methylomirabilia	**-0.624**	0.387	0.169	**-0.649**		0.983	<0.0001	0.510	<0.0001	<0.0001	<0.0001	0.027	<0.0001	0.145	0.027	0.052	0.861
Planctomycetes	0.321	0.199	-0.428	0.040	0.004		0.806	0.0004	0.646	0.295	0.666	0.015	0.015	0.252	0.021	0.972	0.227
Bacteroidia	0.526	0.113	-0.211	0.546	**-0.713**	-0.041		0.450	<0.0001	0.152	<0.0001	0.059	<0.0001	0.001	0.001	0.894	0.863
Anaerolineae	-0.245	-0.466	0.187	0.178	-0.110	-0.547	-0.126		0.166	0.674	0.805	0.004	0.054	0.604	0.001	0.502	0.494
Verrucomicrobiia	0.565	0.109	-0.156	0.488	**-0.700**	0.077	**0.933**	-0.229		0.109	0.001	0.039	<0.0001	0.002	0.001	0.944	0.766
Nitrospiria	-0.300	0.384	0.202	-0.341	**0.688**	-0.174	-0.237	-0.071	-0.264		0.0001	0.999	0.334	0.931	0.132	0.0002	0.765
Latescibacterota_ insertae_sedis_class	-0.327	0.223	0.054	-0.390	**0.786**	0.072	**-0.608**	-0.041	**-0.533**	**0.583**		0.070	0.001	0.592	0.001	0.001	0.208
Phycisphaerae	0.009	-0.148	0.413	0.274	-0.359	-0.391	0.309	0.460	0.336	0.000	-0.297		0.837	0.146	0.109	0.858	0.090
Dehalococcoidia	**-0.715**	0.056	0.283	-0.443	**0.635**	-0.393	**-0.705**	0.315	**-0.673**	0.161	**0.513**	-0.035		0.084	0.0001	0.590	0.011
Polyangiia	0.197	0.255	-0.220	0.417	-0.241	0.190	**0.500**	0.087	0.492	-0.015	0.090	0.240	-0.284		0.719	0.164	0.017
Acidobacteriae	-0.487	-0.193	0.243	0.010	0.358	-0.373	**-0.502**	**0.525**	**-0.522**	0.249	**0.503**	0.265	**0.581**	0.060		0.147	0.047
Gemmatimonadia	-0.107	0.374	0.032	0.115	0.318	0.006	-0.022	-0.112	-0.012	**0.574**	**0.523**	0.030	-0.090	0.231	0.240		0.515
KD4-96	-0.212	0.304	0.026	0.159	0.029	-0.201	-0.029	0.114	0.050	-0.050	0.209	0.279	0.406	0.384	0.324	0.109	

rank correlation for the sediments also revealed significant and strong relationships between the relative abundances of Bacteriodia and Verrucomicrobiia, and significant and strongly negative correlations between Methylomirabilia and Latescibacterota_insertae_sedis_class, Methylomirabilia and Bacteroidia, and Gammaproteobacteria and Dehalococcoidia, among several other significant and moderately strong relationships.

4.4.2 Putative Pathogens

Bacterial orders, such as Pseudomonadales, Rickettsiales, Enterobacteriales, and Legionellales, include putative pathogens, and these taxa were present in differing relative abundances form the cave water and sediment (**Figure 4.12**). Taking the total of these four orders into consideration, from 5% to 35% relative abundances in the communities could represent putative pathogens. Although KN145, primarily classified as having developed cover, had the highest relative abundances of these taxa. The cave streams from KN14, KN62, and KN24 had higher relative abundances for these groups over time, where other cave streams had lower relative abundances over time. Specifically, the relative abundances of Pseudomonadales increased in all caves except KN103 and KN145 over time, but the relative abundances for Rickettsiales generally decreased from the cave streams over time. The relative abundances of Enterobacteriales, which contains the genera *Escherichia*, *Shigella*, *Klebsia*, *Salmonella*, and *Pleosiomonas*, increased over time, especially from KN14 and RN5 (**Figure 4.12**). These results do not reflect the microbial loads from CFUs of coliforms or *E. coli* measured from the cave streams. Lastly, the relative abundances for Legionellales decreased in all cave streams except KN24 over time. This order also had higher relative abundances from KN103 and KN145 in 2019 compared to the other cave streams. These locations experienced the least amount of overall LULC and development over the study period, which may have had an influence on the stream composition that led to a decrease in the contribution of Legionellales to microbial communities.

4.5 Correlations Between Taxonomic Groups, LULC, and Environmental Variables

Pearson’s correlation tests were performed using major LULC categories and human population densities near the caves to determine the strength and significance of linear relationships against the relative abundances of microbial classes from all of the cave stream samples and all of the cave sediment samples (**Table 4.14** and **Table 4.15**). For all the cave streams, the relative abundances of Verrucomicrobiia, Planctomycetes, and Cyanobacteria

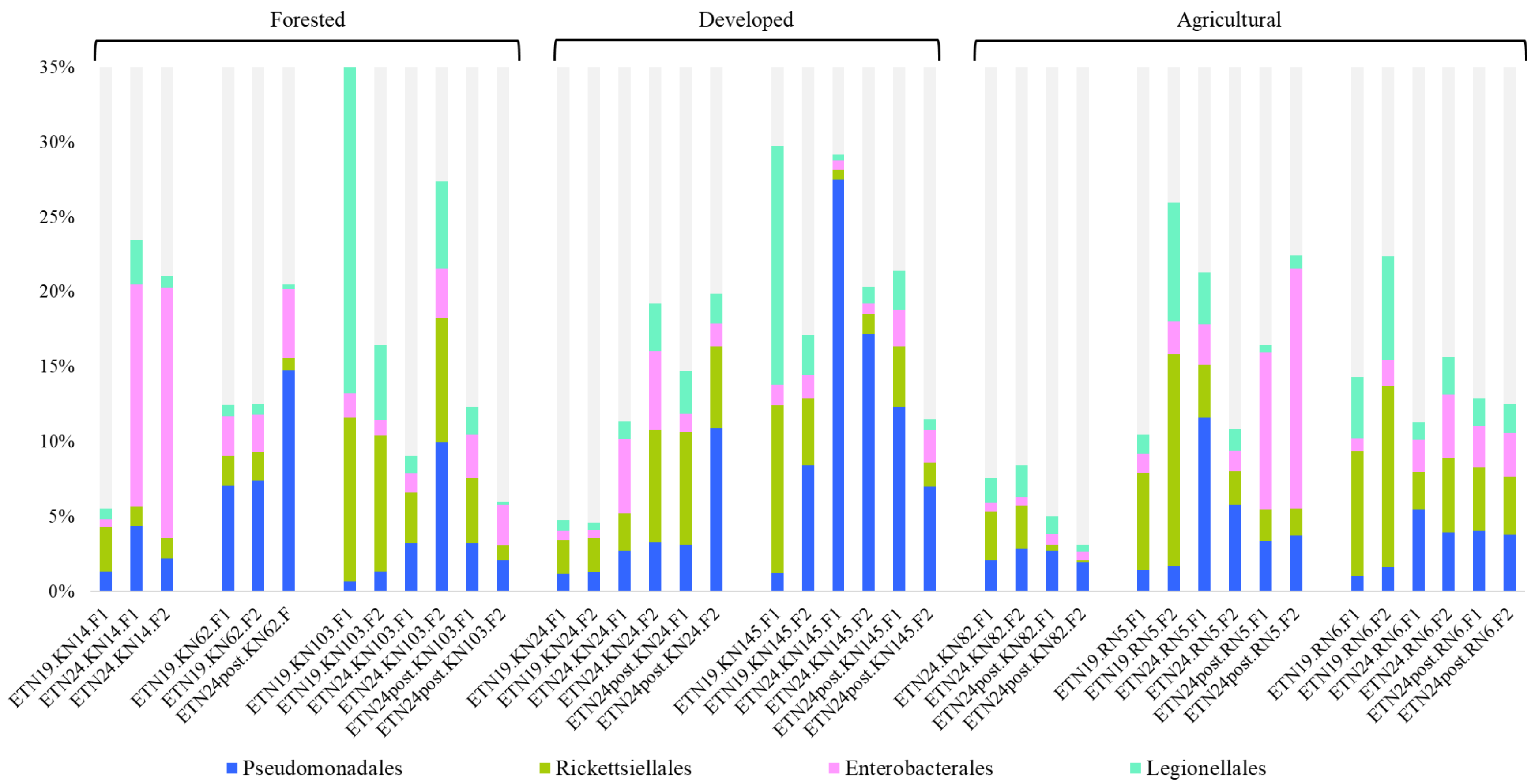

Figure 4.12. Relative abundances of 16S rRNA gene sequences from cave streams at the order level. Putative pathogens are highlighted while all other orders are grayed out.

Table 4.14. Pearson's significance (r) tests for class-level taxa from the cave streams against LULC for major categories (1-km buffer) and population density within a 5-km radius around the caves. Statistically significant values (p-value <0.05) are highlighted in green, and moderately strong correlations are highlighted in yellow.

Taxonomic Class	**% Development**		**% Agriculture**		**% Forest**		**Population**	
	r	**p-value**	**r**	**p-value**	**r**	**p-value**	**r**	**p-value**
Gammaproteobacteria	0.167	0.304	-0.174	0.283	-0.028	0.864	0.227	0.159
Bacteria_unclassified	0.014	0.929	-0.171	0.292	0.297	0.063	0.031	0.847
Bacteroidia	-0.065	0.690	-0.284	0.075	0.211	0.192	0.015	0.925
Alphaproteobacteria	0.094	0.564	0.030	0.856	-0.043	0.790	-0.053	0.744
Verrucomicrobiia	-0.332	0.037	0.129	0.428	-0.059	0.720	-0.149	0.358
Planctomycetes	-0.419	0.007	0.322	0.043	-0.115	0.482	-0.227	0.158
Saccharimonadia	0.009	0.956	0.078	0.634	-0.016	0.922	-0.062	0.702
Actinobacteria	-0.036	0.825	0.440	0.004	-0.665	0.000	0.001	0.993
Vicinamibacteria	0.015	0.925	0.021	0.898	0.185	0.254	-0.183	0.259
Cyanobacteriia	-0.394	0.012	0.415	0.008	-0.232	0.150	-0.309	0.052
Babeliae	-0.089	0.583	-0.093	0.568	0.223	0.166	-0.014	0.933
Acidimicrobiia	-0.278	0.082	0.507	0.001	-0.452	0.003	-0.174	0.283
Omnitrophia	0.104	0.522	-0.206	0.202	0.293	0.067	0.045	0.784
Parcubacteria	0.101	0.537	-0.482	0.002	0.459	0.003	0.123	0.450
Oligoflexia	-0.082	0.616	0.026	0.871	0.296	0.064	-0.179	0.270
Polyangiia	-0.203	0.208	-0.015	0.926	0.447	0.004	-0.412	0.008

Table 4.15. Pearson's significance (r) tests for class-level taxa from the cave sediments against LULC for major categories (1-km buffer) and population density within a 5-km radius around the caves. Statistically significant values ($p<0.05$) highlighted in pink, and moderately strong correlations highlighted in yellow.

Taxonomic Class	**% Development**		**% Agriculture**		**% Forest**		**Population**	
	r	**p-value**	**r**	**p-value**	**r**	**p-value**	**r**	**p-value**
Gammaproteobacteria	-0.051	0.763	-0.176	0.290	0.152	0.363	0.100	0.562
Vicinamibacteria	0.488	0.002	-0.355	0.029	-0.074	0.659	0.437	0.008
Bacteria_unclassified	-0.301	0.066	0.248	0.134	0.048	0.775	-0.378	0.023
Alphaproteobacteria	-0.171	0.304	-0.098	0.557	0.203	0.221	-0.149	0.386
Methylomirabilia	0.030	0.859	0.270	0.101	-0.206	0.214	-0.094	0.587
Planctomycetes	0.492	0.002	-0.349	0.032	0.059	0.724	0.384	0.021
Bacteroidia	0.069	0.678	-0.302	0.065	-0.025	0.880	0.248	0.145
Anaerolineae	-0.557	0.000	0.454	0.004	-0.064	0.704	-0.465	0.004
Verrucomicrobiia	0.099	0.554	-0.329	0.044	0.030	0.856	0.205	0.230
Nitrospiria	-0.218	0.188	0.280	0.089	-0.059	0.727	-0.303	0.072
Latescibacterota_ insertae_sedis_class	-0.233	0.159	0.387	0.016	-0.032	0.848	-0.398	0.016
Phycisphaerae	-0.466	0.003	0.073	0.665	0.240	0.147	-0.352	0.035
Dehalococcoidia	-0.214	0.198	0.419	0.009	-0.181	0.276	-0.267	0.116
Polyangiia	-0.081	0.628	0.110	0.510	-0.190	0.254	-0.125	0.467
Acidobacteriae	-0.628	0.000	0.561	0.000	0.070	0.678	-0.750	0.000
Gemmatimonadia	-0.104	0.534	-0.035	0.836	0.243	0.142	-0.225	0.186
KD4-96	-0.110	0.511	0.111	0.509	-0.018	0.915	-0.160	0.352

significantly but weakly correlated to the percentage of developed and agricultural cover. The relative abundances of Acidimicrobiia and Parcubacteria strongly correlated to agricultural cover, and neither taxon significantly correlated to forested LULC. The relative abundances of Polyangiia negatively but weakly correlated to higher populations. Lastly, the relative abundances of Actinobacteria significantly and negatively correlated to forested cover but positively to agricultural cover, which may be influenced by long-term fertilization stimulating the growth of Actinobacteria (Dai et al., 2018).

For the sediment samples, there were significant relationships among microbial classes and developed and agricultural cover, but not to forested cover. Higher human population densities strongly and significantly correlated lower relative abundances of Acidobacteriae andAnaerolineae, whereas there were positive relationships among Vicinamibacteria and Planctomycetes. Overall, these results suggested a connection between LULC and microbial community composition, although the analyses do not account for watershed-scale differences or distinguishing between inflowing and outflowing cave streams.

A CCA was done to evaluate potential relationships among microbial community compositions, environmental, and LULC parameters (**Figure 4.13**). Over 90% of variance could be explained by the first two axes. Cave communities clustered primarily according to prevalent LULC category and not to watershed. For instance, communities from all sampling times for KN145 clustered along the development vector and communities from all sampling times for RN6 clustered near the forested vector. The distribution of communities from KN14 and KN62 could be explained by developed and forested cover. However, the communities from RN5 and KN82 from 2019 and 2024 post-Helene both clustered near the agricultural vector, which suggested a change in community compositions prior to Hurricane Helene in 2024 and that the communities after the Hurricane become more similar to 2019 conditions. The communities from KN24 also shifted from developed cover in 2019 to forested cover for 2024 sampling, which may suggest an improvement in environmental and land use parameters around KN24 that would have affected microbial community compositions.

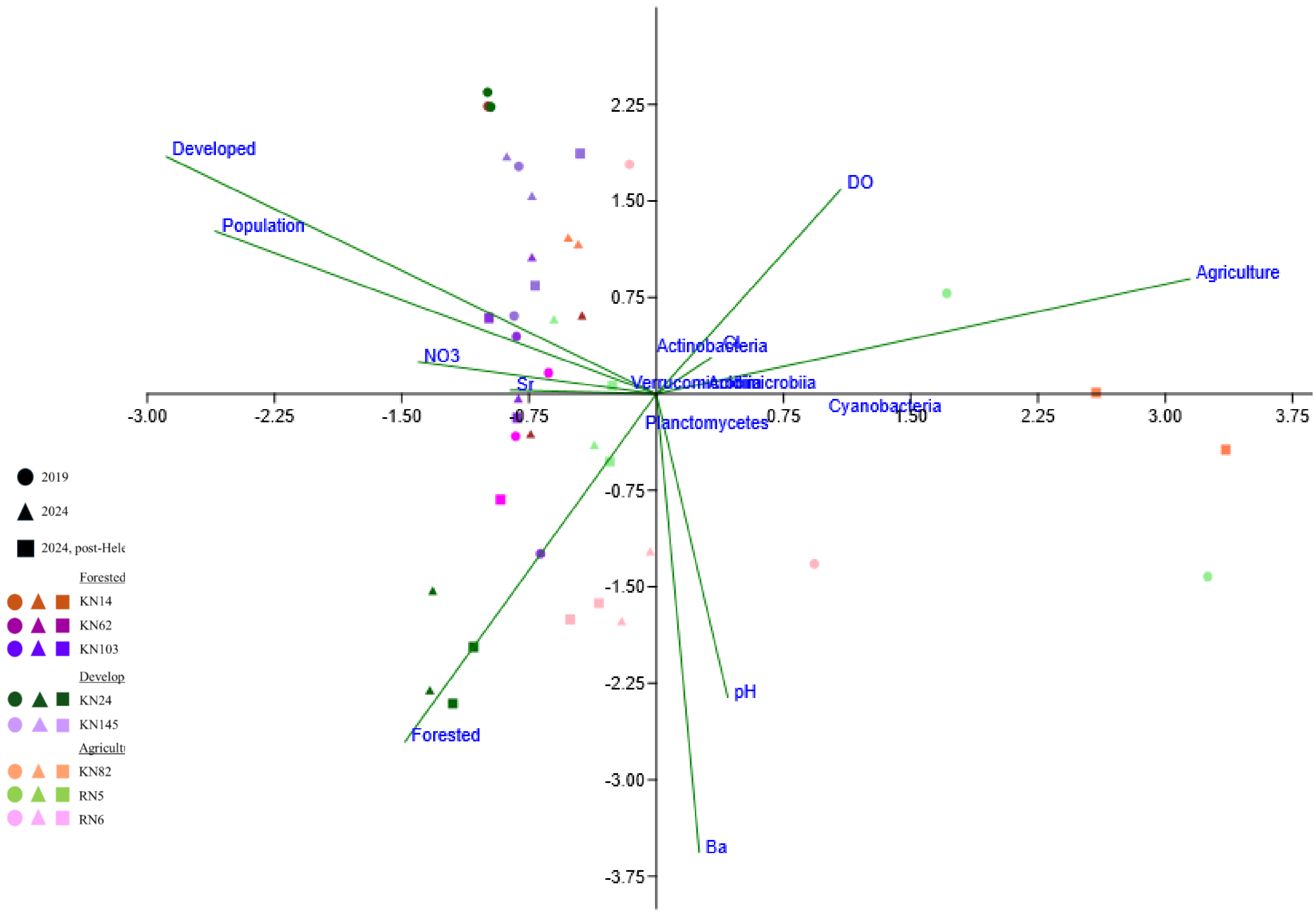

Figure 4.13. Cannonical correspondence analysis of selected class-level taxa which were statistically significant among different LULC caves. Colored shapes indicate caves. The first axis explains 68.1% of the variance and second axis explains 22.0% of the variance.

CHAPTER FIVE: CONCLUSIONS

As natural landscapes shift towards non-natural landscapes classified as developed and urban or agricultural, surface and groundwater systems are expected to change due to the spread of impervious surfaces, increased input of anthropogenic chemicals (e.g., from fertilizers or industrial effluent), changes to water uptake and release for water treatment plant usage, and disposal or leakage of wastewater effluent or septic failure. Although caves and karst systems are generally considered resilient systems, they are also non-renewable over geologic time (Gunn et al., 2000; Van Beynen and Townsend, 2005). Karst systems can rapidly respond to water transport from surface runoff, which carries with it particulates, pathogens, and nutrients. These potential contaminants make their way into local aquifers. Surface flooding, which may increase in frequency and severity due to climate change, can further affect karst systems, as well as the rates and types of biogeochemical cycles and microbial communities. Increased exposure to anthropogenic disturbances, such as from deforestation, development, agriculture, construction or mining, can further impact karst systems. For regions highly dependent on karst aquifer for daily freshwater need, health risks are also possible.

The impacts of changing LULC in karst areas have not been widely studied. The study selected eight caves in the KMSA to evaluate the impacts of LULC, and from Hurricane Helene flooding, on water quality and microbial ecology over a 5-year period. The questions posed in this study were straight-forward, starting with what microbial groups are found in cave streams affected by different LULC categories, whether there were microbial loads attributed to potential anthropogenic contamination (e.g., from coliform and *E. coli* counts), and how water quality based on environmental and geochemical parameters, including trace metals, may correlate to LULC categories and microbial community compositions. Studies like this will benefit future researchers interested in mitigating groundwater quality risks where anthropogenic activities have the potential to alter landscapes.

Based on the environmental, geochemical, and microbial data, there were distinctions based on a cave's hydrology. Caves with direct surface influence (i.e., inflowing cave streams, or those that receive surface runoff; KN24, KN62, KN82) had consistently elevated solute concentrations, such as for ions like chloride, nitrate, and potassium that may indicate contamination from septic and wastewater, or fertilizers. Caves with little to no direct surface influence (i.e., outflowing cave streams) had lower solute concentrations. Caves with LULC categories linked to development and agriculture also had higher microbial loads, and these caves also had microbial community compositions with higher relative abundances of groups considered to be putative pathogens. EPA water quality recommendations were surpassed for some of these caves, as well. As such, for these systems, there appeared to be persistent LULC impacts on the cave microbial communities.

The current study focused on caves that were not meant to be used for drinking water. However, communication with landowners and other local people indicated that some people still consider karst streams and springs to be clean and safe for drinking, irrigation, and livestock care. Throughout the KMSA, city-provided drinking water is treated and regulated, but numerous households that use independent, non-community water sources, such as wells and karst springs, are unregulated and untested. Based on the measured microbial loads from this study, as well as the microbial community compositions for the cave streams that included several putative pathogens, there is a risk that some landowners have access to unhealthy water. The human health implications and likelihood of disease outbreaks in communities because of microbial contamination in karst groundwater are not well understood globally, and should be studied more intently across the KMSA, and especially where LULC changes shift karst landscapes away from natural conditions.

REFERENCES

3M, 2017a, Aerobic Count Plate: Petrifilm Interpretation Guide.

-, 2017b, Rapid *E. coli*/Coliform Count Plate: Petrifilm Interpretation Guide.

Addesso, R., Gonzalez-Pimentel, J. L., D'Angeli, I. M., De Waele, J., Saiz-Jimenez, C., Jurado, V., Miller, A. Z., Cubero, B., Vigliotta, G., and Baldantoni, D., 2021, Microbial community characterizing vermiculations from karst caves and its role in their formation: Microbial Ecology, v. 81, no. 4, p. 884-896.

Al-Asadi, S. A. R., Al-Qurnawi, W. S., Al Hawash, A. B., Ghalib, H. B., and Alkhlifa, N.-H. A., 2020, Water quality and impacting factors on heavy metals levels in Shatt Al-Arab River, Basra, Iraq: Applied Water Science, v. 10, no. 5, p. 1-15.

Alexander, M., 1971, Microbial Ecology, John Wiley & Sons, 511 p.

Allison, S. D., and Martiny, J. B. H., 2008, Resistance, resilience, and redundancy in microbial communities: Proceedings of the National Academy of Sciences, v. 105, no. 1, p. 11512-11519.

Anderson, J. R., Hardy, E. E., Roach, J. T., and Witmer, R. E., 1976, A land use and land cover classification system for use with remote sensor data, *in* U.S. Geological Survey, ed., Geological Survey Professional Paper, v. 964, p. 7-9.

Apprill, A., McNally, S., Parsons, R., and Weber, L., 2015, Minor revision to V4 region SSU rRNA 806R gene primer greatly increases detection of SAR11 bacterioplankton: Aquatic Microbial Ecology, v. 75, no. 2, p. 129-137.

Bahar, M. M., and Yamamuro, M., 2008, Assessing the influence of watershed land use patterns on the major ion chemistry of river waters in the Shimousa Upland, Japan: Chemistry and Ecology, v. 24, no. 5, p. 341-355.

Bakalowicz, M., 2005, Karst groundwater: a challenge for new resources: Hydrogeology Journal, v. 13, no. 1, p. 148-160.

Baker, M. A., Valett, H. M., and Dahm, C. N., 2000, Organic carbon supply and metabolism in a shallow groundwater ecosystem: Ecology, v. 81, no. 11, p. 3133-3148.

Barton, H. A., Taylor, M. R., and Pace, N. R., 2004, Molecular phylogenetic analysis of a bacterial community in an oligotrophic cave environment: Geomicrobiology Journal, v. 21, no. 1, p. 11-20.

Bickford, T. M., Lindsey, B. D., and M.R., B., 1996, Bacteriological quality of ground water used for household supply, Lower Susquehanna River Basin, Pennsylvania and Maryland, U.S. Geological Survey Water-Resources Investigations Report 1996–4212, 31 p., https://pubs.er.usgs.gov/publication/wri964212.

Biedunkova, O., and Kuznietsov, P., 2024, Dataset on heavy metal pollution assessment in freshwater ecosystems: Scientific Data, v. 11, no. 1, p. 12-41.

Bolstad, P. V., and Swank, W. T., 1997, Cumulative impacts of landuse on water quality in a southern Appalachian watershed: Water Resources Bulletin, v. 33, p. 519-533.

Bontemps, Z., Alonso, L., Pommier, T., Hugoni, M., and Moënne-Loccoz, Y., 2022, Microbial ecology of tourist Paleolithic caves: Science of The Total Environment, v. 816, p. 151492.

Bouwer, E., and McCarty, P., 1984, Modeling of trace organics biotransformation in the subsurface: Ground Water, v. 22, p. 433-440.

Boyer, D. G., and Pasquarell, G. C., 1999, Agricultural land use impacts on bacterial water quality in a karst groundwater aquifer: Journal of the American Water Resources Association, v. 35, no. 2, p. 291-300.

Brad, T., Iepure, S., and Sarbu, S. M., 2021, The chemoautotrophically based movile cave groundwater ecosystem, a hotspot of subterranean biodiversity: Diversity, v. 13, no. 10, p. 128, https://doi.org/10.3390/d13030128.

Centers for Disease Control and Prevention, 2021, CDC-SafeWatch safe water for community health, Available online: https://www.cdc.gov/nceh/ehs/safe-watch/index.html.

Chen, Z., Auler, A. S., Bakalowicz, M., Drew, D., Griger, F., Hartmann, J., Jiang, G., Moosdorf, N., Richts, A., Stevanovic, Z., Veni, G., and Goldscheider, N., 2017, The world karst aquifer mapping project: concept, mapping procedure and map of Europe: Hydrogeology Journal, v. 25, no. 3, p. 771-785.

Chiarini, V., Duckeck, J., and De Waele, J., 2022, A global perspective on sustainable show cave tourism: Geoheritage, v. 14, no. 3, p. 82, https://doi.org/10.1007/s12371-022-00717-5.

Choudhury, T. R., Acter, T., Alam, A. M., Sowrav Sheikh Fahim Faysal, Safiur, R. M., A.M., C. S., and Sahamshad, Q. B., 2024, Appraisal of heavy metal contamination and their source apportionment identification in five river water systems of the coastal areas in Bangladesh: Regional Studies in Marine Science, v. 70, p. 103378.

Clinton, B., D., and Vose, J. M., 2005, Variation in stream water quality in an urban headwater stream in the southern Appalachians: Water, Air, & Soil Pollution, v. 169, p. 331-353.

Cordeiro, G., Beldi, J. S., García-Ruiz, S., Van Britsom, G., Cizek-Stroh, A., Robouch, P., and Hoekstra , E., 2018, Determination of the mass fractions of total aluminium, nickel, antimony and zinc in food simulant B, FCM-18-02 "Proficiency Test Report," JRC113663, 41 p.

Culver, D., 1985, Trophic relationships in aquatic environments: Stygologia, v. 1, p. 43-53.

Cunningham, K. I., Northup, D. E., Pollastro, R. M., Wright, W. G., and Larock, E. J., 1995, Bacteria, fungi and biokarst in Lechuguilla Cave, Carlsbad Caverns National Park, New Mexico: Environmental Geology, v. 25, no. 1, p. 2-8.

Dai, Z., Su, W., Chen, H., Barberán, A., Zhao, H., Yu, M., Yu, L., Brookes, P. C., Schadt, C. W., Chang, S. X., and Xu, J., 2018, Long-term nitrogen fertilization decreases bacterial diversity and favors the growth of Actinobacteria and Proteobacteria in agro-ecosystems across the globe: Global Change Biology, v. 24, no. 8, p. 3452-3461.

Dein, J., Gilmer, D., Ray, H., Sasthav, C., and Armsworth, P., 2019, The state of surface water quality in Knox County, University of Tennessee, Knoxville: Available from: https://consci.utk.edu/wp-content/uploads/2019/08/State-of-the-Watershed.pdf.

Drew, D., and Hötzl, H., 1999, Karst hydrogeology and human activities, International Conributions to Hydrogeology: Rotterdam, the Netherlands, A.A. Balkema.

Engel, A. S., Lee, N., Porter, M. L., Stern, L. A., Bennett, P. C., and Wagner, M., 2003, Filamentous "Epsilonproteobacteria" dominate microbial mats from sulfidic cave springs: Applied and Environmental Microbiology, v. 69, no. 9, p. 5503-5511.

Engel, A. S., Stern, L. A., and Bennett, P. C., 2004, Microbial contributions to cave formation: New insights into sulfuric acid speleogenesis: Geology, v. 32, no. 5, p. 369-372.

Fadlillah, L. N., Utami, S., Rachmawati, A. A., Jayanto, G. D., and Widyastuti, M., 2023, Ecological risk and source identifications of heavy metals contamination in the water and surface sediments from anthropogenic impacts of urban river, Indonesia: Heliyon, v. 9, no. 4, p. e15485.

Farnleitner, A. H., Wilhartitz, I., Ryzinska, G., Kirschner, A. K. T., Stadler, H., Burtscher, M. M., Hornek, R., Szewzyk, U., Herndl, G., and Mach, R. L., 2005, Bacterial dynamics in spring water of alpine karst aquifers indicates the presence of stable autochthonous microbial endokarst communities: Environmental Microbiology, v. 7, no. 8, p. 1248-1259.

Fashina, L., Luffman, I., Joyner, T. A., and Nandi, A., 2022, Geospatial assessment of karst spring water quality in Northeast Tennessee, USA: Geosciences, v. 12, no. 8, p. 303-317.

Fernández-Ortega, J., Barberá, J. A., and Andreo, B., 2024, Real-time karst groundwater monitoring and bacterial analysis as early warning strategies for drinking water supply contamination: Science of The Total Environment, v. 912, p. 169539.

Fillinger, L., Hug, K., Trimbach, A. M., Wang, H., Kellermann, C., Meyer, A., Bendinger, B., and Griebler, C., 2019, The D-A-(C) index: A practical approach towards the microbiological-ecological monitoring of groundwater ecosystems: Water Research, v. 163, p. 114902.

Ford, D. C., and Williams, P. W., 2007, Karst hydrogeology and geomorphology, John Wiley & Sons, Ltd., 578 p.

Freckman, D. W., Blackburn, T., Brussaard, L., Hutchings, P., Palmer, M., and Snelgrove, P., 1997, Linking biodiversity and ecosystem functioning of soils and sediments: Ambio, v. 26, p. 556-562.

Frenzel, S. A., and Couvillion, C. S., 2002, Fecal indicator bacteria in streams along a gradient of residential development: Journal of the American Water Resources Association, v. 38, no. 1, p. 265-273.

Frindte, K., Allgaier, M., Grossart, H. P., and Eckert, W., 2016, Redox stability regulates community structure of active microbes at the sediment–water interface: Environmental Microbiology Reports, v. 8, no. 5, p. 798-804.

Ghiorse, W. C., and Wilson, J. T., 1988, Microbial ecology of the terrestrial subsurface: Advances in Applied Microbiology, v. 33 p. 107-172.

Gibert, J., Dole-Oliver, M., Marmonier, P., and Vervier, P., 1990, Surface water- groundwater ecotones, *in* Naiman, R., and De´camps, H., eds., The ecology and management of aquatic-terrestrial ecotones, Volume 4: UNESCO Paris and Parthenon Publishing Group, Carnforth, England, p. 199-225.

Gibert, J., Stanford, J. A., Dole-Olivier, M.-J., and Ward, J. V., 1994, Basic attributes of groundwater ecosystems and prospects for research, *in* Gibert, J., Danielopol, D. L., Stanford, J.A., eds., Groundwater Ecology: San Diego, CA., Academic Press, p. 571.

Gladstone, N. S., Perez, K. E., Pieper, E. B., Carter, E. T., Dooley, K. E., Shoobs, N. F., Engel, A. S., and Niemiller, M. L., 2019, A new species of stygobitic snail in the genus Antrorbis Hershler & Thompson, 1990 (Gastropoda, Cochliopidae) from the Appalachian Valley and Ridge of eastern Tennessee, USA: ZooKeys, v. 898, p. 103-120.

Gladstone, N. S., Pieper, E. B., Keenan, S. W., Paterson, A. T., Slay, M. E., Dooley, K., Engel, A. S., and Niemiller, M. L., 2021, Discovery of the Blue Ridge Springsnail, Fontigens orolibas, Hubricht, 1957 (Gastropoda: Emmericiidae) in east Tennessee and its conservation implications: Freshwater Mollusk Biology and Conservation, v. 24, no. 1, p. 34-42.

Goldscheider, N., Chen, Z., Auler, A. S., Bakalowicz, M., Broda, S., Drew, D., Hartmann, J., Jiang, G., Moosdorf, N., Stevanovic, Z., and Veni, G., 2020, Global distribution of carbonate rocks and karst water resources: Hydrogeology Journal, v. 28, no. 5, p. 1661-1677.

Griebler, C., and Avramov, M., 2015, Groundwater ecosystem services: a review: Freshwater Science, v. 34, no. 1, p. 355-367.

Griebler, C., Fillinger, L., Karwautz, C., and Hose, G. C., 2022, Knowledge gaps, obstacles, and research frontiers in groundwater microbial ecology, *in* Junk, W., Wittman, F., and Griebler, C., Encyclopedia of Inland Waters, Elsevier, p. 611-624.

Griebler, C., and Lueders, T., 2009, Microbial biodiversity in groundwater ecosystems: Freshwater Biology, v. 54, no. 4, p. 649-677.

Guan, X., He, R., Zhang, B., Gao, C., and Liu, F., 2023, Seasonal variations of microbial community structure, assembly processes, and influencing factors in karst river: Frontiers in Microbiology, v. 14, p. 1133938.

Guerry, P., LeBlanc, D. J., Falkow, S., 1973, General method for the isolation of plasmid deoxyribonucleic acid: Journal of Bacteriology, v. 116, no. 2, p. 1064-1066.

Gunn, J., Hardwhick, P., and Wood, P., 2000, The invertebrate community of the Peak-Speedwell Cave system, Derbyshire, England: pressures and considerations for conservation management: Aquatic Conservation, Marine and Freshwater Ecosystems, v. 10, no. 5, p. 353-369.

Hammer, Ø., Harper, D. A. T., and Ryan, P. D., 2001, PAST: PAleontological STatistics software package for education and data analysis: Palaeontologia Electronica, v. 4, no. 1, p. 9.

Hampson, P. S., Treece, M. W., Johnson, G. C., Ahlstedt, S. A., and Connell, J. F., 2000, Water Quality in the Upper Tennessee River Basin, Tennessee, North Carolina, Virginia, and Georgia 1994–98: U.S. Geological Survey Circular 1205, 32 p., https://pubs.water.usgs.gov/circ1205/.

Hathaway, J., Garcia, M., Balasch, M., Spilde, M., Stone, F., Dapkevicius, M., Amorim, I., Gabriel, R., Borges, P., and Northup, D., 2012, Comparison of bacterial diversity in Azorean and Hawaiian lava tube cave microbial mats: Geomicrobiology Journal, v. 31, p. 205-220.

He, G., Zhao, X., and Yu, M., 2021, Exploring the multiple disturbances of karst landscape in Guilin World Heritage Site, China: Catena, v. 203, p. 43-59.

Heinz, B., Birk, S., Liedl, R., Geyer, T., Straub, K. L., Andresen, J., Bester, K., and Kappler, A., 2008, Water quality deterioration at a karst spring (Gallusquelle, Germany) due to combined sewer overflow: Evidence of bacterial and micro-pollutant contamination: Environmental Geology, v. 57, p. 797-808.

Hirsch, P., and Rades-Rohkol, E., 1983, Microbial diversity in a groundwater aquifer in northern Germany: Microbiology, v. 24, p. 183-200.

Hofmann, R., and Griebler, C., 2018, DOM and bacterial growth efficiency in oligotrophic groundwater: absence of priming and co-limitation by organic carbon and phosphorus: Aquatic Microbial Ecology, v. 81, no. 1, p. 55-71.

Howarth, F. G., 1983, The conservation of cave invertebrates, *in* Mylroie, J.E. (ed.) Proceedings of the First International Cave Management Symposium, Murray, Kentucky, p. 57-64.

Howarth, F. G., James, S. A., McDowell, W., Preston, D. J., and Imada, C. T., 2007, Identification of roots in lava tube caves using molecular techniques: implications for conservation of cave arthropod faunas: Journal of Insect Conservation, v. 11, no. 3, p. 251-261.

Huebsch, M., Horan, B., Blum, P., Richards, K. G., Grant, J., and Fenton, O., 2013, Impact of agronomic practices of an intensive dairy farm on nitrogen concentrations in a karst aquifer in Ireland: Agriculture, Ecosystems & Environment, v. 179, p. 187-199.

Hughes, J., Whisnant, R., Weller, L., Eskaf, S., Richardson, M., Morrissey, S., and Altz-Stamm, B., 2005, Drinking water and wastewater infrastructure in Appalachia: The University of North Carolina at Chapel Hill, 150 p.

Hunsaker, C. T., and Levine, D. A., 1995, Hierarchical approaches to the study of water quality in rivers: BioScience, v. 45, no. 3, p. 193-203.

Jianfeng, C., and Timothy, T., 2021, Fast, accurate, and robust analysis of environmental samples according to US EPA Method 6010D, Thermo Scientific, https://assets.thermofisher.com/TFS-Assets/CMD/Application-Notes/an-74146-icp-oes-env-samples-epa-method-6010d-an74146-en.pdf.

Jiang, L., and O'Neill, B. C., 2017, Global urbanization projections for the shared socioeconomic pathways: Global Environmental Change, v. 42, p. 193-199.

Johnson, T. B., McKay, L. D., Layton, A. C., Jones, S. W., Johnson, G. C., Cashdollar, J. L., Dahling, D. R., Villegas, L. F., Fout, G. S., Williams, D. E., and Sayler, G., 2011, Viruses and bacteria in karst and fractured rock aquifers in East Tennessee, USA: Ground Water, v. 49, no. 1, p. 98-110.

Jurado, V., Laiz, L., Rodriguez-Nava, V., Boiron, P., Hermosin, B., Sanchez-Moral, S., and Saiz-Jimenez, C., 2010, Pathogenic and opportunistic microorganisms in caves: International Journal of Speleology, v. 39, no. 1, p. 15-24.

Justus, C. M., Pasini, A., Raminelli, J., and Azeredo Gonçalves, L. S., 2020, Chemical elements in the water of the São Pedro river basin, Faxinal - Paraná: Agricultural Siences, v. 41, no. 3, p. 743.

Kaiser, R. A., Polk, J. S., Datta, T., Parekh, R. R., and Agga, G. E., 2022, Occurrence of antibiotic resistant bacteria in urban karst groundwater systems: Water, v. 14, no. 6, p. 960.

Karwautz, C., Zhou, Y., Kerros, M.-E., Weinbauer, M. G., and Griebler, C., 2022, Bottom-up control of the groundwater microbial food-web in an alpine aquifer: Frontiers in Ecology and Evolution, v. 10, p. 854228.

Keenan, S. W., Patterson, A., Niemiller, M. L., and Slay, M. E., 2017, Observations of the first stygobiont snail (Hydrobiidae, Fontigens sp.) in Tennessee: Conference: 17th International Congress of Speleology, p. 91-94.

Kiehl, A., 2024, Helene by the numbers: How much rain fell in Tennessee? How high did rivers crest? How many died?, Knoxville News Sentinel: Knoxville News Sentinel, Knoxville News Sentinel, p. 1-4.

Krescic, N., and Stevanovic, Z., 2010, Groundwater Hydrogeology of Springs, Management and Sustainability: Oxford, United Kingdom, 573 p.

Lee, N., Meisinger, D., Aubrecht, R., Kovacik, L., Saiz-Jimenez, C., Baskar, S., Baskar, R., Liebl, W., Porter, M., and Engel, A., 2012, Caves and karst environments, *in* Bell, E.M., ed., Life at Extremes: Environments, Organisms, and Strategies for Survival, Wallingford, U.K., p. 320-344.

Liao, H.-W., Jiang, Z.-C., Zhou, H., Qin, X.-Q., Huang, Q.-B., and Wu, H.-Y., 2023, Heavy metal pollution and health risk assessment in karst basin around a lead-zinc mine: Chinese Journal of Environment Science, v. 11, p. 6085-6094.

Lindsey, B. D., J.S., R., and T.M., Z., 2002, Microbiological quality of water from noncommunity supply wells in carbonate and crystalline aquifers of Pennsylvania: U.S. Geological Survey Water-Resources Investigations Report 2001–4268, 30 p., https://pubs.er.usgs.gov/publication/wri014268.

Liu, Y., Huang, X., Yang, H., and Zhong, T., 2014, Environmental effects of land-use/cover change caused by urbanization and policies in Southwest China Karst area – A case study of Guiyang: Habitat International, v. 44, p. 339-348.

Luo, C., Routh, J., Dario, M., Sarkar, S., Wei, L., Luo, D., and Liu, Y., 2020, Distribution and mobilization of heavy metals at an acid mine drainage affected region in South China, a post-remediation study: Science of The Total Environment, v. 724, p. 138122.

Madsen, E., and Ghiorse, W., 1993, Groundwater microbiology: subsurface ecosystem processess, *in* Ford, T., ed., Aquatic Microbial Ecology- An Ecological Approach: Oxford, UK, Blackwell, p. 167-213.

Magesh, N. S., Chandrasekar, N., and Elango, L., 2017, Trace element concentrations in the groundwater of the Tamiraparani river basin, South India: Insights from human health risk and multivariate statistical techniques: Chemosphere, v. 185, p. 468-479.

Mapili, K., Rhoads, W. J., Coughter, M., Pieper, K. J., Edwards, M. A., and Pruden, A., 2022, Occurrence of opportunistic pathogens in private wells after major flooding events: A four state molecular survey: Science of the Total Environment, v. 826, p. 153901.

Medina, M. J., Antić, D., Borges, P. A. V., Borko, Š., Fišer, C., Lauritzen, S.-E., Martín, J. L., Oromí, P., Pavlek, M., Premate, E., Puliafico, K. P., Sendra, A., and Reboleira, A. S. P. S., 2023, Temperature variation in caves and its significance for subterranean ecosystems: Scientific Reports, v. 13, no. 1, p. 20735.

Milici, R. C., 1973, The stratigraphy of Knox County, Tennessee: Tennessee Division of Geology Bulletin, no. 70, p. 9-24.

Mitchell, K., and Takacs-Vesbach, C., 2008, A comparison of methods for total community DNA preservation and extraction from various thermal environments: Journal of the Industrial Microbiology and Biotechnology, v. 35, p. 1139-1147.

Moneymaker, B., 1929, The Caves of East Tennessee [Masters of Science in Education], University of Tennessee, 49-50 p.

Motta, A. L. L., Motta, N. L., Sales, D. d. S., Sales, C. M. R., Nunes, C. H., and Viana, R. d. S., 2025, Heavy metal water contamination: Anthropogenic sources and environmental and public health implications: Revista de Gestão Social e Ambiental, v. 19, no. 5, p. e012300, https://doi.org/10.24857/rgsa.v19n5-069.

Neimiller, M. L., Carter, E. T., Gladstone, N. S., Neimiller, D. K., Hayter, L. E., Engel, A. S., Miller, B. T., and Fitzpatrick, B. M., 2021, Distribution, ecology, life history, and conservation status of the Berry Cave Salamander (*Gyrinophilus gulolineatus*): Herpetological Conservation and Biology, v. 16, no. 3, p. 686-703.

Overbo, A., Heger, S., and Gulliver, J., 2021, Evaluation of chloride contributions from major point and nonpoint sources in a northern U.S. state: Science of The Total Environment, v. 764, p. 144-179.

Palmer, A. N., 1990, Chapter 8. Groundwater processes in karst terranes, *in* Higgins, C. G., and Coates, D. R., eds., Groundwater Geomorphology: The Role of Subsurface Water in Earth-Surface Processes and Landforms, v. 252, Geological Society of America, p. 177-210.

Panno, S. V., Hackley, K. C., Hwang, H. H., and Kelly, W. R., 2001, Determination of the sources of nitrate contamination in karst springs using isotopic and chemical indicators: Chemical Geology, v. 139, p. 113-128.

Parada, A. E., Needham, D. M., and Fuhrman, J. A., 2016, Every base matters: assessing small subunit rRNA primers for marine microbiomes with mock communities, time series and global field samples: Environmental Microbiology, v. 18, no. 5, p. 1403-1414.

Pedersen, K., Arlinger, J., Hallbeck, L., and Pettersson, C., 1996, Diversity and distribution of subterranean bacteria in groundwater at Oklo in Gabon, Africa, as determined by 16S rRNA gene sequencing: Molecular Ecology, v. 5, no. 3, p. 427-436.

Pérez-Castresana, G., CastañedaRoldán, E., García Suastegui, W. A., Morán Perales, J. L., Cruz Montalvo, A., and Handal Silva, A., 2019, Evaluation of health risks due to heavy metals in a rural population exposed to Atoyac River pollution in Puebla, Mexico: Water, v. 11, no. 2, p. 277, https://doi.org/10.3390/w11020277.

Piano, E., Biagioli, F., Nicolosi, G., Coleine, C., Poli, A., Prigione, V., Zanellati, A., Addesso, R., Varese, G. C., Selbmann, L., and Isaia, M., 2023, Tourism affects microbial assemblages in show caves: Science of The Total Environment, v. 871, p. 162106.

Power, J., and Schepers, J., 1989, Nitrate contamination of groundwater in North America: Agriculture, Ecosystems & Environment, v. 26, no. 3-4, p. 165-187.

Prescott, R. D., Zamkovaya, T., Donachie, S. P., Northup, D. E., Medley, J. J., Monsalve, N., Saw, J. H., Decho, A. W., Chain, P. S. G., and Boston, P. J., 2022, Islands within islands: Bacterial phylogenetic structure and consortia in Hawaiian lava caves and fumaroles: Frontiers in Microbiology, v. 13, p. 934708.

Probst, A. J., Ladd, B., Jarett, J. K., Geller-Mcgrath, D. E., Sieber, C. M. K., Emerson, J. B., Anantharaman, K., Thomas, B. C., Malmstrom, R. R., Stieglmeier, M., Klingl, A., Woyke, T., Ryan, M. C., and Banfield, J. F., 2018, Differential depth distribution of microbial function and putative symbionts through sediment-hosted aquifers in the deep terrestrial subsurface: Nature Microbiology, v. 3, no. 3, p. 328-336.

Pueyo, M., Mateu, J., Rigol, A., Vidal, M., López-Sánchez, J. F., and Rauret, G., 2008, Use of the modified BCR three-step sequential extraction procedure for the study of trace element dynamics in contaminated soils: Environmental Pollution, v. 152, no. 2, p. 330-341.

Quast, C., Pruesse, E., Yilmaz, P., Gerken, J., Schweer, T., Yarza, P., Peplies, J., and Glöckner, F. O., 2012, The SILVA ribosomal RNA gene database project: improved data processing and web-based tools: Nucleic Acids Research, v. 41, no. D1, p. 590-596.

Ramey, M., 1971, TN KN82 Cave Narrative, TCS narrative file for Knox County, Tennessee, Tennessee Cave Survey Inc. https://tennesseecavesurvey.org/, p. 55-56.

Rauret, G., Lopez-Sanchez, J. F., Sahuquillo, A., Rubio, R., Davidson, C., Ure, A., and Quevauviller, P., 1999, Improvement of the BCR three step sequential extraction procedure prior to the certification of new sediment and soil reference materials: Journal of Environmental Monitoring, v. 1, no. 1, p. 57-61.

Reboleira, A. S., Borges, P., Gonçalves, F., Serrano, A., and Oromí, P., 2011, The subterranean fauna of a biodiversity hotspot region - Portugal: an overview and its conservation: International Journal of Speleology, v. 40, no. 1, p. 23-37.

Reboleira, A. S. P. S., Abrantes, N., Oromí, P., and Gonçalves, F., 2013, Acute toxicity of copper sulfate and potassium dichromate on stygobiont proasellus: General aspects of groundwater ecotoxicology and future perspectives: Water, Air, & Soil Pollution, v. 224, no. 5, p. 1550.

Schirmer, M., Leschik, S., and Musolff, A., 2013, Current research in urban hydrogeology – A review: Advances in Water Resources, v. 51, p. 280-291.

Schloss, P. D., 2020, Reintroducing mothur: 10 years later: Applied and Environmental Microbiology, v. 86, no. 2, p. e02343-02319.

Schloss, P. D., Westcott, S. L., Ryabin, T., Hall, J. R., Hartmann, M., Hollister, E. B., Lesniewski, R. A., Oakley, B. B., Parks, D. H., Robinson, C. J., Sahl, J. W., Stres, B., Thallinger, G. G., Van Horn, D. J., and Weber, C. F., 2009, Introducing mothur: Open-source, platform-independent, community-supported software for describing and comparing microbial communities: Applied and Environmental Microbiology, v. 75, no. 23, p. 7537-7541.

Somerville, C. C., Knight, I. T., Straube, W. L., and Colwell, R. R., 1989, Simple, rapid method for direct isolation of nucleic acids from aquatic environments: Applied and Environmental Microbiology, v. 55, no. 3, p. 548-554.

Spens, J., Evans, A. R., Halfmaerten, D., Knudsen, S. W., Sengupta, M. E., Mak, S. S. T., Sigsgaard, E. E., Hellström, M., and Yu, D., 2016, Comparison of capture and storage methods for aqueous macrobial eDNA using an optimized extraction protocol: advantage of enclosed filter: Methods in Ecology and Evolution, v. 8, no. 5, p. 635-645.

Stevanović, Z., 2019, Karst waters in potable water supply: a global scale overview: Environmental Earth Sciences, v. 78, no. 23, p. 662.

Stim, K., 1995, A phylogenetic analysis of microorganisms isolated from subsurface environments: Molecular Ecology, v. 4, p. 1-10.

Tennessee Department of Environmental Conservation, 2007, Watershed water quality management plan, Division of Water Pollution Control, Tennessee Department of Environment and Conservation, Division of Water Resources; Nashville, Tennessee.

Tennessee Department of Health, 2003, Private Water Supply, Environmental Health Topics: https://www.tn.gov/health/cedep/environmental/environmental-health-topics/eht/private-water-supply.html.

Trajano, E., 2000, Cave faunas in the atlantic tropical rain forest: Composition, ecology, and conservation: Biotropica, v. 32, no. 4b, p. 882-893.

U.S. Environmental Protection Agency, 2006, National primary drinking water regulations: Groundwater rule; Final rule, Volume 71: Federal Register, Federal Register, p. 65574-65660.

-, 2012, Recreational water quality criteria and methods, Water quality criteria, Office of Water: https://www.epa.gov/wqc/recreational-water-quality-criteria-and-methods.

-, 2016, Definition and procedure for the determination of the method detection limit, Office of Water: https://www.epa.gov/cwa-methods.

-, 2018, EPA Method 6010D (SW-846): Inductively Coupled Plasma, ThermoFischer Scientific: https://www.epa.gov/esam.

-, 2024, National Primary Drinking Water Regulations, Office of Water: https://www.epa.gov/ground-water-and-drinking-water/national-primary-drinking-water-regulations.

Van Beynen, P., and Townsend, K., 2005, A disturbance index for karst environments: Environmental Management, v. 36, no. 1, p. 101-116.

Vesper, D., 2001, Contaminant transport in karst aquifers: Theoretical and Applied Karstology, v. 13, no. 14, p. 101-111.

Viles, H. A., 2003, Conceptual modeling of the impacts of climate change on karst geomorphology in the UK and Ireland: Journal for Nature Conservation, v. 11, no. 1, p. 59-66.

Wang, H., and Zhang, Q., 2019, Research advances in identifying sulfate contamination sources of water environment by using stable isotopes: International Journal of Environmental Research and Public Health, v. 16, no. 11, p. 1914.

Wang, Z., Torres, M., Paudel, P., Hu, L., Yang, G., and Chu, X., 2020, Assessing the karst groundwater quality and hydrogeochemical characteristics of a prominent dolomite aquifer in Guizhou, China: Water, v. 12, no. 9, p. 25-84.

White, W., 2002, Karst hydrology: recent developments and open questions: Engineering Geology, v. 65, no. 2-3, p. 85-105.

Xu, C., Li, Z., and Li, D., 2020, Heavy metal content and health risk assessment of karst cave water in Guizhou: Fresenius Environmental Bulletin, v. 29, no. 4, p. 2378-2389.

Xu, C., Yan, H., and Zhang, S., 2021, Heavy metal enrichment and health risk assessment of karst cave fish in Libo, Guizhou, China: Alexandria Engineering Journal, v. 60, no. 1, p. 1885-1896.

Yang, P., Wang, Y., Wu, X., Chang, L., Ham, B., Song, L., and Groves, C., 2020a, Nitrate sources and biogeochemical processes in karst underground rivers impacted by different anthropogenic input characteristics: Environmental Pollution, v. 265, p. 114835.

Yang, Y., Wang, Y., Hou, X., Lin, Y., Yang, L., Hou, X., and Zheng, C., 2020b, Can low-temperature point discharge Be used as atomic emission source for sensitive determination of cyclic volatile methylsiloxanes?: Analytica Chimica Acta, v. 1124, p. 121-128.

Yavari-Bafghi, M., Rezaei Somee, M., Amoozegar, M. A., Dastgheib, S. M. M., and Shavandi, M., 2023, Genome-resolved analyses of oligotrophic groundwater microbial communities along phenol pollution in a continuous-flow biodegradation model system: Frontiers in Microbiology, v. 14, p. 147-162.

Yuan, J., Xu, F., Deng, G., Tang, Y., and Li, P., 2017, Hydrogeochemistry of shallow groundwater in a karst aquifer system of Bijie City, Guizhou Province.: Water, v. 9, p. 625, https://doi.org/10.3390/w9080625.

Zampella, R. A., Procopio, N. A., Lathrop, R. G., and Dow, C. L., 2007, Relationship of land-use/land-cover patterns and surface-water quality in the Mullica River Basin: Journal of the American Water Resources Association, v. 43, no. 3, p. 594-604.

Zarcinas, B. A., 2002, Comparison of the lead 168-nm and 220-nm analytical lines in high iron and aluminium matrices by inductively coupled plasmaoptical emission spectrometry: The Science of the Total Environment, v. 295, p. 241-244.

Zhang, C., Yu, Z.-G., Zeng, G.-M., Jiang, M., Yang, Z.-Z., Cui, F., Zhu, M.-Y., Shen, L.-Q., and Hu, L., 2014, Effects of sediment geochemical properties on heavy metal bioavailability: Environment International, v. 73, p. 270-281.

Zhang, C., and Yuan, D., 2004, The relationship between water quality and land use in the typical karst groundwater basin in Guizhou: Chin. J. Water Resour. Res., v. 18, p. 134-137.

Zhao, M., Zeng, C., Liu, Z., a nd Wang, S., 2010, Effect of different land use/land cover on karst hydrogeochemistry: A paired catchment study of Chenqi and Dengzhanhe, Puding, Guizhou, SW China: Journal of Hydrology, v. 388, no. 1-2, p. 121-130.

Zhou, J., Bruns, M., Tiedje, J. M., 1996, DNA recovery from soils of diverse composition: Applied and Environmental Microbiology, v. 62, no. 2, p. 316-322.

Zhu, H.-Z., Zhang, Z.-F., Zhou, N., Jiang, C.-Y., Wang, B.-J., Cai, L., Wang, H.-M., and Liu, S.-J., 2021, Bacteria and metabolic potential in karst caves revealed by intensive bacterial cultivation and genome assembly: Applied and Environmental Microbiology, v. 87, no. 6, p. e02440-02420.

APPENDICES

Appendix A

Table A.1. Trace elements concentrations for the cave streams. Concentrations are in ppm (mg/L). BDL = below detection limit, based on the Qtegra Limit of Detection for each element.

Element	**As**	**Ba**	**Cd**	**Cu**	**Fe**	**Mg**	**Mn**	**P**	**Pb**	**Si**	**Sr**
Limit of Detection	0.001	0.01	0.0001*	0.0001*	0.001	0.01	0.00001	0.01	0.001	0.01	0.0001*
ETN.190711.KN14	BDL	0.03	BDL	0.0002	BDL	29.9	BDL	BDL	BDL	4.9	0.08
ETN.240816.KN14	BDL	0.04	BDL	BDL	BDL	302	0.0012	BDL	BDL	4.9	0.08
ETN.190627.KN24	0.002	0.02	BDL	0.0005	BDL	4.4	BDL	0.04	0.001	3.4	0.11
ETN.240813.KN24	0.001	0.03	0.0003	BDL	BDL	5.8	0.0006	0.03	BDL	3.8	0.14
ETN.240930.KN24	BDL	0.02	BDL	BDL	BDL	6.1	0.00007	0.04	BDL	3.6	0.13
ETN.190709.KN62	0.001	0.04	BDL	0.0002	BDL	11.4	BDL	BDL	BDL	3.5	0.09
ETN.240908.KN62	BDL	0.05	BDL	BDL	BDL	12.6	0.0007	BDL	BDL	3.7	0.11
ETN.241004.KN62	0.001	0.05	BDL	0.0007	BDL	13.3	0.0005	BDL	BDL	3.4	0.10
ETN.190625.KN82	0.001	0.03	BDL	0.0008	0.07	7.5	0.04	BDL	BDL	3.7	0.15
ETN.240816.KN82	0.001	0.03	BDL	0.0002	BDL	7.0	0.007	BDL	BDL	3.6	0.14
ETN.241005.KN82	0.002	0.03	0.0001	0.0002	BDL	11.8	0.0003	BDL	0.001	2.3	0.12
ETN.190803.KN103	0.001	0.04	BDL	BDL	BDL	33.6	BDL	BDL	BDL	4.3	0.04
ETN.240908.KN103	0.001	0.04	BDL	BDL	BDL	36.1	BDL	BDL	BDL	4.5	0.04
ETN.241004.KN103	BDL	0.04	BDL	BDL	BDL	34.2	BDL	BDL	BDL	4.4	0.04
ETN.190808.KN145	BDL	0.04	BDL	BDL	BDL	34.7	BDL	BDL	BDL	4.8	0.05
ETN.240915.KN145	0.001	0.04	BDL	BDL	BDL	37.0	BDL	BDL	BDL	4.9	0.06
ETN.241002.KN145	BDL	0.04	BDL	BDL	BDL	35.7	0.0005	BDL	BDL	4.7	0.06
ETN.190728.RN5	BDL	0.02	BDL	BDL	BDL	24.0	0.00005	BDL	BDL	4.2	0.03
ETN.240911.RN5	BDL	0.02	BDL	BDL	BDL	32.1	BDL	BDL	BDL	4.5	0.03
ETN.241006.RN5	0.001	0.02	BDL	BDL	BDL	30.9	0.0010	BDL	BDL	4.4	0.03
ETN.190728.RN6	0.002	0.04	BDL	BDL	BDL	21.0	BDL	BDL	BDL	4.0	0.02
ETN.240918.RN6	BDL	0.05	BDL	BDL	BDL	30.3	BDL	BDL	BDL	4.3	0.03
ETN.241006.RN6	0.002	0.05	BDL	BDL	BDL	29.9	BDL	BDL	BDL	4.3	0.03

*These detection limits used the MDL

Table A.2. Extracted trace element concentrations and standard deviations measured from the cave sediments, reported duplicates. Concentrations are in ppm. BDL = below detection limit, based on the Qtegra Limit of Detection for each element.

Sample ID	Al	As	Ba	Cd	Cu	Fe	Mn	Mo	Ni	Pb	Sr	Zn
Limit of Detection	0.1	0.01	0.001	0.1	1	1	0.1	1*	1	1	0.0001	1
ETN.190711.KN14.S1	65.08 ± 21.18	0.48 ± 0.21	8.75 ± 1.37	BDL	1.54 ± 1.16	3.32 ± 0.41	97.81 ± 27.53	BDL	BDL	BDL	6.72 ± 1.45	4.60 ± 0.19
ETN.190711.KN14.S2	45.22 ± 6.31	0.53 ± 0.21	11.29 ± 2.58	BDL	BDL	5.32 ± 0.33	92.67 ± 26.86	BDL	BDL	BDL	6.93 ± 1.02	4.28 ± 0.72
ETN.240816.KN14.S1	96.50 ± 46.27	0.57 ± 0.11	14.25 ± 1.34	BDL	1.41 ± 1.36	2.45 ± 0.41	46.11 ± 3.60	BDL	BDL	BDL	4.84 ± 0.16	3.43 ± 0.72
ETN.240816.KN14.S2	50.32 ± 14.80	0.27 ± 0.20	9.95 ± 0.30	BDL	BDL	1.07 ± 0.35	55.60 ± 41.91	BDL	BDL	BDL	5.10 ± 2.05	4.02 ± 1.36
ETN.190627.KN24.S1	51.71 ± 10.97	0.23 ± 0.22	41.74 ± 4.66	BDL	BDL	4.67 ± 0.62	1433.62 ± 187.75	BDL	1.73 ± 0.10	BDL	14.73 ± 2.53	17.23 ± 0.20
ETN.190627.KN24.S2	71.18 ± 2.46	0.65 ± 0.01	36.45 ± 1.19	BDL	BDL	3.19 ± 0.30	1099.72 ± 29.17	BDL	1.68 ± 0.06	BDL	13.89 ± 0.43	15.74 ± 0.29
ETN.230813.KN24.S1	48.38 ± 2.17	0.32 ± 0.17	41.51 ± 1.57	0.13 ± 0.03	BDL	BDL	494.84 ± 40.85	BDL	1.07 ± 0.15	BDL	17.06 ± 0.82	15.02 ± 0.88
ETN.230813.KN24.S2	52.65 ± 12.24	0.46 ± 0.19	28.20 ± 4.57	BDL	1.22 ± 0.64	1.21 ± 0.29	586.24 ± 105.83	BDL	1.01 ± 0.18	BDL	13.50 ± 1.10	13.45 ± 1.72
ETN.240930.KN24.S1	52.31 ± 1.42	0.28 ± 0.03	35.08 ± 1.59	BDL	BDL	BDL	528.04 ± 64.96	BDL	BDL	BDL	16.09 ± 0.15	18.64 ± 1.77
ETN.240930.KN24.S2	38.90 ± 3.71	BDL	30.78 ± 4.65	BDL	1.24 ± 0.88	BDL	297.40 ± 33.12	BDL	BDL	BDL	16.26 ± 2.00	12.23 ± 1.53
ETN.190709.KN62.S1	39.24 ± 10.45	0.82 ± 0.15	15.49 ± 2.72	BDL	BDL	BDL	172.38 ± 38.47	BDL	BDL	BDL	4.42 ± 0.27	8.02 ± 1.66
ETN.190709.KN62.S2	26.17 ± 2.06	BDL	15.42 ± 2.39	BDL	BDL	BDL	58.91 ± 9.55	BDL	BDL	BDL	2.45 ± 0.05	2.83 ± 0.31
ETN.241004.KN62.S1	53.67 ± 9.34	0.19 ± 0.05	17.08 ± 1.86	BDL	1.04 ± 0.18	BDL	188.52 ± 77.28	BDL	BDL	BDL	9.38 ± 0.95	7.90 ± 2.49
ETN.241004.KN62.S2	49.88 ± 16.99	0.54 ± 0.32	16.75 ± 1.50	BDL	BDL	BDL	228.94 ± 37.49	BDL	BDL	BDL	8.88 ± 1.21	7.90 ± 2.49
ETN.190625.KN82.S1	31.46 ± 19.92	0.32 ± 0.17	31.16 ± 16.49	0.27 ± 0.07	BDL	BDL	274.31 ± 117.07	BDL	1.81 ± 0.58	BDL	4.64 ± 1.88	11.38 ± 3.17
ETN.240816.KN82.S1	49.14 ± 11.35	0.18 ± 0.18	28.31 ± 5.48	0.24 ± 0.02	BDL	BDL	266.93 ± 50.95	BDL	BDL	BDL	2.94 ± 0.53	14.18 ± 2.05
ETN.240816.KN82.S2	60.27 ± 8.35	0.48 ± 0.29	34.14 ± 1.55	0.27 ± 0.01	BDL	BDL	390.63 ± 12.44	BDL	1.03 ± 0.03	BDL	3.01 ± 0.10	15.57 ± 0.46

*This detection limits uses the MDL

Table A.2. Continued.

Sample ID	Al	As	Ba	Cd	Cu	Fe	Mn	Mo	Ni	Pb	Sr	Zn
ETN.241005.KN82.S1	66.87 ± 15.63	0.38 ± 0.15	31.94 ± 5.85	0.22 ± 0.04	BDL	1.06 ± 0.56	933.79 ± 224.68	BDL	BDL	BDL	2.30 ± 0.42	9.25 ± 2.03
ETN.190625.KN82.S2	30.13 ± 1.01	0.56 ± 0.01	41.33 ± 9.19	0.27 ± 0.08	0.49 ± 0.15	BDL	1338.64 ± 343.04	BDL	3.41 ± 0.73	1.22 ± 0.10	5.34 ± 1.64	12.52 ± 2.17
ETN.241005.KN82.S1	49.14 ± 11.35	0.18 ± 0.18	28.31 ± 5.48	0.24 ± 0.02	0.25 ± 0.03	BDL	266.93 ± 50.95	0.01 ± 0.01	0.84 ± 0.18	0.19 ± 0.06	2.94 ± 0.53	14.18 ± 2.05
ETN.241005.KN82.S2	60.27 ± 8.35	0.48 ± 0.29	34.14 ± 1.55	0.27 ± 0.01	0.28 ± 0.07	BDL	390.63 ± 12.44	BDL	1.03 ± 0.03	0.33 ± 0.15	3.01 ± 0.10	15.57 ± 0.46
ETN.190803.KN103.S1	66.87 ± 15.63	0.38 ± 0.15	31.94 ± 5.85	0.22 ± 0.04	0.21 ± 0.02	1.06 ± 0.56	933.79 ± 224.68	BDL	0.97 ± 0.17	0.87 ± 0.26	2.30 ± 0.42	9.25 ± 2.03
ETN.190803.KN103.S2	104.69 ± 43.24	0.29 ± 0.01	36.94 ± 8.55	0.13 ± 0.04	0.19 ± 0.10	2.33 ± 1.35	562.40 ± 160.79	BDL	0.44 ± 0.18	0.71 ± 0.23	1.99 ± 0.24	5.02 ± 1.44
ETN.240908.KN103.S1	53.99 ± 4.14	0.22 ± 0.01	20.67 ± 1.53	BDL	0.70 ± 0.21	33.05 ± 21.88	1431.19 ± 283.35	BDL	0.24 ± 0.11	2.13 ± 0.07	26.14 ± 6.59	3.29 ± 0.62
ETN.240908.KN103.S2	38.20 ± 4.30	0.44 ± 0.42	18.55 ± 0.77	0.02 ± 0.01	0.61 ± 0.21	11.27 ± 2.03	936.97 ± 223.80	BDL	0.20 ± 0.14	1.58 ± 0.50	34.54 ± 2.22	3.74 ± 0.16
ETN.241004.KN103.S1	47.84 ± 8.02	0.75 ± 0.04	20.86 ± 1.57	0.02 ± 0.01	0.57 ± 0.52	BDL	297.47 ± 15.34	BDL	0.29 ± 0.13	0.57 ± 0.14	11.26 ± 0.15	5.22 ± 0.17
ETN.241004.KN103.S2	32.34 ± 4.90	0.76 ± 0.14	14.45 ± 1.85	0.02 ± 0.01	0.23 ± 0.12	BDL	134.07 ± 42.14	BDL	0.13 ± 0.01	0.31 ± 0.12	7.47 ± 2.00	3.76 ± 0.41
ETN.190808.KN145.S1	21.26 ± 3.40	0.34 ± 0.10	15.16 ± 1.32	0.14 ± 0.02	0.24 ± 0.09	BDL	19.57 ± 6.35	BDL	0.44 ± 0.21	0.51 ± 0.02	5.61 ± 1.65	3.69 ± 0.19
ETN.190808.KN145.S2	19.24 ± 4.31	0.45 ± 0.27	16.19 ± 1.85	0.17 ± 0.04	1.12 ± 1.20	BDL	21.11 ± 7.19	BDL	0.61 ± 0.33	0.24 ± 0.05	5.59 ± 1.56	3.97 ± 0.78
ETN.240915.KN145.S1	13.08 ± 7.94	0.34 ± 0.10	17.24 ± 0.18	0.17 ± 0.01	0.35 ± 0.22	BDL	30.64 ± 5.07	0.03 ± 0.02	0.72 ± 0.02	0.36 ± 0.06	8.24 ± 1.39	4.84 ± 0.49
ETN.240915.KN145.S2	13.32 ± 4.80	0.37 ± 0.01	22.42 ± 1.80	0.19 ± 0.01	0.10 ± 0.05	BDL	26.51 ± 2.33	0.02 ± 0.02	0.64 ± 0.01	0.46 ± 0.29	7.90 ± 1.03	2.97 ± 0.46
ETN.241002.KN145.S1	15.98 ± 2.06	0.56 ± 0.20	12.36 ± 2.79	0.13 ± 0.04	0.25 ± 0.07	BDL	22.65 ± 9.39	BDL	0.49 ± 0.26	0.44 ± 0.22	5.17 ± 1.94	3.40 ± 0.38
ETN.241002.KN145.S2	26.07 ± 7.83	0.71 ± 0.16	16.21 ± 1.22	0.14 ± 0.02	0.43 ± 0.12	BDL	21.20 ± 4.20	BDL	0.55 ± 0.11	0.21 ± 0.01	6.66 ± 1.32	4.85 ± 0.04
ETN.190728.RN5.S1	5.25 ± 4.57	0.33 ± 0.03	4.02 ± 1.14	0.11 ± 0.02	0.15 ± 0.08	BDL	50.11 ± 9.19	BDL	0.51 ± 0.28	0.15 ± 0.03	9.07 ± 2.06	1.99 ± 0.21
ETN.190728.RN5.S2	3.80 ± 0.94	0.67 ± 0.19	7.40 ± 0.53	0.09 ± 0.03	0.25 ± 0.06	BDL	31.82 ± 0.70	0.02 ± 0.02	0.73 ± 0.18	0.31 ± 0.10	10.83 ± 1.88	2.42 ± 0.12
ETN.240911.RN5.S1	4.19 ± 3.54	0.35 ± 0.11	7.92 ± 1.21	0.13 ± 0.02	0.31 ± 0.07	BDL	30.35 ± 5.70	BDL	0.17 ± 0.12	0.42 ± 0.18	17.77 ± 2.94	1.93 ± 0.26
ETN.240911.RN5.S2	3.02 ± 0.93	0.52 ± 0.11	6.19 ± 1.32	0.04 ± 0.01	0.08 ± 0.01	BDL	10.57 ± 1.59	BDL	0.15 ± 0.01	0.28 ± 0.07	11.12 ± 0.98	1.30 ± 0.06

Table A.2. Continued.

Sample ID	Al	As	Ba	Cd	Cu	Fe	Mn	Mo	Ni	Pb	Sr	Zn
ETN.241006.RN5.S1	10.45 ± 4.84	0.28 ± 0.18	17.99 ± 1.82	0.08 ± 0.04	0.22 ± 0.08	BDL	14.30 ± 2.69	BDL	0.16 ± 0.07	0.98 ± 0.01	13.60 ± 4.60	2.85 ± 0.18
ETN.241006.RN5.S2	1.64 ± 0.20	0.19 ± 0.02	2.22 ± 0.51	0.04 ± 0.02	0.26 ± 0.17	BDL	19.86 ± 2.14	BDL	0.08 ± 0.04	BDL	11.51 ± 0.11	0.66 ± 0.10
ETN.190728.RN6.S1	86.34 ± 27.02	BDL	20.02 ± 4.95	0.05 ± 0.02	0.27 ± 0.07	2.61 ± 1.39	191.74 ± 79.21	BDL	0.69 ± 0.14	0.10 ± 0.06	0.55 ± 0.12	2.86 ± 0.49
ETN.190728.RN6.S2	97.87 ± 13.45	0.44 ± 0.01	22.48 ± 4.58	0.03 ± 0.02	0.08 ± 0.06	3.45 ± 0.14	123.03 ± 34.12	BDL	0.75 ± 0.03	0.10 ± 0.08	0.58 ± 0.21	2.58 ± 0.33
ETN.240918.RN6.S1	49.41 ± 20.20	0.22 ± 0.14	24.27 ± 7.40	0.02 ± 0.01	0.13 ± 0.09	BDL	29.72 ± 9.96	BDL	0.65 ± 0.07	0.13 ± 0.01	1.82 ± 0.38	2.51 ± 0.71
ETN.240918.RN6.S2	56.41 ± 15.83	0.54 ± 0.01	31.76 ± 6.96	BDL	0.08 ± 0.02	BDL	31.46 ± 7.84	BDL	0.32 ± 0.04	0.35 ± 0.08	1.65 ± 0.23	1.20 ± 0.37
ETN.241006.RN6.S1	76.05 ± 22.32	0.50 ± 0.05	37.82 ± 1.43	0.04 ± 0.02	0.12 ± 0.09	2.79 ± 0.87	1049.40 ± 61.52	BDL	0.56 ± 0.12	0.55 ± 0.10	2.10 ± 0.13	1.39 ± 0.22
ETN.241006.RN6.S2	115.35 ± 30.25	0.32 ± 0.14	46.78 ± 6.15	0.08 ± 0.02	0.19 ± 0.10	5.97 ± 1.59	1207.00 ± 153.88	BDL	0.96 ± 0.30	1.51 ± 0.65	2.45 ± 0.24	2.57 ± 0.34
ETN.241006.RN5.S2	1.64 ± 0.20	0.19 ± 0.02	2.22 ± 0.51	0.04 ± 0.02	0.26 ± 0.17	BDL	19.86 ± 2.14	BDL	0.08 ± 0.04	BDL	11.51 ± 0.11	0.66 ± 0.10
ETN.190728.RN6.S1	86.34 ± 27.02	BDL	20.02 ± 4.95	0.05 ± 0.02	0.27 ± 0.07	2.61 ± 1.39	191.74 ± 79.21	BDL	0.69 ± 0.14	0.10 ± 0.06	0.55 ± 0.12	2.86 ± 0.49

Table A.3. Extracted concentrations of Ca, Mg, Na, P, Si and standard deviations measured from the cave sediments, reported duplicates. Concentrations are in ppm. BDL = below detection limit, based on the reporting limit for each element.

Sample ID	**Ca**	**Mg**	**Na**	**P**	**Si**
Limit of Detection	10	0.1	0.001	10	1
ETN.190711.KN14.S1	16725.19 ± 4880.92	8959.28 ± 3750.37	13.89 ± 1.62	BDL	77.47 ± 7.80
ETN.190711.KN14.S2	16605.92 ± 3758.76	8558.97 ± 3642.09	14.21 ± 4.80	11.89 ± 0.40	95.45 ± 16.86
ETN.240816.KN14.S1	9203.82 ± 490.19	3182.44 ± 199.69	7.41 ± 3.01	BDL	142.94 ± 12.37
ETN.240816.KN14.S2	10569.21 ± 6837.84	5283.03 ± 4540.59	7.62 ± 5.10	BDL	87.58 ± 2.32
ETN.190627.KN24.S1	7537.83 ± 1993.78	435.75 ± 66.17	9.60 ± 0.71	48.95 ± 27.99	211.04 ± 11.53
ETN.190627.KN24.S2	6060.80 ± 159.87	635.63 ± 56.33	11.71 ± 0.29	11.74 ± 0.12	225.34 ± 12.42
ETN.230813.KN24.S1	9064.19 ± 1296.07	1275.01 ± 333.11	10.96 ± 0.86	12.08 ± 1.06	234.60 ± 9.60
ETN.230813.KN24.S2	5609.55 ± 404.16	385.97 ± 45.70	8.85 ± 1.88	37.90 ± 1.46	179.83 ± 29.65
ETN.240930.KN24.S1	6646.24 ± 900.90	754.33 ± 363.39	9.31 ± 0.35	20.49 ± 1.36	226.31 ± 13.96
ETN.240930.KN24.S2	9517.85 ± 1932.30	863.05 ± 499.58	10.27 ± 1.10	20.83 ± 7.27	191.39 ± 14.53
ETN.190709.KN62.S1	4022.65 ± 200.66	521.97 ± 9.20	12.51 ± 2.04	BDL	153.67 ± 20.72
ETN.190709.KN62.S2	1551.67 ± 23.78	155.11 ± 13.35	6.72 ± 0.33	BDL	111.51 ± 10.46
ETN.241004.KN62.S1	13005.07 ± 1547.76	2018.06 ± 206.29	43.82 ± 4.09	BDL	140.63 ± 19.49
ETN.241004.KN62.S2	12123.08 ± 1967.51	2105.08 ± 235.18	39.74 ± 7.38	BDL	141.06 ± 14.94
ETN.190625.KN82.S1	7675.39 ± 5408.56	2328.28 ± 1060.74	5.67 ± 3.79	62.18 ± 35.43	132.75 ± 72.32
ETN.190625.KN82.S2	7839.89 ± 4086.49	1954.10 ± 929.68	4.95 ± 1.68	10.10 ± 1.49	115.71 ± 27.72
ETN.240816.KN82.S1	5798.58 ± 1824.12	2360.19 ± 574.10	2.82 ± 1.58	BDL	100.96 ± 25.85
ETN.240816.KN82.S2	6300.85 ± 1062.83	2467.38 ± 346.24	1.56 ± 0.26	BDL	110.73 ± 6.30
ETN.241005.KN82.S1	4254.22 ± 1470.58	1743.73 ± 473.92	0.96 ± 0.55	BDL	113.57 ± 22.41
ETN.241005.KN82.S2	2484.10 ± 1108.66	1053.74 ± 465.59	BDL	BDL	154.73 ± 35.18
ETN.190803.KN103.S1	22245.11 ± 6357.15	592.69 ± 49.25	26.33 ± 2.46	BDL	190.22 ± 18.98
ETN.190803.KN103.S2	37829.82 ± 3755.07	706.31 ± 101.00	25.86 ± 1.30	BDL	168.48 ± 1.47
ETN.240908.KN103.S1	7356.54 ± 867.98	289.51 ± 15.48	18.26 ± 0.47	17.07 ± 4.05	211.14 ± 8.17
ETN.240908.KN103.S2	4931.66 ± 723.67	205.89 ± 43.81	9.47 ± 2.80	BDL	141.72 ± 26.36
ETN.241004.KN103.S1	2538.42 ± 25.36	94.76 ± 2.70	3.51 ± 0.80	BDL	110.87 ± 5.04
ETN.241004.KN103.S2	5364.36 ± 1208.39	257.01 ± 54.80	9.85 ± 3.92	BDL	176.20 ± 49.91

Table A.3. Continued.

Sample ID	**Ca**	**Mg**	**Na**	**P**	**Si**
ETN.190808.KN145.S1	19231.10 ± 6221.89	10488.63 ± 4722.56	14.82 ± 4.43	BDL	102.85 ± 9.09
ETN.190808.KN145.S2	20047.27 ± 6625.14	11114.68 ± 5067.76	16.37 ± 4.98	BDL	107.55 ± 10.94
ETN.240915.KN145.S1	28462.50 ± 6065.39	16474.75 ± 3677.38	21.82 ± 3.86	BDL	92.09 ± 4.16
ETN.240915.KN145.S2	26301.06 ± 4660.32	15061.80 ± 2791.27	18.87 ± 3.26	18.00 ± 4.91	127.63 ± 12.67
ETN.241002.KN145.S1	18233.96 ± 8236.50	10333.98 ± 5550.43	15.06 ± 7.52	BDL	82.02 ± 20.39
ETN.241002.KN145.S2	22697.14 ± 5264.95	11411.23 ± 4451.33	18.04 ± 4.82	423.65 ± 86.16	114.90 ± 13.16
ETN.190728.RN5.S1	28608.12 ± 7111.31	15758.17 ± 3920.58	23.68 ± 6.42	BDL	83.23 ± 12.79
ETN.190728.RN5.S2	30871.67 ± 1667.25	16966.96 ± 443.70	26.44 ± 3.32	10.41 ± 3.94	110.45 ± 8.17
ETN.240911.RN5.S1	34626.56 ± 7534.67	13823.28 ± 3602.91	37.31 ± 8.50	BDL	98.46 ± 14.13
ETN.240911.RN5.S2	35929.95 ± 1764.15	20693.81 ± 861.68	37.30 ± 3.87	BDL	108.61 ± 11.50
ETN.241006.RN5.S1	25794.55 ± 7009.32	9680.29 ± 4161.01	21.78 ± 6.15	63.19 ± 3.00	214.50 ± 31.32
ETN.241006.RN5.S2	35968.84 ± 1484.49	19603.59 ± 1748.91	35.40 ± 3.08	BDL	91.80 ± 9.57
ETN.190728.RN6.S1	482.98 ± 147.69	158.66 ± 59.01	BDL	BDL	79.44 ± 28.17
ETN.190728.RN6.S2	374.25 ± 146.84	138.21 ± 55.83	BDL	BDL	90.79 ± 16.14
ETN.240918.RN6.S1	2138.50 ± 859.52	706.73 ± 240.61	0.45 ± 0.01	125.33 ± 58.14	172.68 ± 55.47
ETN.240918.RN6.S2	1498.58 ± 544.13	564.77 ± 196.83	BDL	25.25 ± 12.10	175.79 ± 32.87
ETN.241006.RN6.S1	3608.90 ± 430.37	1464.15 ± 59.04	0.16 ± 0.01	BDL	127.55 ± 8.69
ETN.241006.RN6.S2	3811.36 ± 444.70	1560.88 ± 162.16	5.11 ± 0.40	BDL	178.14 ± 23.67

Table A.4. Average colony forming units (CFU) and standard deviations per mL for aerobic bacteria, total coliforms, and *E. coli* measured from raw cave stream water. NM= not measured.

Sample ID	**Aerobic bacteria**	**Total coliform**	***E. coli***
ETN.190711.KN14	NM	NM	NM
ETN.240816.KN14	77 ± 7.5	1 ± 0.6	0
ETN.190627.KN24	NM	252*	1*
ETN.230813.KN24	400 ± 53.7	24 ± 2.9	1 ± 1.2
ETN.240930.KN24	402 ± 56.1	15 ± 2.7	1 ± 1.2
ETN.190709.KN62	NM	NM	NM
ETN.241004.KN62	425 ± 87.1	6 ± 1.8	3 ± 2
ETN.190625.KN82	NM	402*	NM
ETN.240816.KN82	347 ± 15.0	9 ± 2.9	0 ± 0.5
ETN.241005.KN82	415 ± 73.7	13 ± 1.5	0
ETN.190803.KN103	NM	NM	0*
ETN.240908.KN103	79 ± 1.2	2 ± 0.3	0
ETN.241004.KN103	213 ± 37.3	1 ± 0.6	1 ± 0.6
ETN.190808.KN145	NM	NM	0*
ETN.240915.KN145	933 ± 17.0	4 ± 0.3	0
ETN.241002.KN145	1202 ± 87.0	4 ± 1.3	0 ± 0.6
ETN.190728.RN5	NM	7*	NM
ETN.240911.RN5	1400 ± 158.7	4 ± 1.0	0
ETN.241006.RN5	285 ± 40.0	2 ± 0.8	1±1
ETN.190728.RN6	NM	6*	1*
ETN.240918.RN6	151 ± 33.5	1 ± 0.6	0 ± 0.6
ETN.241006.RN6	236 ± 24.6	1 ± 0.5	0

*These data are missing triplicate standard deviations

VITA

Maya Robles was born March 23rd, 2002, in Ann Arbor, Michigan. They grew up in Texas, within traveling range of their mother's family in Central Mexico. From a young age, creativity was encouraged, and Maya gained a desire to study the natural sciences. With an added love for water and swimming, Maya pursued division II athletics at Henderson State University, a small university in Arkansas, where they studied biology. Maya is fond of time spent swimming at the local lake by the university. Meanwhile, Maya conducted undergraduate research, where they discovered a love for the outdoors and caving through field-based science. Maya was awarded a grant from The Explorers Club and was supported by the Ronald E. McNair program. Maya also was fortunate to have the support of several faculty throughout their time at Henderson. Maya eagerly dedicated hours of their time to cave mapping and biological monitoring of caves in the Ozarks with the Cave Research Foundation, wondering how to continue similar work in the future. This led them to the University of Tennessee to study under the mentorship of Annette Engel, distinguished cave scientist, conservationist, feminist, and ally. The knowledge gained from studies in Geology revealed context to the natural systems that Maya was already fascinated by, and the combined benefit of living in Eastern Tennessee, surrounded by incredible mountains, rivers, and caves, further enhanced the experience. Maya hopes to become further involved in the caving community and conservation-based projects in the future and is excited for the next chapter in life.